NASA Contractor Report 3166

Kinetic Energy Budgets in Areas of Convection

Henry E. Fuelberg

CONTRACT NAS8-32838
AUGUST 1979

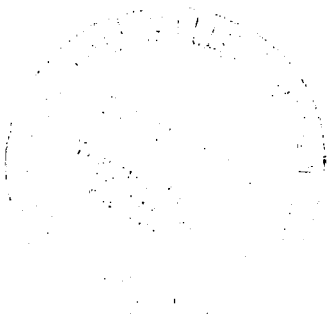

NASA

NASA Contractor Report 3166

Kinetic Energy Budgets in Areas of Convection

Henry E. Fuelberg
Saint Louis University
St. Louis, Missouri

Prepared for
Marshall Space Flight Center
under Contract NAS8-32838

National Aeronautics
and Space Administration

**Scientific and Technical
Information Branch**

1979

TABLE OF CONTENTS

		Page
LIST OF FIGURES		v
LIST OF TABLES		viii
1.	STATEMENT OF THE PROBLEM	1
	a. Introduction	1
	b. Previous studies	2
	c. Objectives	5
2.	THEORETICAL CONSIDERATIONS	6
3.	DATA AND ANALYTICAL PROCEDURES	8
	a. The AVE data sets	8
	b. Analytical procedures	10
4.	SYNOPTIC CONDITIONS	12
	a. AVSSE I period	12
	b. AVSSE II period	13
	c. AVE VII period	25
5.	RESULTS	34
	a. Average kinetic energy budget for each experiment	34
	1) AVSSE I period	34
	2) AVSSE II period	35
	3) AVE VII period	39
	4) Time series analyses	41

TABLE OF CONTENTS (Continued)

Page

b. Energy budgets of individual areas of convection..... 45

1) Texas convection area..... 45

2) Gulf Coast convection area..... 54

c. Energy budgets versus MDR values..... 63

d. Spatial maps of kinetic energy budget terms.. 76

1) AVSSE I at 0000 GMT 28 April 1975..... 76

2) AVSSE II at 2100 GMT 6 May 1975..... 81

3) AVE VII at 1200 GMT 3 May 1978..... 86

6. SUMMARY AND CONCLUSIONS..... 91

REFERENCES..... 93

ACKNOWLEDGEMENTS..... 96

LIST OF FIGURES

Figure		Page
1	Areas encompassed by the AVSSE I and II and AVE VII experiments	9
2	Synoptic conditions at the beginning of the AVSSE I period, 1200 GMT 27 April 1975	13
3	Radar summary charts for the AVSSE I period	14
4	Synoptic conditions at the end of the AVSSE I period, 1200 GMT 28 April 1975	17
5	Synoptic conditions at the beginning of the AVSSE II period, 1200 GMT 6 May 1975	19
6	Radar summary charts for the AVSSE II period	20
7	Synoptic conditions near the end of the AVSSE II period	24
8	Synoptic conditions at the beginning of the AVE VII period, 0000 GMT 2 May 1978	26
9	Radar summary charts for the AVE VII period	27
10	Synoptic conditions at the end of the AVE VII period, 1200 GMT 3 May 1978	33
11	Time series of kinetic energy budget terms integrated from the surface to 100 mb for the entire AVSSE II area	42
12	Time series of kinetic energy budget terms integrated from the surface to 100 mb for the entire AVE VII area	44
13	Pressure-time cross section of vertical motion (ω) in $\mu b\ s^{-1}$ for the Texas convection area during AVSSE II	49
14	Pressure-time cross section of generation of kinetic energy ($-\vec{V}\cdot\vec{\nabla}\phi$) for the Texas convection area during AVSSE II in $W\ m^{-2}/100$ mb	49

LIST OF FIGURES (Continued)

Figure		Page
15	Pressure-time cross section of dissipation of kinetic energy for the Texas convection area during AVSSE II in W m^{-2}/100 mb.....	51
16	Pressure-time cross section of the horizontal flux divergence of kinetic energy ($\vec{V}\cdot k\vec{V}$) for the Texas convection area during AVSSE II in W m^{-2}/100 mb.....	51
17	Pressure-time cross section of the vertical flux divergence of kinetic energy ($\partial\omega k/\partial p$) for the Texas convection area during AVSSE II in W m^{-2}/100 mb.....	53
18	Pressure-time cross section of the local change of kinetic energy ($\partial K/\partial t$) for the Texas convection area during AVSSE II in W m^{-2}/100 mb.....	53
19	Pressure-time cross section of vertical motion (ω) in $\mu b\ s^{-1}$ for the Gulf Coast area of convection during AVE VII.....	56
20	Pressure-time cross section of generation of kinetic energy ($-\vec{V}\cdot\vec{\nabla}\phi$) for the Gulf Coast area of convection during AVE VII in W m^{-2}/mb.....	57
21	Pressure-time cross section of dissipation of kinetic energy for the Gulf Coast area of convection during AVE VII in W m^{-2}/100 mb.....	58
22	Pressure-time cross section of the horizontal flux divergence of kinetic energy ($\vec{V}\cdot k\vec{V}$) for the Gulf Coast area of convection during AVE VII in W m^{-2}/100 mb.....	60
23	Pressure-time cross section of the vertical flux divergence of kinetic energy ($\partial\omega k/\partial p$) for the Gulf Coast area of convection during AVE VII in W m^{-2}/100 mb.....	61
24	Pressure-time cross section of the local change of kinetic energy ($\partial K/\partial t$) for the Gulf Coast convection area during AVE VII in W m^{-2}/100 mb..	62

LIST OF FIGURES (Continued)

Figure		Page
25	Vertical profiles of term $-\vec{V}\cdot\vec{\nabla}\phi$ for the MDR 3-6 category of several AVE type experiments.....	72
26	Vertical profiles of the dissipation term for the MDR 3-6 category of several AVE type experiments.....	72
27	Vertical profiles of term $\frac{DK}{Dt}$ for the MDR 3-6 category of several AVE type experiments.....	74
28	Vertical profiles of term $\vec{\nabla}\cdot k\vec{V}$ for the MDR 3-6 category of several AVE type experiments.....	74
29	Vertical profiles of term $\partial\omega k/\partial p$ for the MDR 3-6 category of several AVE type experiments...	75
30	Vertical profiles of term $\partial K/\partial t$ for the MDR 3-6 category of several AVE type experiments.....	75
31	Spatial fields of kinetic energy budget terms for the 400-100 mb layer of AVSSE I at 0000 GMT 28 April 1975.....	78
32	Spatial fields of kinetic energy budget terms for the 400-100 mb layer of AVSSE II at 2100 GMT 6 May 1975.....	82
33	Spatial fields of kinetic energy budget terms for the 400-100 mb layer of AVE VII at 1200 GMT 3 May 1978.....	87

LIST OF TABLES

Table		Page
1	Manually digitized radar (MDR) data code (National Weather Service, 1977).....	9
2	Average kinetic energy budget for the three standard observation times of the AVSSE I experiment.....	34
3	Average kinetic energy budget for the entire AVSSE II period.....	36
4	Kinetic energy budget for North America, 13-18 April 1970, during a period of short synoptic wave development (Ward and Smith, 1976).....	37
5	Average kinetic energy budget for the entire AVE VII period.....	39
6	Average kinetic energy budget for the limited area enclosing the convection in central Texas during AVSSE II at 2100 GMT 6 May 1975.....	46
7	Average kinetic energy budget for the limited area enclosing the convection along the Gulf Coast during AVE VII at 1200 GMT 3 May 1978.....	55
8	Comparisons of energy budget studies for grid points of MDR 0.....	64
9	Comparisons of energy budget studies for grid points of MDR 3-6.....	67
10	Comparisons of energy budget studies for grid points of MDR 5-6.....	71

KINETIC ENERGY BUDGETS IN AREAS OF CONVECTION

by

Henry E. Fuelberg

Department of Earth and Atmospheric Sciences
Saint Louis University
St. Louis, Missouri 63103

1. STATEMENT OF THE PROBLEM

a. Introduction

Severe thunderstorms are mesoscale phenomena whose formation is influenced by meteorological conditions on both larger and smaller atmospheric scales. After formation, severe thunderstorms affect the wind and thermal structure of the surrounding atmospheric environment on all scales and thereby influence the formation of additional storms. Understanding the complex interactions between thunderstorms and their environments is a great challenge to meteorology. Improvements in forecasting severe thunderstorms, and other weather events, will occur as our knowledge of scale interactions increases.

Understanding the energy budget of the thunderstorm environment is one way of furthering our knowledge about how thunderstorms form and interact with their surroundings. This research computes synoptic-scale kinetic energy budgets at 3 h intervals for volumes that encompass numerous severe thunderstorms. The energy processes prior, during, and after the storms are studied to gain a better understanding of severe storm development, evolution, and scale interaction. The results also indicate the atmospheric variability of kinetic energy near such storms which will help NASA define the desired resolutions for remote sensing systems. Rawinsonde and satellite data from NASA's Atmospheric Variability Experiments (AVE's) are used in this research.

b. Previous studies

Numerous kinetic energy budget studies have been performed for individual synoptic-scale weather systems such as cyclones and anticyclones. These systems with wavelengths of several thousand kilometers and lifetimes of several days are important components of the average energy budget computed for larger areas and longer time periods. Kung and Smith (1974) have summarized this research and noted that a single mature cyclone can account for 1/4 to 1/3 of the middle-latitude atmospheric energetics. Recent studies on this topic have been conducted by Vincent and Chang (1975), Ward and Smith (1976), Kornegay and Vincent (1976), and Chien and Smith (1977). The energetics of middle latitude cyclones have been found to be highly variable between individual case studies and between different time periods of the same case study. By interpretation of the dissipation term, several studies have shown that subgrid-scale processes can supply, as well as remove, energy from the synoptic scale. (e.g., Chen And Bosart, 1977; Kung and Baker, 1975; Ward and Smith, 1976; Vincent and Chang, 1975).

Nearly all of the computed kinetic energy budgets on the synoptic scale have used rawinsonde data at the customary 12 h intervals, in which case shorter period features were not resolved. Therefore much remains to be learned about synoptic-scale energy variability at shorter time intervals.

Compared to investigations of the synoptic scale, few studies have considered kinetic energy budgets of the environments of mesoscale events such as severe thunderstorms (a lack of mesoscale data is a serious obstacle to such research). Three such studies have used data from the mesoscale network of nine rawinsonde stations operated by the National Severe Storms Laboratory (NSSL) to describe the kinetic energy budgets of the environments of mesoscale

phenomena (McInnis and Kung, 1972; Kung and Tsui, 1975; Tsui and Kung, 1977). Areas of convection were found to be centers of major energy generation, transport, and dissipation. Some of the processes were an order of magnitude larger than corresponding processes on the synoptic scale. Large generation of kinetic energy by cross-contour flow was nearly balanced by dissipation to subgrid scales of motion, while boundary terms and local changes were relatively small. A relation between variations in energy variables and the growth and decay of storms was noted.

The relationship between energy processes and the life cycle of convective activity is difficult to assess when mesoscale data (such as NSSL data) are used because many intense storm systems do not remain within such limited data-rich areas during their complete life cycles. In an attempt to overcome this problem, Fuelberg and Scoggins (1977, 1978) studied the energy variability of the synoptic-scale flow in which large areas of intense convection were imbedded, using AVE IV data. The energetics of the synoptic-scale flow were described before, during, and after the formation of two intense squall lines.

Although convective areas and their surroundings interact to affect energy exchanges on scales that are not resolved in specific detail with synoptic-scale data, previous research has shown that large areas of intense convection in concert do affect the surroundings to an extent that changes can be detected using synoptic-scale data. On the other hand, small areas of non-severe thunderstorms would not affect the surroundings enough to be measured with synoptic-scale data. Hence, the approach of Fuelberg and Scoggins (1978) probably would not detect the environmental changes due to scattered non-severe thunderstorms. However, Ninomiya (1971a and b) observed kinematic and thermodynamic changes in the synoptic-scale flow near tornado-producing thunderstorms attributable

to latent heat release. In addition, Danard (1964, 1966), using numerical methods with and without the inclusion of latent heat release, found that the production of kinetic energy due to rising air and cross-contour flow was enhanced considerably by latent heat release. This effect was of the same order of magnitude as that caused solely by dry adiabatic processes.

Fuelberg and Scoggins (1977, 1978) observed large generation of kinetic energy in the general flow surrounding the intense convection. Horizontal transport of kinetic energy out of the areas of convection and transfer of kinetic energy to subgrid scale motion also were shown to be important processes. Temporal variations in the energy budget terms were related to the life cycles of the convection; maximum generation and transport of energy occurred near the time of maximum storm intensity while smaller values were observed during the development and decay stages. Spatial fields of the energy budget terms showed that the most intense energy processes occurring during the AVE IV period were associated with the intense convection. Additional studies of this type should be undertaken to further investigate the effects of intense convection on atmospheric energy.

A large region of accurate conventional mesoscale data, at the surface and aloft, would be ideal for a kinetic energy study of severe storms; currently, however, such data are scarce. The 1979 SESAME-AVE field experiments will provide additional subsynoptic scale rawinsonde data for this type of research, but only six days of data collection are planned. As we learn more how to exploit satellite observations, alternative data bases will be obtained for real time use. Since it is not now possible to compute kinetic energy budgets of areas enclosing severe storms using satellite-derived data alone, it is necessary to obtain results based upon existing data sources. At the present time, however, various types of

satellite imagery are a valuable supplement to rawinsonde data. This combination of data sources is expected to be weighted more and more toward the satellite as time evolves to yield better and better understandings of the relations between severe storm development and evolution, and energy conversions and transports on the various scales.

c. Objectives

This research related synoptic-scale kinetic energy variability to severe storm occurrences during three AVE periods that encompassed intense convection. Several of the tasks were possible only because the AVE rawinsonde data were available at 3 h intervals, rather than 12 h intervals. The specific items that were investigated are:

1) The relation between spatial fields of kinetic energy budget terms and the locations and movements of convection and other discernible map features,

2) A description of the average kinetic energy budgets for each entire AVE area,

3) A description of the synoptic-scale kinetic energy budgets in the vicinities of severe storms,

4) The relation between temporal variations in kinetic energy budget terms and the life cycles of convective activity, and

5) The relation between kinetic energy variability and the intensity of convective activity.

2. THEORETICAL CONSIDERATIONS

The kinetic energy budget equation for a fixed volume in the isobaric coordinate system is given by Smith (1969) as:

$$\frac{\partial K}{\partial t} = \underset{\sigma p}{\iint} -\vec{V}\cdot\vec{\nabla}_p\phi - \underset{\sigma p}{\iint}\vec{\nabla}_p\cdot k\vec{V} - \underset{\sigma p}{\iint}\frac{\partial \omega k}{\partial p} + \underset{\sigma p}{\iint}\vec{V}\cdot\vec{F} + \int_{\sigma} k_0 \frac{\partial p_0}{\partial t} \qquad (1)$$

(a) (b) (c) (d) (e) (f)

where $\underset{\sigma p}{\iint} = \frac{1}{gA} \iiint dx\,dy\,dp$,

$\vec{V}$ is the horizontal wind vector,

$\omega = \frac{dp}{dt}$ is the vertical motion in isobaric coordinates,

$k = (u^2 + v^2)/2$ is horizontal kinetic energy per unit mass,

$K = \underset{\sigma p}{\iint} k$,

$\phi = gz$ is geopotential height,

$\vec{F}$ is frictional force,

A is the area of computation σ, and

$_0$ is a subscript denoting surface values.

Local changes in kinetic energy for a fixed volume, term (a) above, are due to five processes. Term (b) represents kinetic energy generation (Kung, 1966) or conversion of potential to kinetic energy (Smith, 1970) due to cross-contour flow. Terms (c) and (d) are the horizontal and vertical components of flux divergence of kinetic energy. Term (f) represents changes in kinetic energy due to changes in mass of the volume being studied. Term (e) conceptually represents thermodynamic frictional processes, but when computed as a residual to the kinetic energy equation, it also represents a transfer of energy between grid and subgrid scales of motion, due mostly to unresolvable eddy processes. (Smith and

Adhikary, 1974; Kung and Smith, 1974). The term is often called the "dissipation" term.

The residual dissipation term also contains errors accumulated from other terms in the kinetic energy equation, but error simulations have shown that these are not the dominant components of the dissipation term (Vincent and Chang, 1975; Kornegay and Vincent, 1976; Ward and Smith, 1976). Since the resolvable scales of motion in a given study are generally known, this residual term allows one to infer the importance of motions which are not readily detectable with the input data scale and computational procedures being used. For example, if synoptic-scale data are used, the net effect on kinetic energy of mesoscale and microscale processes that are not adequately described by the input data can be inferred.

3. DATA NND ANALYTICAL PROCEDURES

a. The AVE data sets

Data from three AVE-type experiments were used in the research--AVSSE I (27-28 April 1975), AVSSE II (6-7 May 1975), and AVE VII (2-3 May 1978). Figure 1 shows boundaries of each of the three experiment areas; approximately 23 rawinsonde stations participated in each experiment. The AVE data were collected during periods of intense convective activity and have synoptic-scale spatial separation, but are at 3 or 6 h time intervals. Data reduction procedures used to process the AVE rawinsonde data are described by Fuelberg (1974) while the data at 25 mb intervals are given by Fucik and Turner (1975a and b) for AVSSE I and II and Davis et al. (1978) for AVE VII. During AVSSE I many of the special rawinsonde soundings were missing; therefore, in the present study, only the 12 h regular data were used. Data from all time periods were used for the studies of AVSSE II and the AVE VII periods.

Manually Digitized Radar (MDR) data were used to determine objectively the intensity and location of radar-observed convection. For AVSSE I and II, these data were obtained from NOAA's Techniques Development Laboratory on magnetic tape and then plotted manually; for AVE VII, they were read from the radar summary charts sent over the NAFAX circuit. Table 1 is an explanation of the MDR code now in use. When hourly MDR data were available, plots were made each hour for 3 h periods centered on each rawinsonde observation time. The three plots were then combined into a single chart for each rawinsonde observation time by using the highest coded value reported for each MDR block. This procedure tends to maximize both areal coverage and intensity, but objectively gives the general location and intensity of the convection under study. When hourly MDR data were not available, values for the individual hours of rawinsonde release were used.

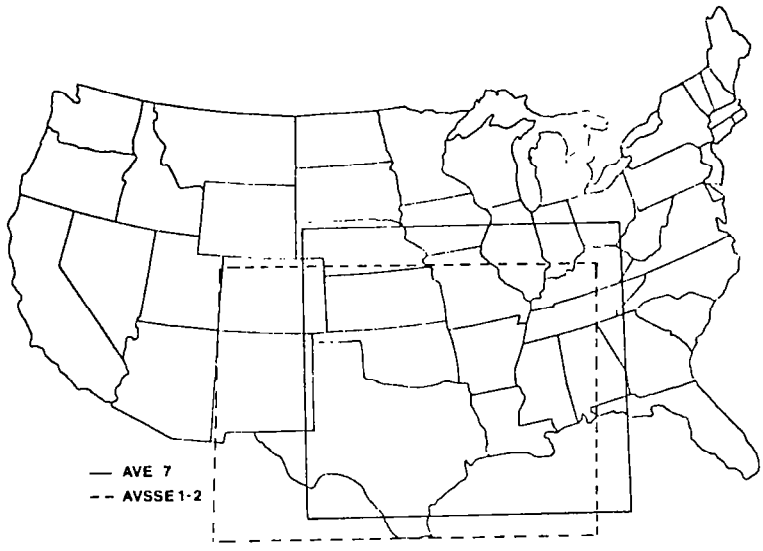

Fig. 1. Areas encompassed by the AVSSE I and II and AVE VII experiments.

Table 1. Manually digitized radar (MDR) data code (National Weather Service, 1977).

Code Number (VIP Level)	Echo Intensity	Rainfall Rate (in/hr) Stratiform	Convective
1	light	less than 0.1	.05 - 0.2
2	moderate	0.1 - 0.5	0.2 - 1.1
3	heavy	0.5 - 1.0	1.1 - 2.2
4	very heavy	1.0 - 2.0	2.2 - 4.5
5	intense	2.0 - 5.0	4.5 - 7.1
6	extreme	greater than 5.0	greater than 7.1

b. Analytical procedures

Rawinsonde data were interpolated from the randomly spaced stations onto an equally spaced grid system with a spacing of 158 km by using an objective analysis scheme by Barnes (1964). Although a careful manual analysis of data is preferable to any automatic objective scheme that has been devised, the number of charts required rendered hand analysis unfeasible for this study. The procedure developed by Barnes is commonly referred to as successive corrections to a first-guess field. The final gridded fields retain as much detail as can be justified from the input data and show very good agreement with hand analyses. Since the average spatial separation of rawinsonde stations over the United States is about 400 km, the smallest resolvable wavelength using such data is about 800 km.

Gridded analyses of the required input data were produced at the surface and at 50 mb intervals from 900 to 100 mb for each observation time. Winds were averaged over 50 mb layers to reduce further random errors. Centered finite differences were used where possible to compute all space and time derivatives. However, forward and backward time differences were used for the first and last observation times of each experiment, respectively.

Grid-point values of terms in (1) [except (e)] were computed at each of the 18 levels previously described and then integrated over 50 mb layers using the trapezoidal rule. The dissipation term [term (e)] was computed as a residual to balance (1) at each grid point in each 50 mb layer. One should recall that this term is interpreted on the basis of the atmospheric motions that can be resolved with the input data and computational procedures being used.

Kinematic values of vertical motion were used. Vertical motion was assumed to be zero at the surface; an adjustment scheme by O'Brien (1970) was applied so that values at 100 mb

would equal zero.

Random errors in input data and truncation error lead to errors in computed terms of the kinetic energy equation, but the magnitudes of these errors are difficult to estimate. The validity of results of an energy study can be inferred on the basis of spatial continuity, vertical consistency, and comparisons with parallel but independent research efforts (McInnis and Kung, 1972). In this regard, the present results appear quite systematic and physically meaningful. An alternate method of assessing accuracy is the introduction of reasonable random errors into the input data and comparing the computed kinetic energy budget with results from unaltered data. Previous investigators who have used this method have concluded that trends of results and their interpretations almost always remain the same regardless of the reasonable errors that were introduced (Vincent and Chang, 1975; Kornegay and Vincent, 1976; Ward and Smith, 1976). Although previous investigators used computational procedures that differ from those used in this study, their general conclusions appear applicable to this study.

4. SYNOPTIC CONDITIONS

Each of the three AVE periods chosen for study was characterized by the occurence of severe thunderstorms within the experiment area.

a. AVSSE I period

Synoptic conditions at the beginning of the AVSSE I period (1200 GMT 27 April 1975) are shown in Fig. 2. At the surface, a dual low pressure center was located over South Dakota and eastern Colorado. A warm front extended from South Dakota southeastward into Arkansas where it became stationary and continued to the coast of Georgia. Cool polar air was located to the north of this frontal zone while warmer, more humid air bathed locations south of the front. A cold front extended along a north-south axis from South Dakota to the Big Bend region of Texas. Cool, dry air was located to the west of this front.

A well defined trough-ridge pattern with wavelengths of about 3000 km was present in the middle and upper troposphere. The conditions at 500 mb at the beginning of AVSSE I are shown in Fig. 2. A ridge extended from Minnesota to Louisiana, roughly through the center of the AVSSE I experiment region. A cold core trough was located over the Rocky Mountains on the western fringes of the experiment region. Southwesterly flow as great as 50 m s^{-1} was located near 300 mb over the western portion of the AVSSE I area.

Intense thunderstorms formed along the eastward moving cold front on 27 April. At the beginning of the period showers and thundershowers were scattered over Texas and the middle Mississippi River Valley (Fig. 3a). Intense thunderstorms with radar tops as high as 15.2 km (50,000 ft) were occurring over western Kansas and the Oklahoma panhandle. Surface hail was reported with some of these storms. This area of storms moved eastward during the day and developed into a

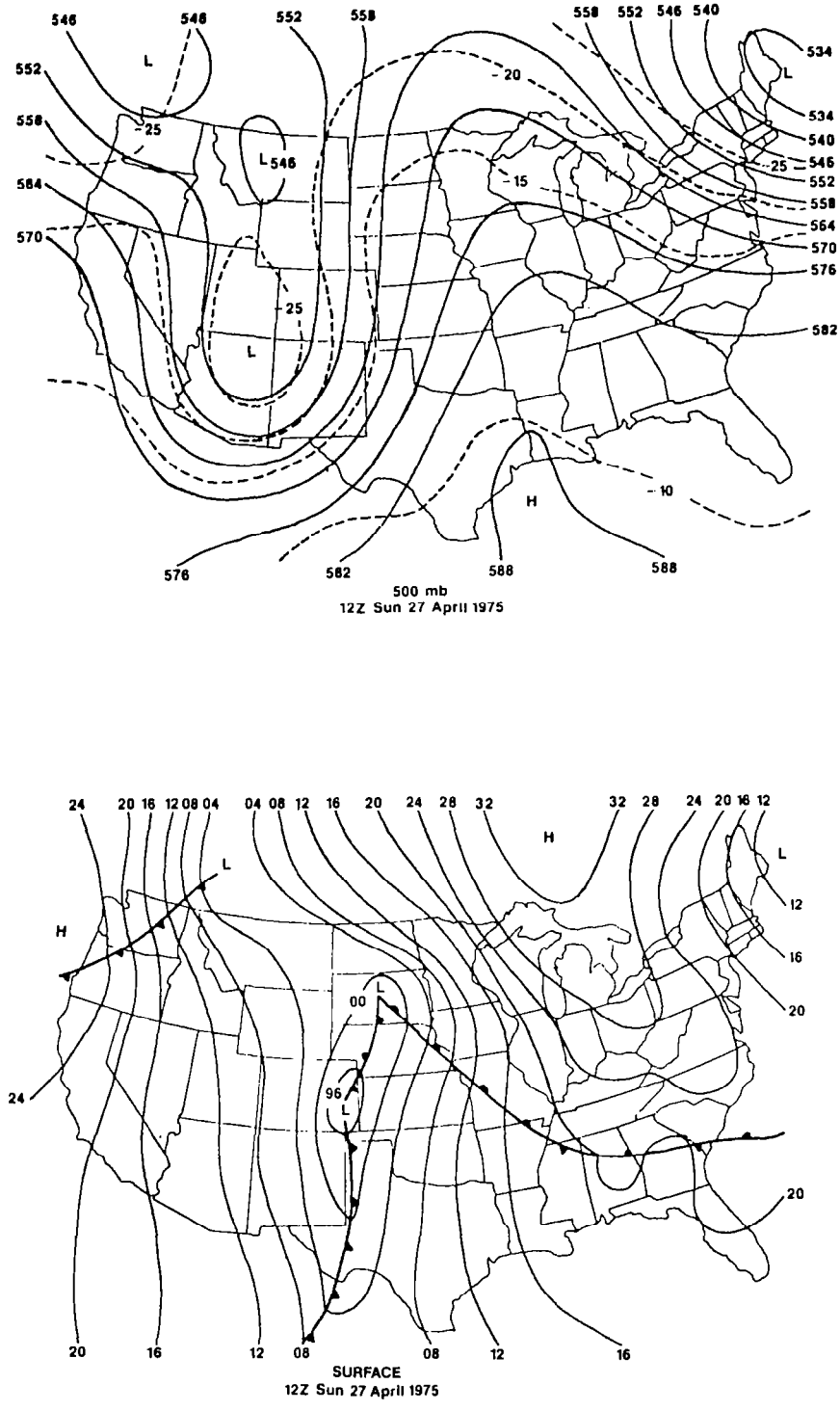

Fig. 2. Synoptic conditions at the beginning of the AVSSE I period, 1200 GMT 27 April 1975.

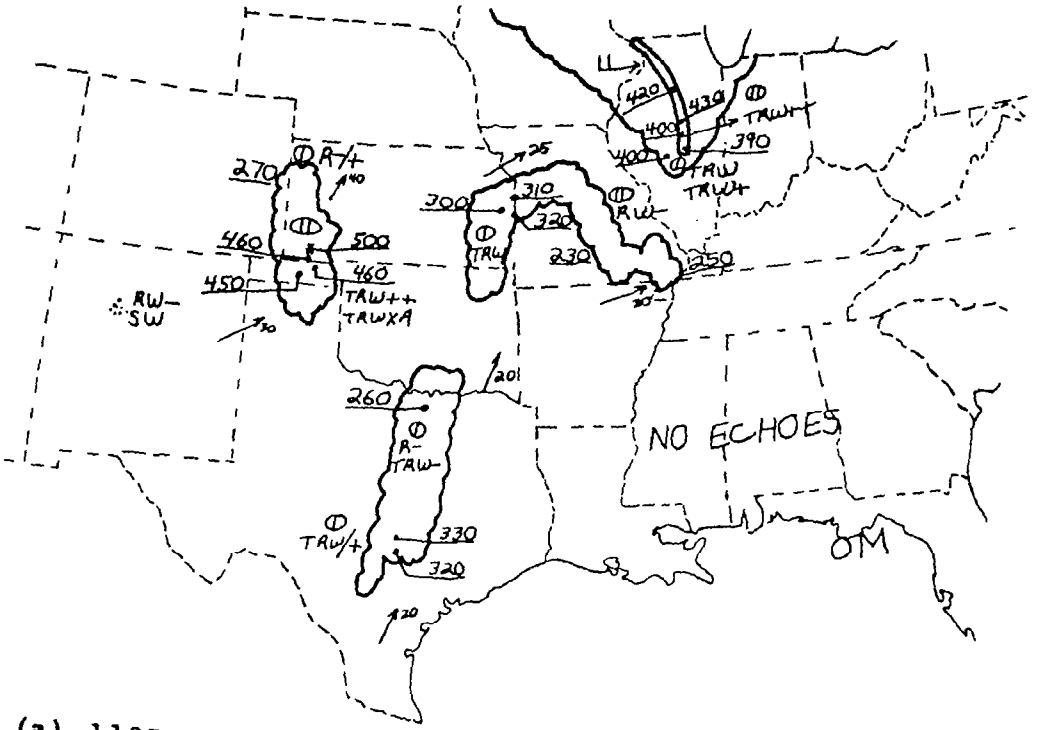

(a) 1135 GMT 27 April 1975

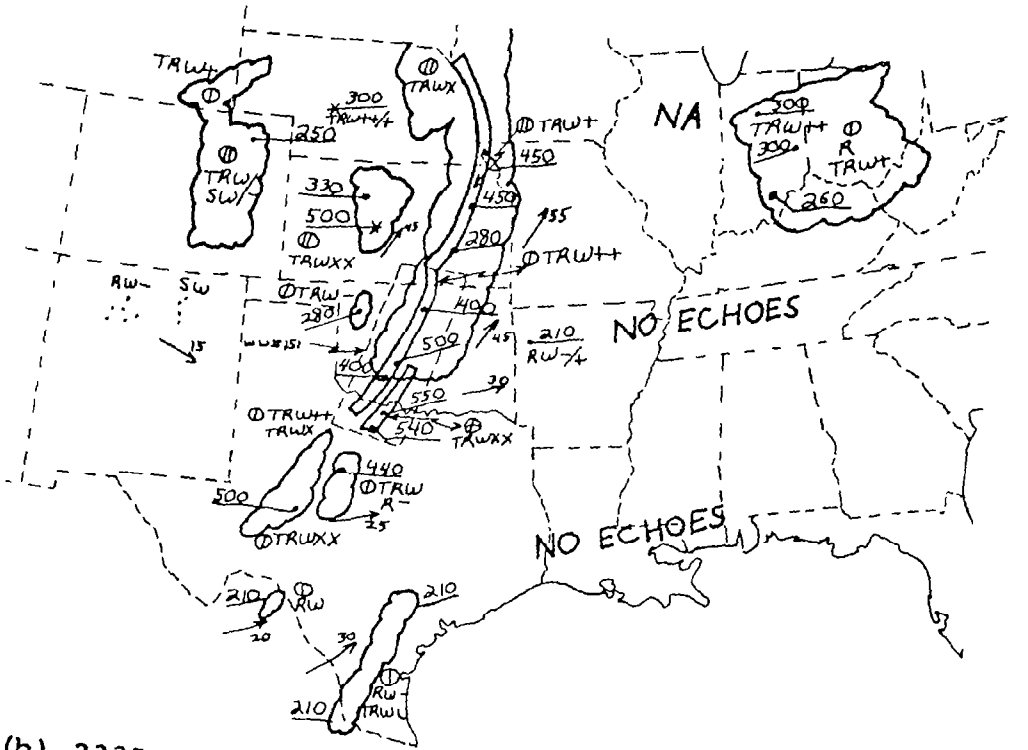

(b) 2335 GMT 27 April 1975

Fig. 3. Radar summary charts for the AVSSE I period.

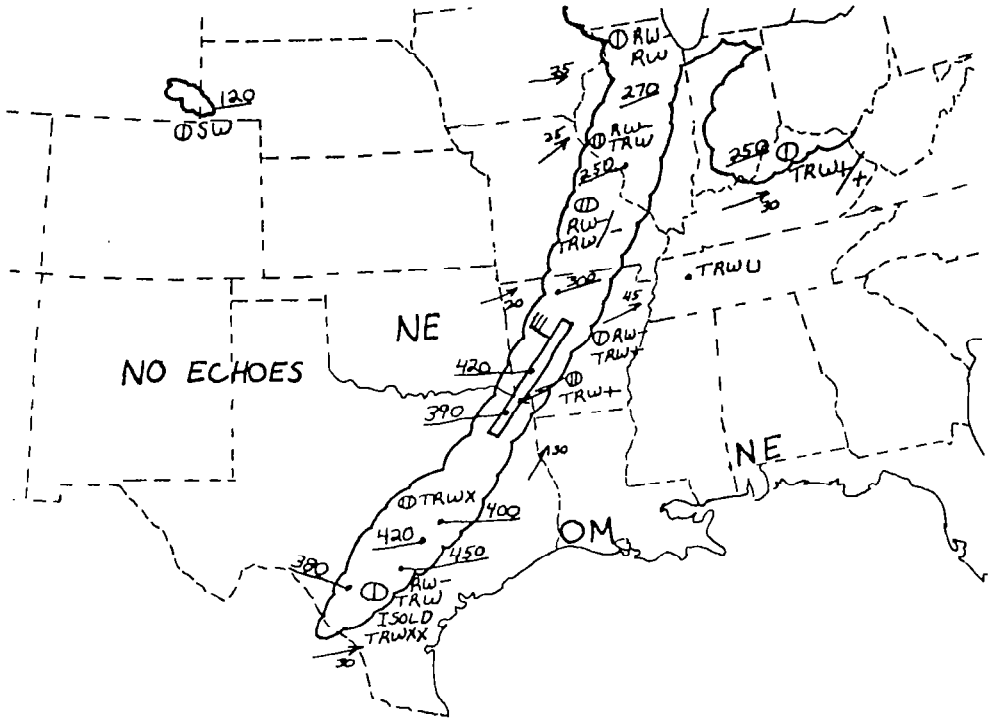

(c) 1135 GMT 28 April 1975

Fig. 3. (Continued)

well defined squall line extending from Nebraska into central Texas. Numerous severe storm watches and warnings were issued for this area of convection which reached peak intensity and areal coverage near 2100 GMT. By 2335 GMT 27 April (Fig. 3b), heavy thunderstorms were still occurring through the Midwest and into Texas. The southern portions of the convection area underwent considerable intensification during the night. By early morning on 28 April (Fig. 3c) a band of showers and storms extended from Illinois to the Texas-Mexico border with the heaviest storms located in southcentral Texas.

The surface map at the end of the period, 1200 GMT 28 April, (Fig. 4) reveals a single intense low pressure area centered over the Nebraska-South Dakota border. An occluded front extended southeastward into Iowa where it split into a cold front that reached into central Texas and a warm front that reached the coast of North Carolina.

At 500 mb, the base of the upper-level trough broadened during the period as a short wave moved northeastward and away from the main trough axis. The short wave was located near the border of South Dakota and Nebraska by 1200 GMT 28 April (Fig. 4). The ridge moved slowly eastward and was located over the Ohio and Tennessee River Valleys by the end of the experiment period.

b. AVSSE II period

The synoptic situation of the AVSSE II period shows similarities to conditions found during AVSSE I. Surface features at the beginning of AVSSE II (1200 GMT 6 May 1975) are shown in Fig. 5. A low pressure area was located over South Dakota with a cold front extending southward into Texas. A warm front stretched from South Dakota eastward into Pennsylvania. Remnants of an old frontal system were located along the lower Mississippi River Valley and across

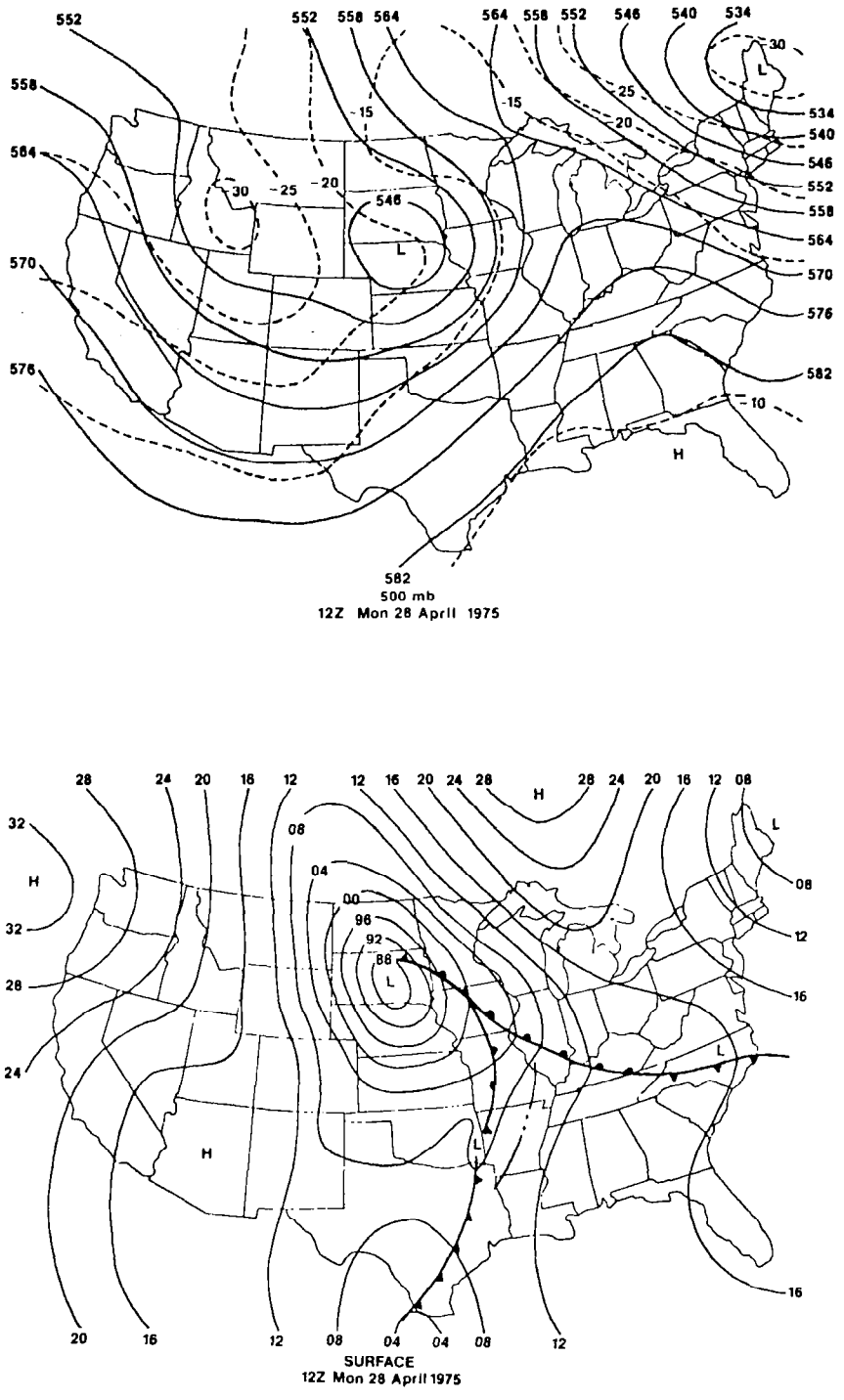

Fig. 4. Synoptic conditions at the end of the AVSSE I period, 1200 GMT 28 April 1975.

Florida.

A closed low pressure center dominated the flow at 500 mb at the start of AVSSE II (Fig. 5). A weak ridge was located along the Mississippi River Valley. The locations of the pressure centers and their wavelengths (~3000 km) are similar to those occurring during AVSSE I. Strongest winds occurred from New Mexico into Nebraska along the eastern side of the low. The AVSSE II experiment area encompassed the southeastern portions of the low and much of the associated downstream ridge.

At the beginning of AVSSE II, 1200 GMT 6 May, convection was confined to the lower Mississippi River Valley where maximum radar tops reached 14.6 km (48,000 ft., Fig. 6a). As the day progressed, this area of convection expanded into Arkansas, Missouri, and Illinois (Fig. 6b). The most intense storm activity of the period, however, formed along the slowly advancing cold front. Storms began forming from Oklahoma to Nebraska at around 1700 GMT while an area of storms in Texas began to form from an area of rainshowers at around 1800 GMT (Fig. 6c). The northern section of storms merged with the area of convection located in the middle Mississippi River Valley and underwent several periods of decay and reintensification during the remainder of the AVSSE II period. Radar tops of 15.2 km (50,000 ft) were quite common in this storm area. The showers in central Texas that began to form near 1400 GMT developed rapidly near 1800 GMT, reached peak coverage and areal intensity (18.6 km, 61,000 ft) near 2100 GMT (Fig. 6d), and had completely dissipated by 0100 GMT 7 May (Fig. 6e-f). Convection was confined to the southeastern portion of the area by the end of the experiment (Fig. 6g-h).

Synoptic conditions at the end of the AVSSE II period are shown in Fig. 7. The surface low pressure center remained

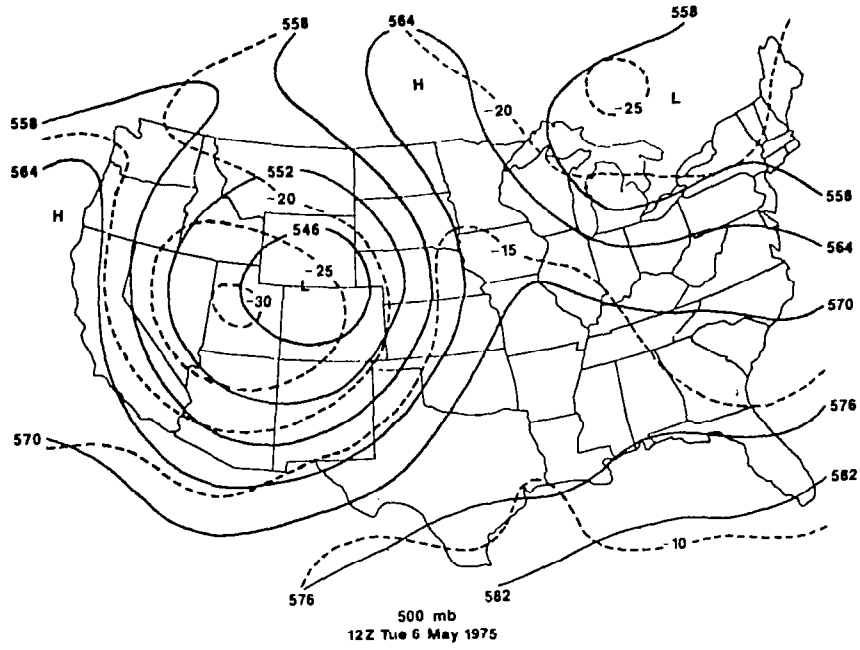

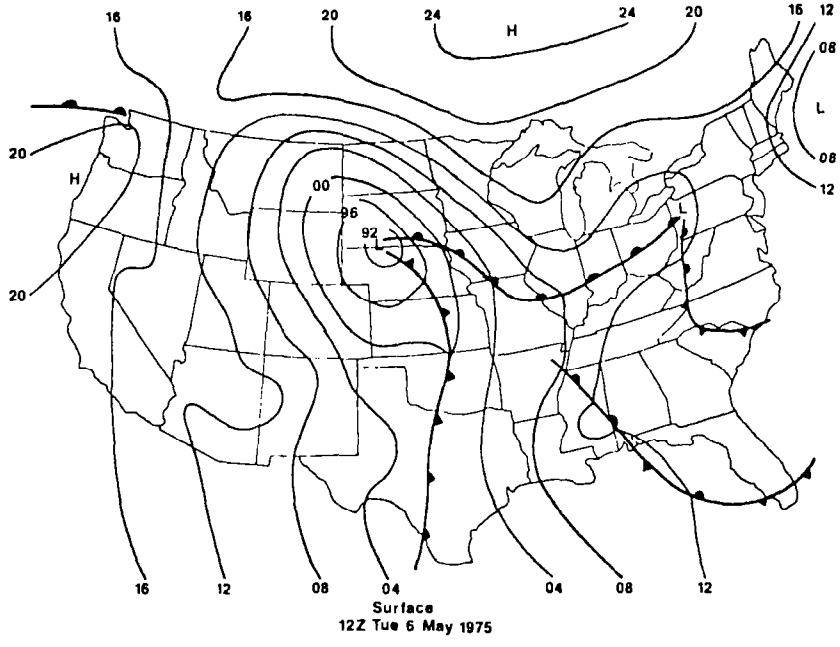

Fig. 5. Synoptic conditions at the beginning of the AVSSE II period, 1200 GMT 6 May 1975.

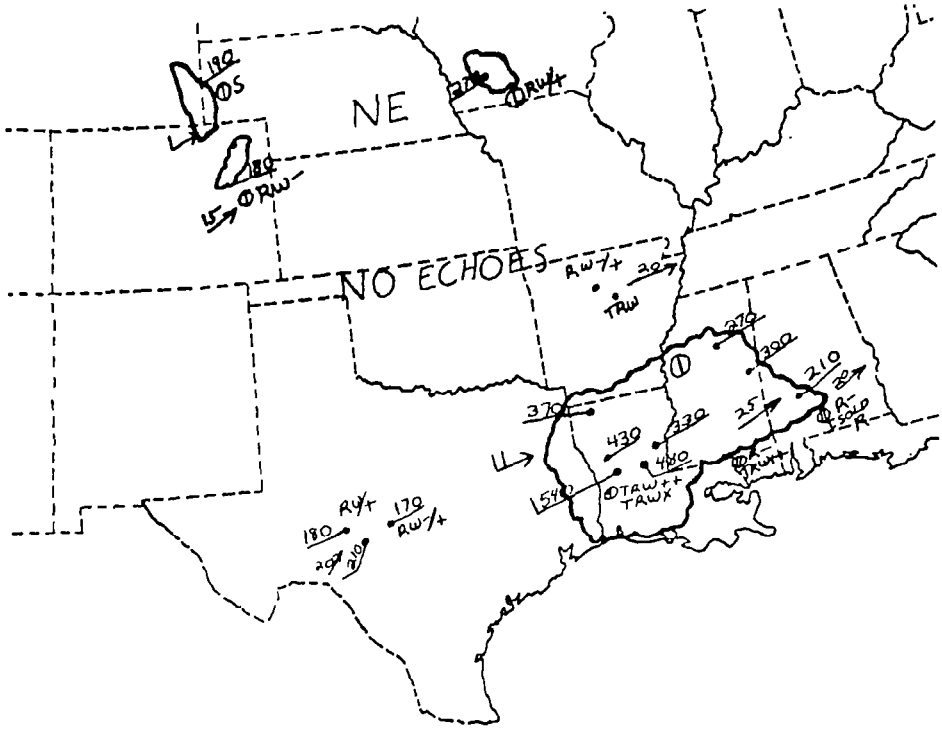

(a) 1135 GMT 6 May 1975

(b) 1435 GMT 6 May 1975

Fig. 6. Radar summary charts for the AVSSE II period.

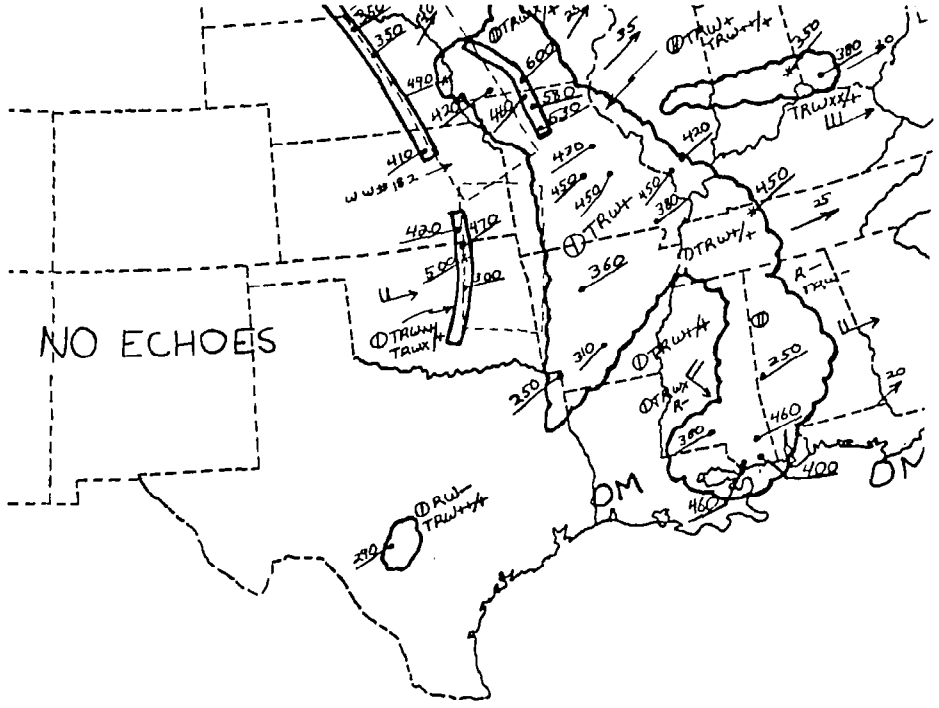

(c) 1735 GMT 6 May 1975

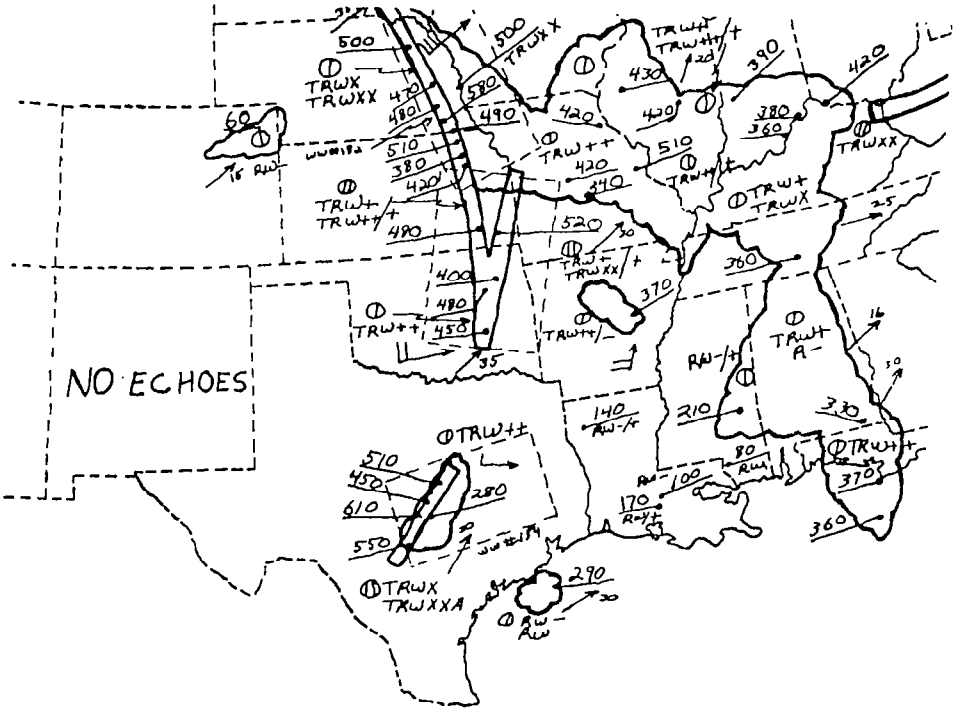

(d) 2035 GMT 6 May 1975

Fig. 6. (Continued)

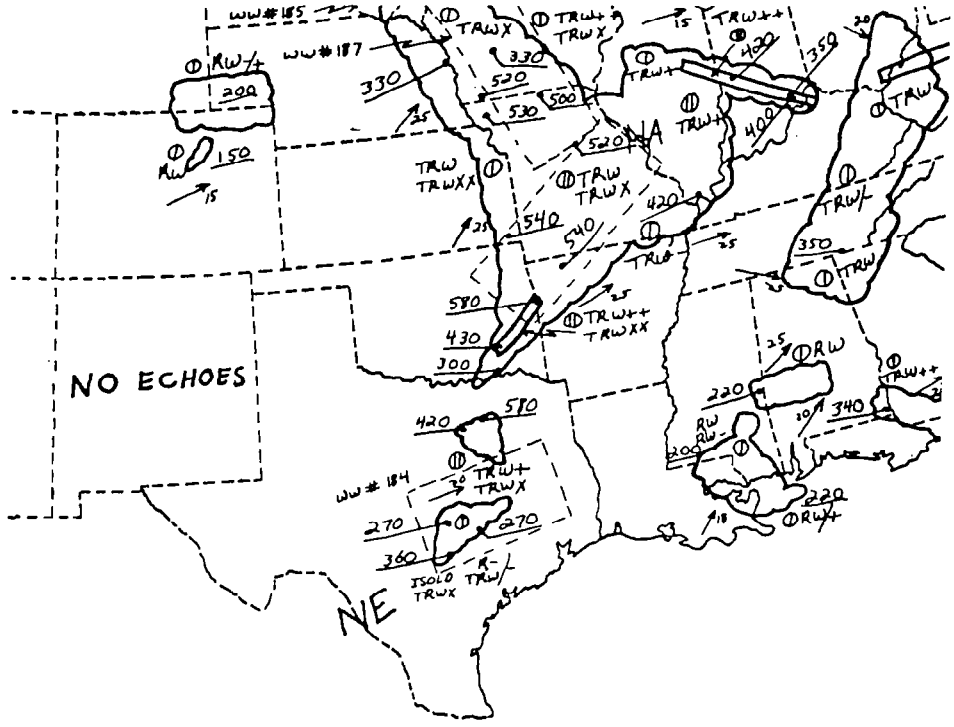

(e) 2335 GMT 6 May 1975

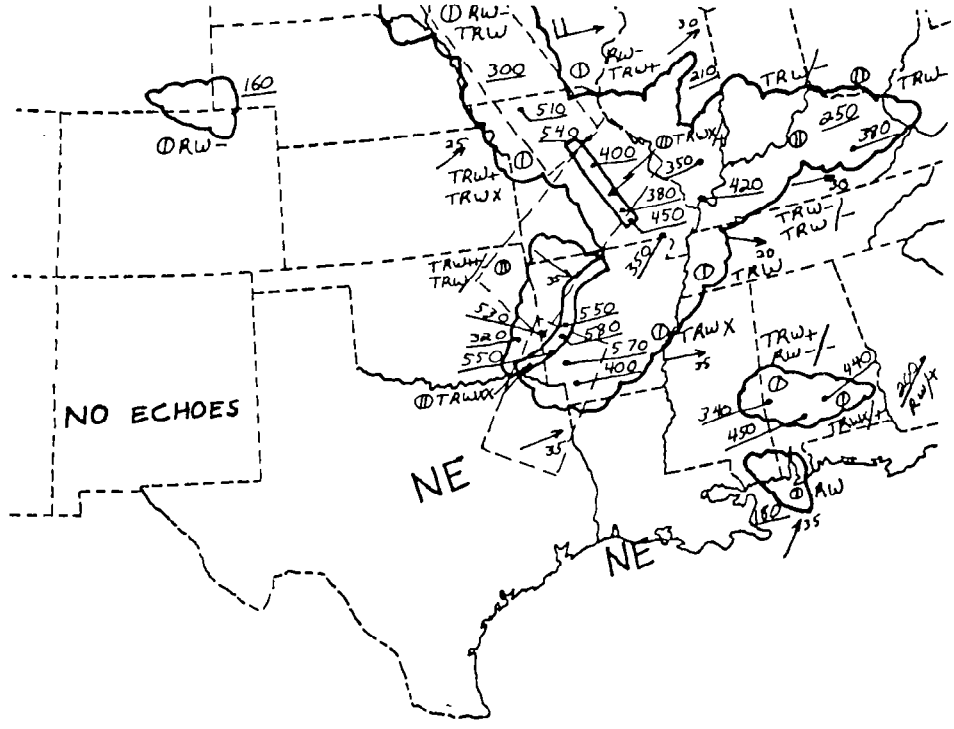

(f) 0235 GMT 7 May 1975

Fig. 6. (Continued)

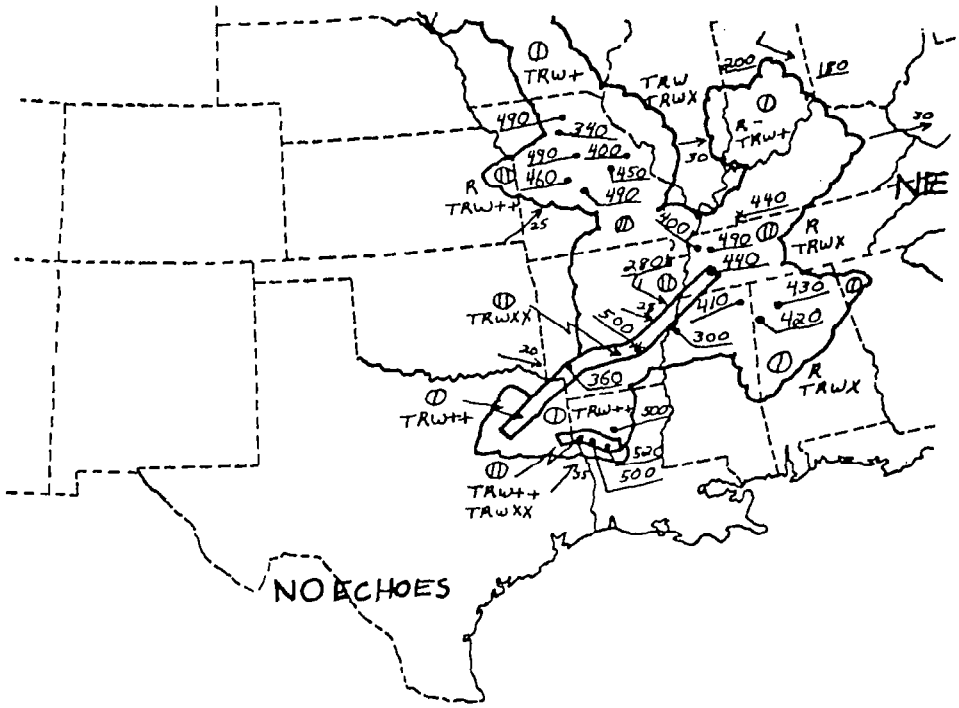

(g) 0735 GMT 7 May 1975

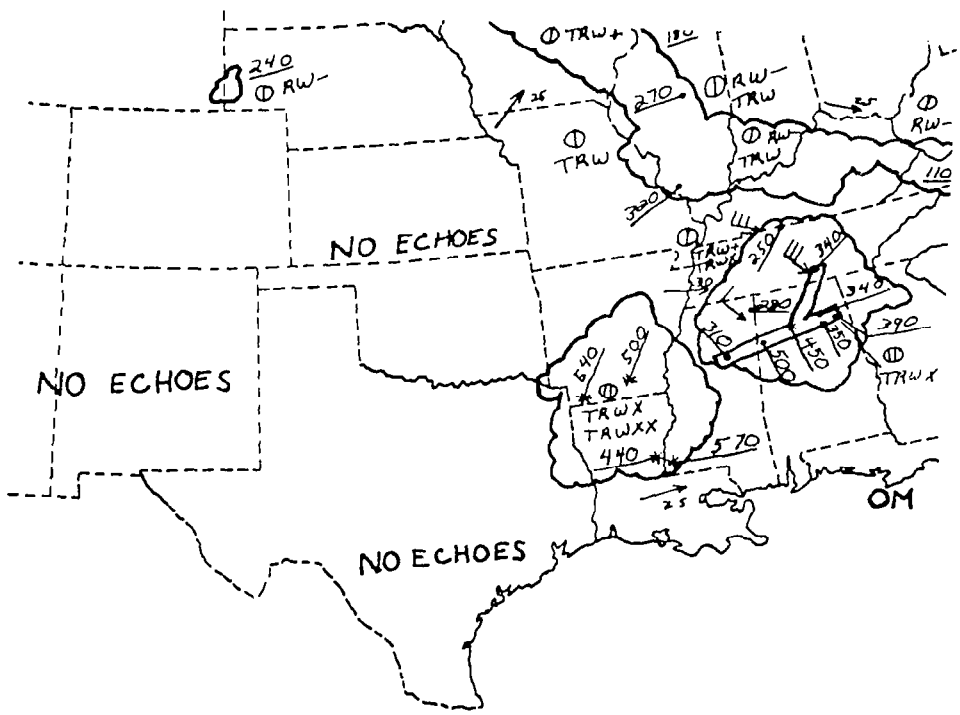

(h) 1135 GMT 7 May 1975

Fig. 6. (Continued)

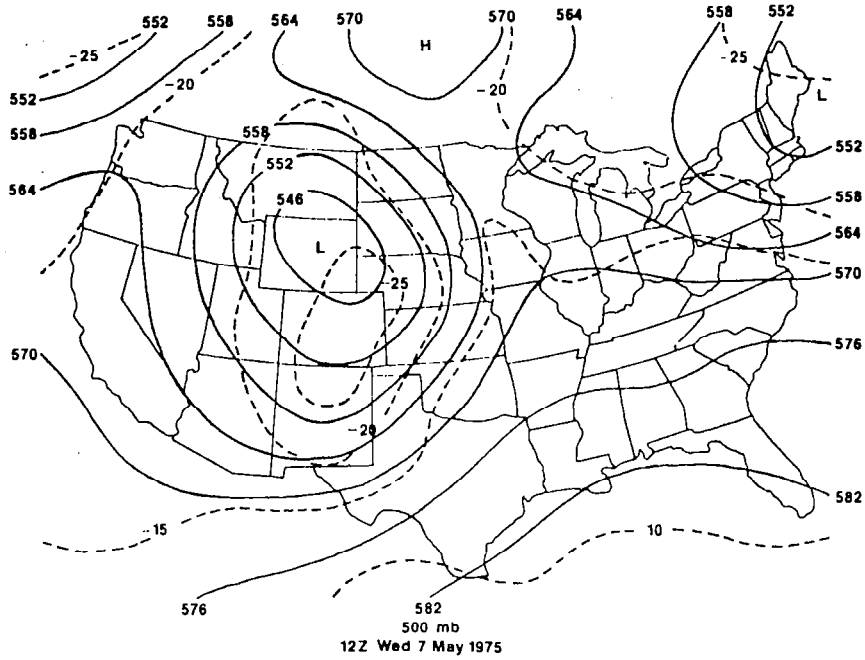

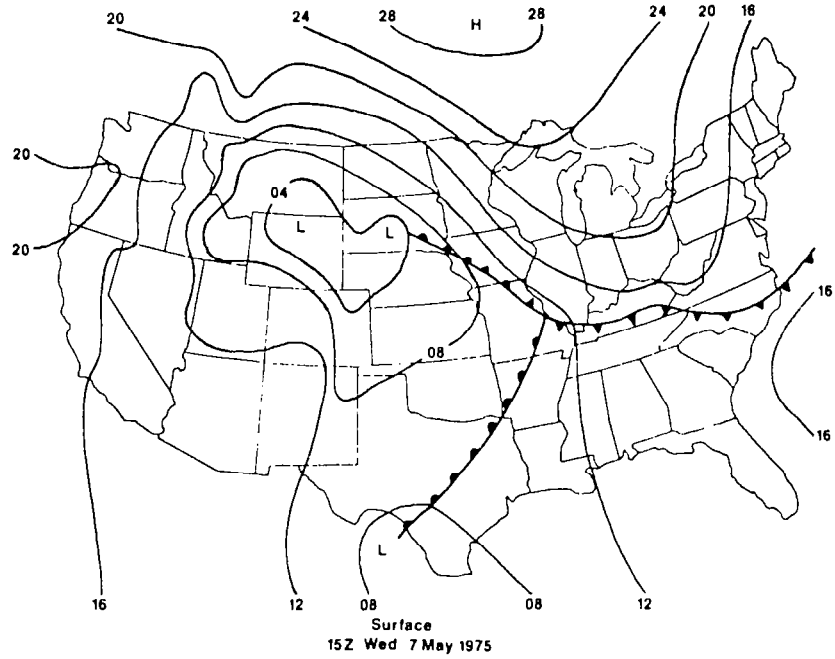

Fig. 7. Synoptic conditions near the end of the AVSSE II period.

nearly stationary and showed gradual weakening during the period. Frontal systems showed only slow movement. Conditions at 500 mb also showed little change. The closed low remained nearly stationary over Wyoming; 24 h height changes over the area were generally less than 30 m.

c. AVE VII period

No major cyclone activity occurred at the surface during the AVE VII period, although intense convection occurred in central Texas and along the coasts of Louisiana and Mississippi. Surface conditions at 0000 GMT 2 May 1978, the start of AVE VII, indicate a frontal system extending from South Carolina, southwestward into Texas (Fig. 8). The Midwest was dominated by high pressure centered in Canada. Temperatures along the Gulf Coast were balmy, but much colder temperatures occurred to the north of the front.

The flow at 500 mb over the AVE VII area was dominated by a closed low over Arizona and a weaker ridge over the Midwest (Fig. 8). A closed low located over the maritime provinces of Canada influenced the flow over the eastern portions of the AVE VII region. The jet stream, with winds as great as 60 m s^{-1}, stretched along the Gulf Coast, while winds through the northern Midwest near the ridge were quite light.

At the beginning of the period, 0000 GMT 2 May, convection was confined to central Texas where radar tops reached 16.8 km (55,000 ft) (Fig. 9a). These storms dissipated during the night. By the next morning at 1200 GMT 2 May (Fig. 9b), thunderstorms already were developing in west Texas. This area of convection moved eastward into Louisiana during the day and night (Fig. 9c-i). An additional area of storms began forming over southern Mississippi and Louisiana near 1800 GMT (Fig. 9d). This area and the advancing storm area from Texas combined to give a large area of intense storms along the Gulf Coast by 0835 GMT 3 May (Fig. 9h). At the end of AVE VII, 1200 GMT 3 May

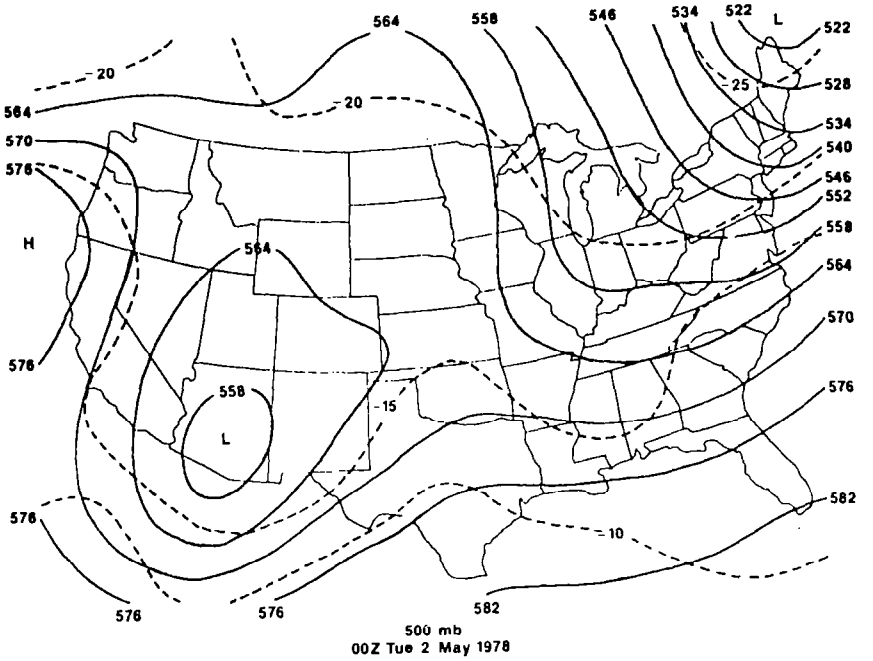

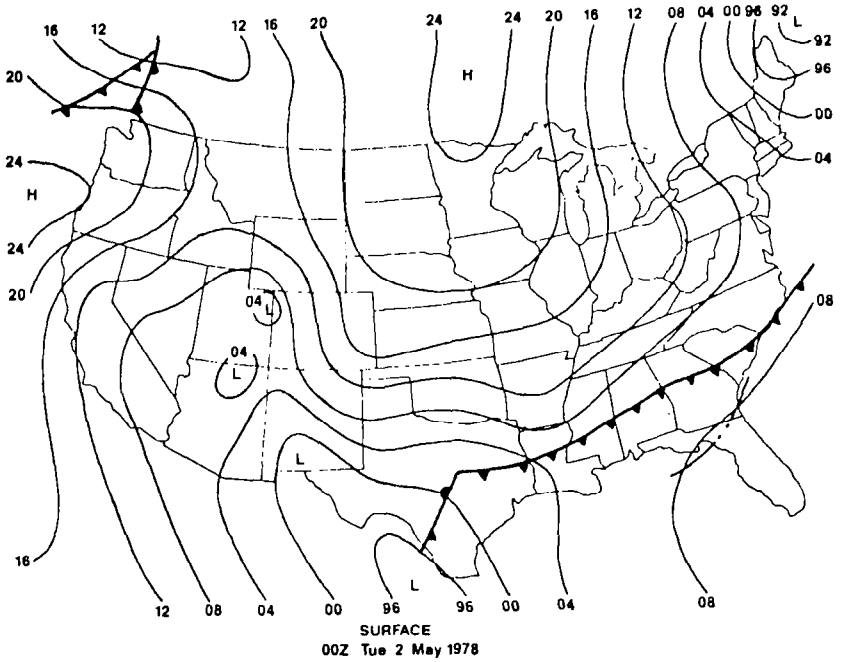

Fig. 8. Synoptic conditions at the beginning of the AVE VII period, 0000 GMT 2 May 1978.

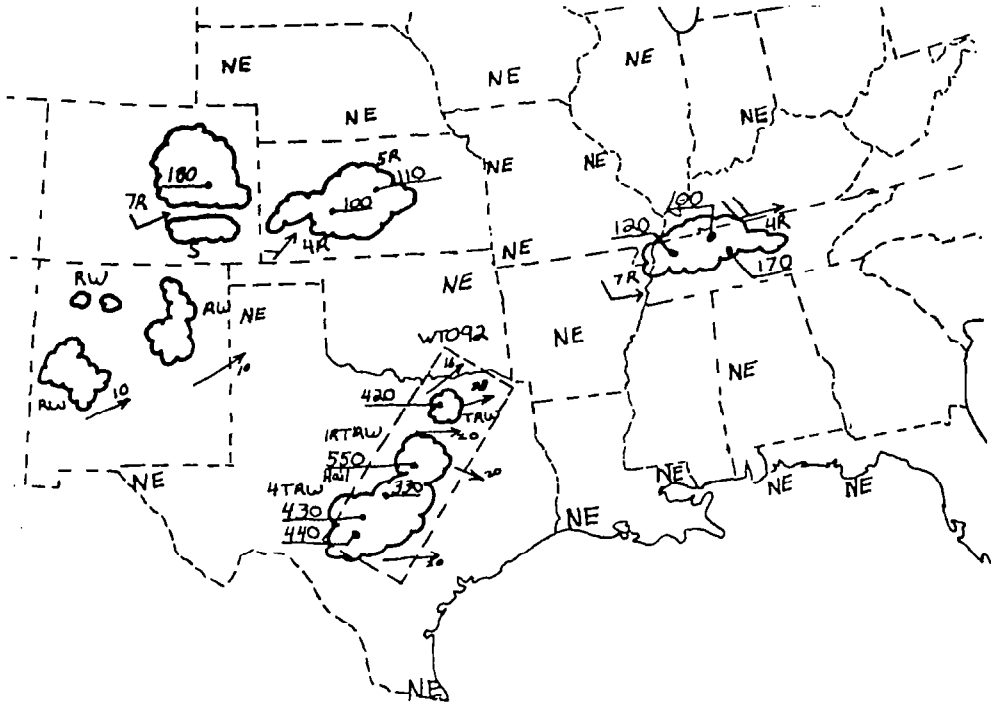

(a) 2335 GMT 1 May 1978

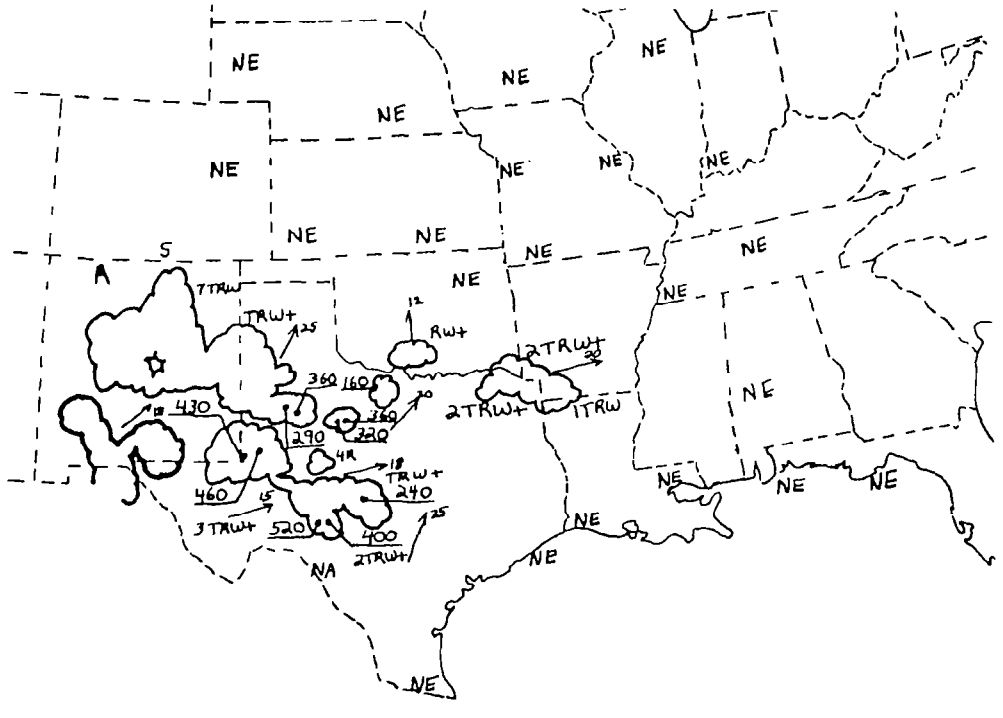

(b) 1135 GMT 2 May 1978

Fig. 9. Radar summary charts for the AVE VII period.

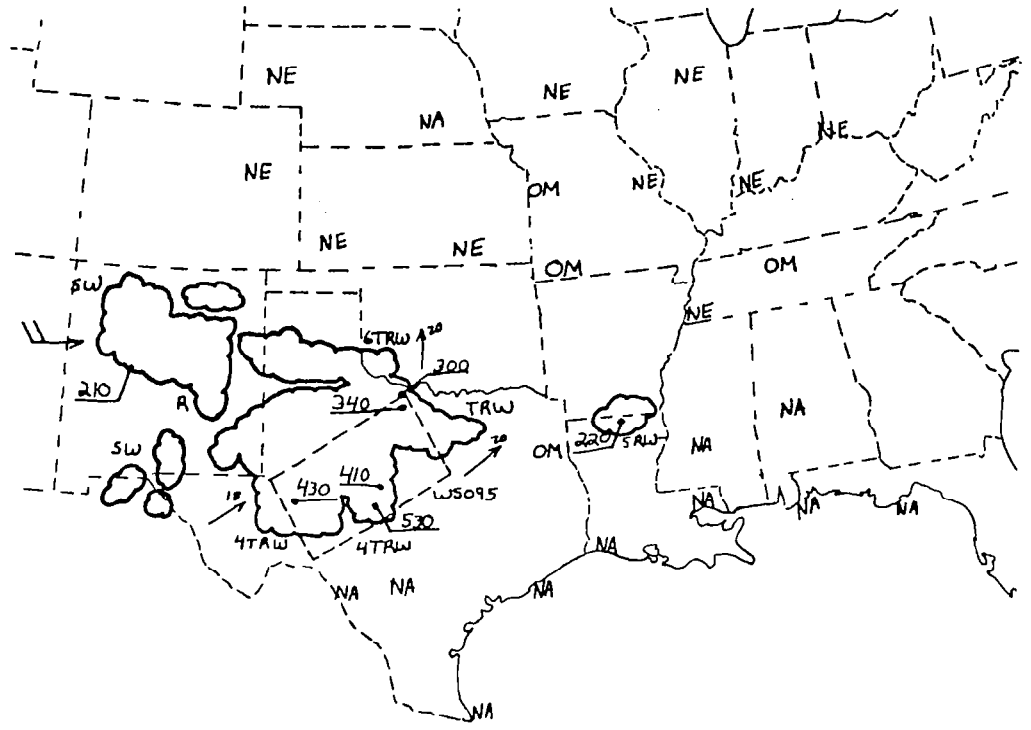

(c) 1435 GMT 2 May 1978

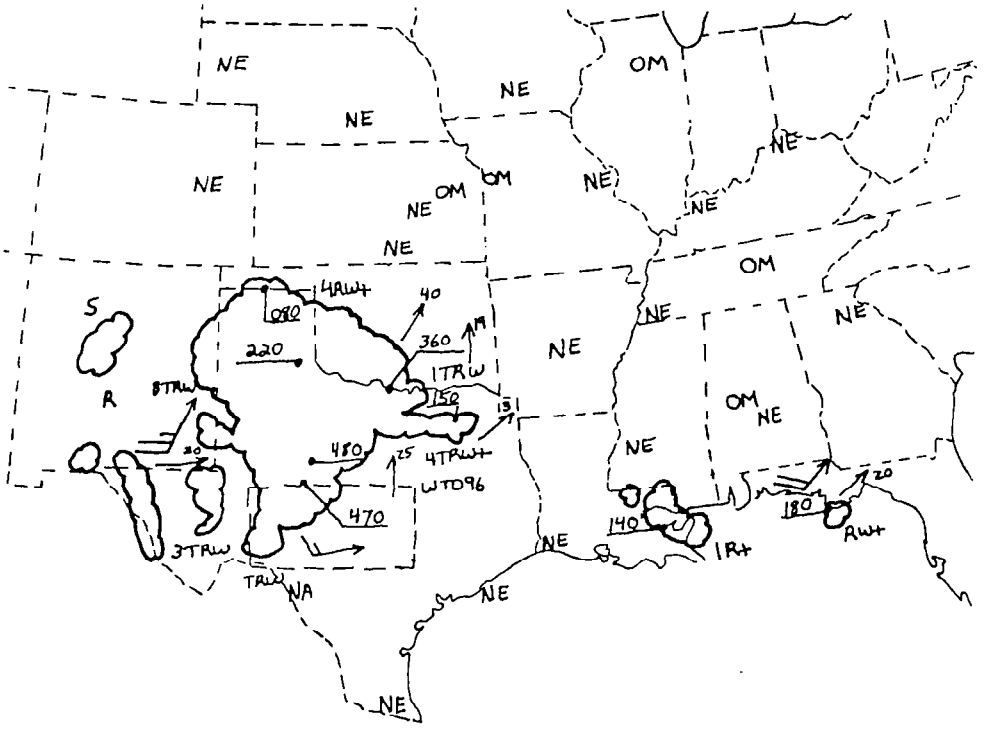

(d) 1735 GMT 2 May 1978

Fig. 9. (Continued)

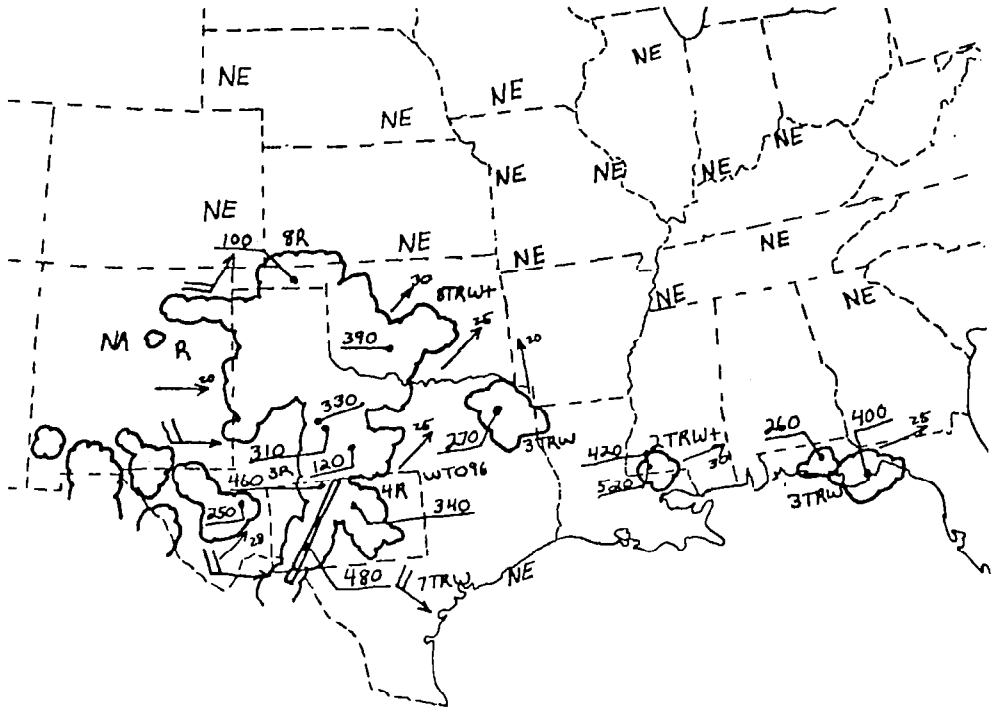

(e) 2035 GMT 2 May 1978

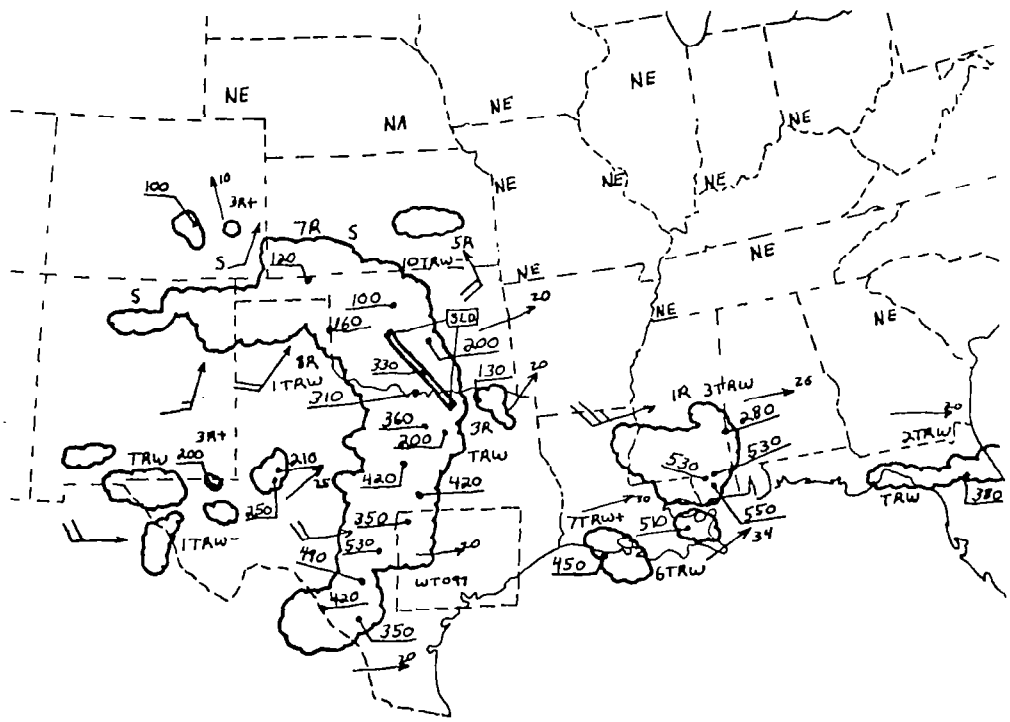

(f) 2335 GMT 2 May 1978

Fig. 9. (Continued)

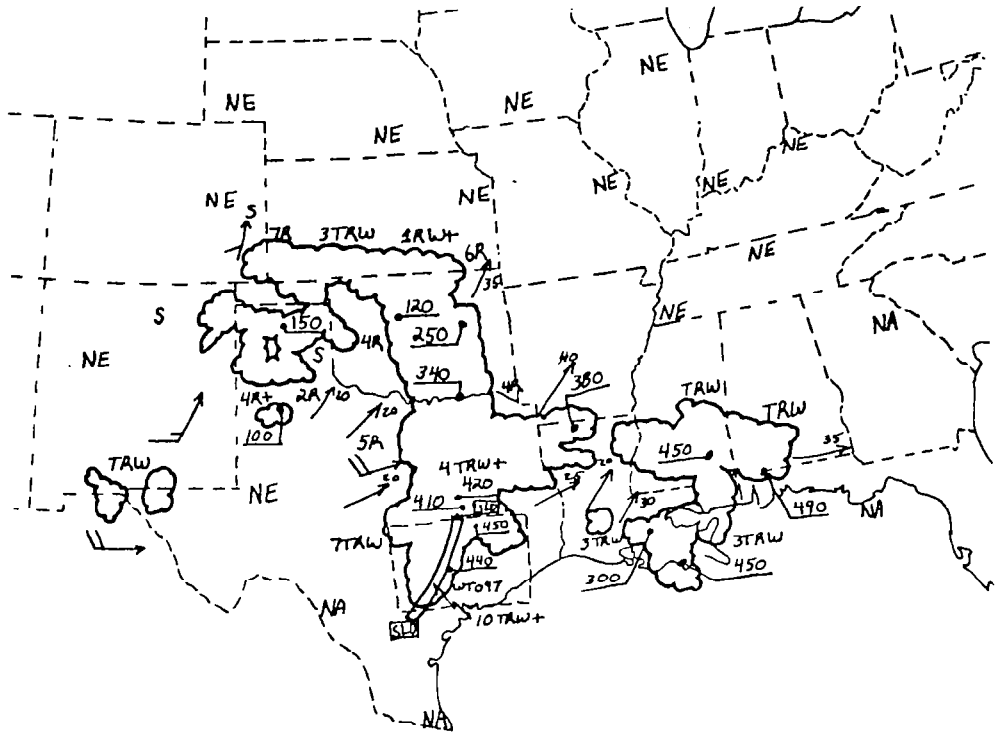

(g) 0235 GMT 3 May 1978

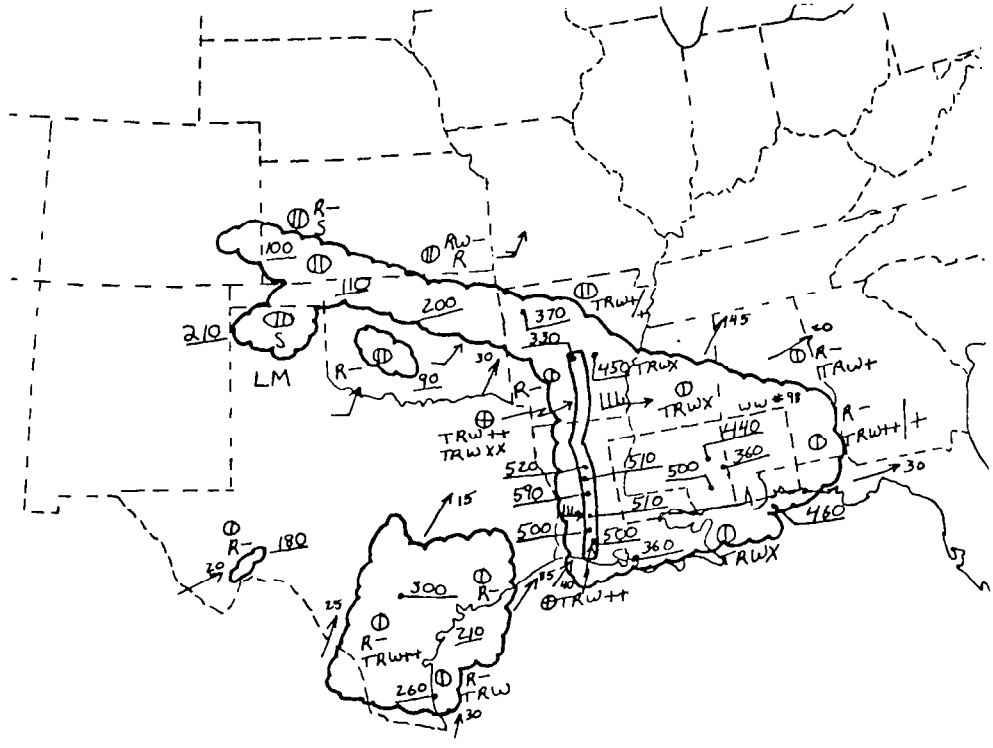

(h) 0835 GMT 3 May 1978

Fig. 9. (Continued)

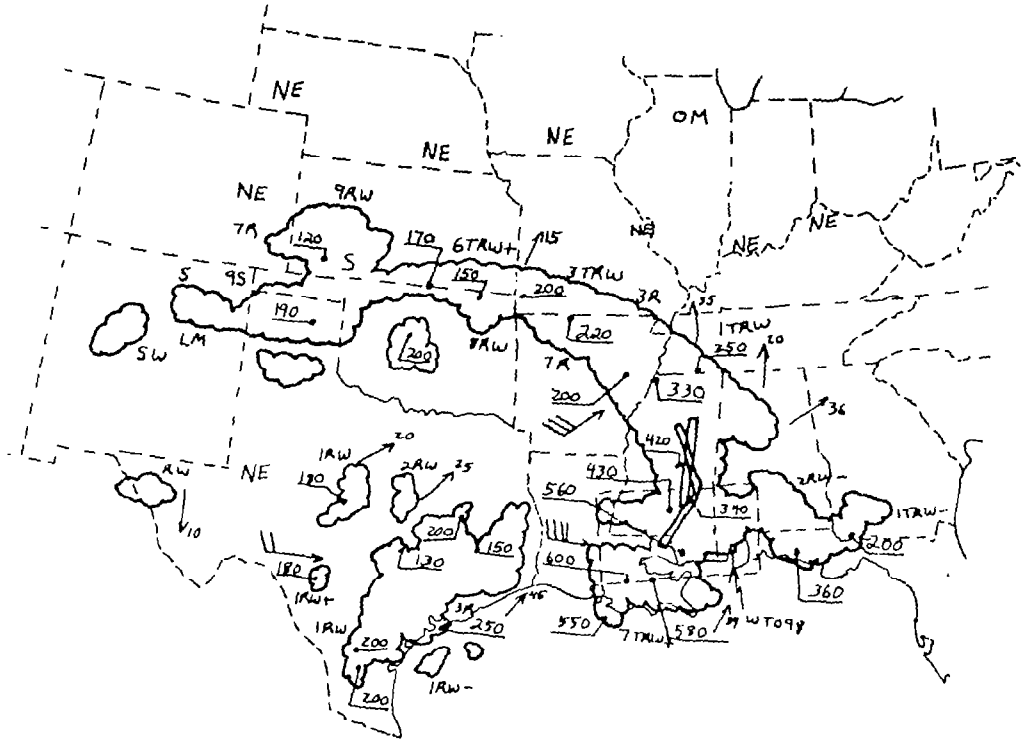

(i) 1135 GMT 3 May 1978

Fig. 9. (Continued)

(Fig. 9i), light rainshowers were occurring in southeast Texas while snow and rainshowers extended in a band from the Texas panhandle to Arkansas. Heavy thunderstorms were located along the coasts of Louisiana and Mississippi.

The surface map for the end of the experiment, 1200 GMT 3 May, (Fig. 10) indicates that the frontal system had moved into the Gulf of Mexico during the period while high pressure continued to influece the flow over the Midwest. The flow at 500 mb was dominated by a closed low centered over the Texas panhandle that had moved eastward from Arizona. This low was located further south than the upper-level lows found during AVSSE I and II and had moved eastward instead of toward the northeast.

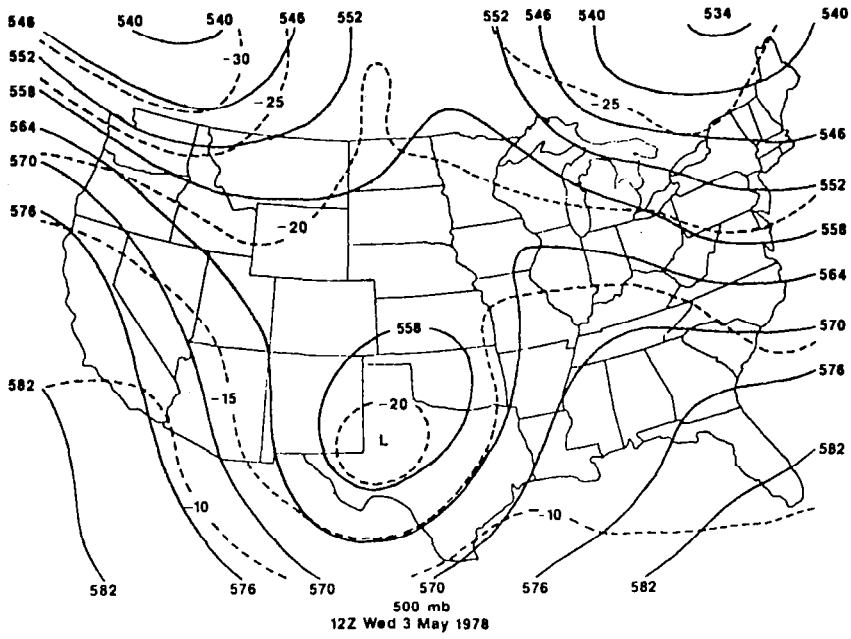

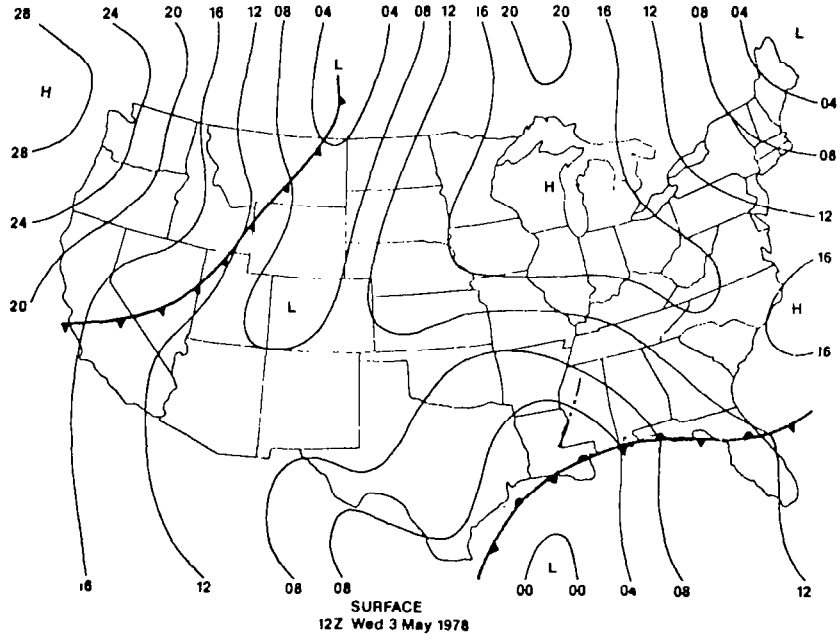

Fig. 10. Synoptic conditions at the end of the AVE VII period, 1200 GMT 3 May 1978.

5. RESULTS

a. Average kinetic energy budget for each experiment

The kinetic energy budget averaged over all time periods for each AVE area describes energetics of the large-scale flow in which the convection is imbedded. Such an average contains properties of the enclosed phenomena plus properties corresponding to interactions with the surrounding environments (Ward and Smith, 1976). Energy processes in the vicinities of individual storm areas will be examined in a later section of this report.

1) AVSSE I period

Table 2 gives the average kinetic energy budget for the combined three AVSSE I observation times. As mentioned earlier, only the budgets at the standard 12 h rawinsonde observation times could be computed because of the large amount of missing data at the times of special sonde releases. The local derivative term indicates that the atmosphere

Table 2. Average kinetic energy budget for the three standard observation times of the AVSSE I experiment.

Pressure Layer (mb)	K (10^5J m^{-2})	$\frac{\partial K}{\partial t}$ (W m^{-2})	$\vec{\nabla}\cdot k\vec{V}$ (W m^{-2})	$\frac{\partial \omega k}{\partial p}$ (W m^{-2})	$-\vec{V}\cdot\vec{\nabla}\phi$ (W m^{-2})	D (W m^{-2})
200-100	4.9	2.4	-6.2	-3.7	-9.7	2.2
300-200	5.8	2.4	-6.0	-0.5	-7.6	3.5
400-300	4.6	0.9	3.2	0.6	0.2	4.5
500-400	3.3	0.4	2.6	-0.1	3.0	-0.1
600-500	2.6	1.3	1.1	1.5	2.7	1.2
700-600	1.7	1.0	0.8	1.2	1.7	1.3
800-700	1.2	-0.4	0.3	0.5	-0.6	1.0
900-800	1.1	-0.7	0.5	0.3	0.2	-0.1
sfc-900	0.4	-0.2	-0.1	0.2	1.5	-1.6
Vertical total	25.6	7.1	-3.8	0.0	-8.6	11.9

below 700 mb experiences a decrease in kinetic energy content during the AVSSE I period, but increases in kinetic energy occur at higher levels, especially near the level of the jet stream. Horizontal flux divergence ($\vec{\nabla}\cdot k\vec{V}>0$) of energy tends to decrease kinetic energy content below 300 mb while horizontal flux convergence ($\vec{\nabla}\cdot k\vec{V}<0$) occurs above 300 mb and serves as an external source of energy to the region. The vertical flux divergence term is generally positive below 300 mb and negative above that level. It indicates the transport of kinetic energy aloft by the widespread upward vertical motion occurring over the area in association with the cyclone activity and convection. Notice that the two boundary terms are important sources of energy in the upper portions of the atmosphere.

Generation of kinetic energy by cross-contour flow is an important source of energy below 300 mb but is the dominant sink of energy at higher levels. Dissipation of energy from grid to subgrid scales of motion (negative dissipation) occurs near the surface due to frictional effects, but kinetic energy is transferred from smaller to larger scales of motion (positive dissipation) above 800 mb.

Considering the entire layer from the surface to 100 mb, it is clear that energy processes occurring near the level of the jet stream dominate the vertical totals of the various budget terms. Local increases in kinetic energy content are due primarily to positive dissipation and horizontal flux convergence. Destruction of kinetic energy at the level of the jet stream by cross-contour flow is the major sink of energy for the total vertical column.

2) AVSSE II period

The average kinetic energy budget of the AVSSE II period (Table 3) shows many similarities with that of the

Table 3. Average kinetic energy budget for the entire AVSSE II period. All seven observation times are included.

Pressure Layer (mb)	K (10^5J m^{-2})	$\frac{\partial K}{\partial t}$ (W m^{-2})	$\vec{V}\cdot k\vec{V}$ (W m^{-2})	$\frac{\partial \omega k}{\partial p}$ (W m^{-2})	$-\vec{V}\cdot\vec{\nabla}\phi$ (W m^{-2})	D (W m^{-2})
200-100	6.0	0.8	-0.8	-2.6	-8.3	5.7
300-200	6.9	1.6	-12.1	1.2	-15.4	6.1
400-300	4.7	1.2	-7.9	1.8	-12.0	7.1
500-400	2.9	0.5	-2.1	0.1	-4.1	2.6
600-500	2.3	0.2	1.5	-0.4	-0.9	2.2
700-600	1.3	0.0	0.5	0.0	-0.1	0.6
800-700	0.7	-0.3	0.2	-0.2	-0.3	0.0
900-800	0.5	-0.2	0.1	0.0	-0.3	0.2
sfc-900	0.2	-0.1	-0.1	0.1	0.1	-0.2
Vertical total	25.5	3.7	-20.7	0.0	-41.3	24.3

AVSSE I period (Table 2). These similarities are expected since synoptic conditions of the two periods also exhibit common features. The vertical totals indicate that local increases in kinetic energy content are again due to positive dissipation and horizontal flux convergence of energy but that destruction of kinetic energy by cross-contour flow nearly cancels out the effects of the source terms. Although the vertical totals of kinetic energy content are roughly the same for both experiments, 25.5×10^5 J m^{-2}, the vertical totals of the various source and sink terms are considerably larger during AVSSE II than in the earlier case due to differing vertical distributions of the various energy processes and due to differing magnitudes of terms in individual layers.

Table 3 shows that the vertical profile of term $\partial K/\partial t$ during AVSSE II is similar to that of AVSSE I (Table 2).

Low-level horizontal flux divergence and upper-level horizontal flux convergence occur during both periods, but during AVSSE II the upper-level convergence is stronger and deeper in vertical extent. The profile of the vertical flux divergence term shows a less well defined structure during AVSSE II than AVSSE I. Except for the surface to 900 mb layer, destruction of kinetic energy by cross-contour flow occurs at all levels during AVSSE II. Values of this term in individual layers are more negative than during AVSSE I. Positive dissipation of kinetic energy is found at all levels except near the ground.

Ward and Smith (1976) have studied the energetics of a period when short synoptic waves with wavelengths of approximately 2000 km were dominant over North America. Although their study encompassed a larger area and a longer time period than the present study, the upper-level flow conditions and energetic properties of their study period (Table 4) show many similarities to those of AVSSE I and II (Tables 2-3). Looking at the vertical totals, these similarities include local increases in kinetic energy content,

Table 4. Kinetic energy budget for North America, 13-18 April 1970, during a period of short synoptic wave development (Ward and Smith, 1976).

Pressure Layer (mb)	K (10^5 J m^{-2})	$\frac{\partial K}{\partial t}$ (W m^{-2})	$\vec{\nabla}\cdot k\vec{V}$ (W m^{-2})	$\frac{\partial \omega k}{\partial p}$ (W m^{-2})	$-\vec{V}\cdot\vec{\nabla}\phi$ (W m^{-2})	D (W m^{-2})
200-100	4.3	0.4	-1.9	-0.3	-3.7	1.9
400-200	10.6	0.8	-5.5	-0.1	-5.0	0.2
600-400	3.9	0.1	-2.0	0.2	-0.4	-1.3
800-600	1.5	0.0	-0.1	0.1	0.6	-0.6
sfc-800	0.6	0.0	-0.1	0.1	1.3	-1.3
Vertical total	20.9	1.3	-9.6	0.0	-7.2	-1.1

horizontal flux convergence of energy, and destruction of kinetic energy by cross-contour flow. Small negative dissipation is indicated in the vertical total of Ward and Smith, but their findings of low-level negative dissipation and upper-level positive dissipation are similar to the present results.

During both AVSSE I and II as well as the period studied by Ward and Smith (1976), there is a tendency for horizontal flux convergence to be accompanied by negative generation. During AVSSE I and II, the flux convergence is due mostly to jet intrusion from the southwest. The explanation offered by Ward and Smith for their values of negative generation seems applicable to the present studies. An important point is that the strong horizontal flux convergence of kinetic energy does not produce an appreciable increase in the contour gradients; only small increases in wind speed are noted. Therefore, the strong winds being transported into the region can produce winds exceeding gradient values such that cross-contour flow from lower to higher heights results in destruction of kinetic energy. According to this hypothesis, systems undergoing increases in contour gradients together with horizontal flux convergence would not be expected to produce negative generation.

In considering possible explanations for positive dissipation, it should first be remembered that this term is computed as a residual and therefore contains errors due to the other terms of the budget equation. Previous error studies have shown, however, that random errors alone do not explain positive dissipation (Vincent and Chang, 1975; Ward and Smith, 1976). Positive dissipation has been associated with convective activity (Ward and Smith, 1976; Chien and Smith, 1977; Fuelberg and Scoggins, 1978), the damping of upstream turbulence (Ward and Smith, 1976), and interaction with very long waves (Kung and Baker, 1975). During AVSSE I

and II, the effects of convection and turbulence may produce positive dissipation but other types of scale interactions may also be significant factors.

3) AVE VII period

The kinetic energy budget averaged over the complete AVE VII period (Table 5) is quite different from the budgets of the AVSSE I and II periods just described. Horizontal flux divergence and transfer of energy to subgrid scales of motion are the sinks of energy in the total vertical column while generation of kinetic energy by cross-contour flow is the major source of kinetic energy. In the vertical total these three processes are opposite those found in AVSSE I and II. Close to the surface, much of the kinetic energy that is generated by cross-contour flow is lost to dissipative effects, but in higher levels, horizontal export of energy out of the volume is the major energy sink, with dissipation being a much smaller factor. Upward vertical motion transports kinetic energy from lower to higher levels of the atmosphere.

Table 5. Average kinetic energy budget for the entire AVE VII period. All eight observation times are included.

Pressure Layer (mb)	K (10^5J m^{-2})	$\frac{\partial K}{\partial t}$ (W m^{-2})	$\vec{\nabla}\cdot k\vec{V}$ (W m^{-2})	$\frac{\partial \omega k}{\partial p}$ (W m^{-2})	$-\vec{V}\cdot\vec{\nabla}\phi$ (W m^{-2})	D (W m^{-2})
200-100	5.4	-0.3	10.7	-2.5	10.0	-2.1
300-200	6.5	-2.5	12.1	-1.5	10.7	-2.6
400-300	3.4	-1.2	3.8	0.3	4.1	-1.2
500-400	2.0	-0.3	1.6	0.5	2.2	-0.4
600-500	1.3	0.2	0.9	1.0	0.6	1.5
700-600	0.8	0.1	0.2	1.2	0.3	1.2
800-700	0.4	0.2	-0.2	0.6	0.4	0.2
900-800	0.4	0.5	-0.1	0.3	1.8	-1.1
sfc-900	0.3	0.2	0.0	0.1	3.1	-2.8
Vertical total	20.5	-3.1	29.0	0.0	33.2	-7.3

The differences in the energy budgets between AVE VII and the AVSSE I-II periods are related to differences in the synoptic situations. Differences in the horizontal flux divergence term can be explained by an inspection of the weather maps. During the AVSSE periods, jet intrusion along the western boundaries of the region occurs and causes flux convergence of energy over the area. During the AVE VII period, however, the strongest winds are located along the eastern boundary of the region leading to flux divergence of energy.

Supergradient winds causing cross-contour flow toward higher values of height yield destruction of kinetic energy in many portions of AVSSE I and II. However, during AVE VII, flow toward lower height values is responsible for generation of kinetic energy. These differing flow patterns are recognizable on carefully analyzed synoptic maps.

Positive dissipation is prevalent during AVSSE I and II, but negative dissipation occurs during AVE VII. There is no ready explanation for this occurrence. One curious fact is that positive dissipation in the free atmosphere often occurs in conjunction with destruction of kinetic energy by cross-contour flow, while negative dissipation seems to occur with positive generation of kinetic energy. This is seen in the present studies (Tables 2, 3, 5) and those by Ward and Smith (1976) (Table 4), Kung and Baker (1975), Chen and Bosart (1977), and Vincent and Chang (1975). Further research will be required to explain the mechanisms which lead to positive dissipation. The importance of the dissipation term to the kinetic energy budget is indicative of the importance of scale interactions in the atmosphere. Small scale motions, that are not directly measured, are having a major effect on synoptic-scale motions.

The preceeding discussion has indicated the general energy processes that occurred during each AVE experiment. Armed with this information, we will describe the temporal

variations in energy that occur over the entire AVE area and over more limited areas surrounding the severe storms.

4) Time series analyses

Because routine rawinsonde soundings are made at 12 h intervals, little is known about kinetic energy processes with periods smaller than 24 h. Kung (1967), who studied the kinetic energy budget for North America over a 5-yr period, noted that cross-contour generation of kinetic energy was larger at 0000 GMT (late afternoon) than at 1200 GMT (early morning). Dissipation of energy from larger to smaller scales of motion also was greater at 0000 GMT than 1200 GMT, but other terms of the kinetic energy budget did not show significant diurnal variations. Depending on the nature and intensity of the synoptic and smaller scale weather phenomena occuring during the AVE periods, temporal variations of the AVE-derived budgets might exhibit either similar or dissimilar fluctuations from the long term averages computed by Kung.

Figure 11 shows a time series of kinetic energy budget terms integrated from the surface to 100 mb over the entire AVSSE II area during the seven observations of the experiment. The vertical flux term is not plotted since its value is zero for the total column. The figure indicates that large variations in generation, dissipation, and horizontal flux divergence occur during the period but that the various energy generation and transport processes tend to cancel each other such that local changes in kinetic energy content are quite small.

Destruction of kinetic energy by cross-contour flow occurs at all observation times but is smaller in magnitude (more nearly generation) at 0000 GMT than at other times. Positive dissipation occurs at most times of AVSSE II except

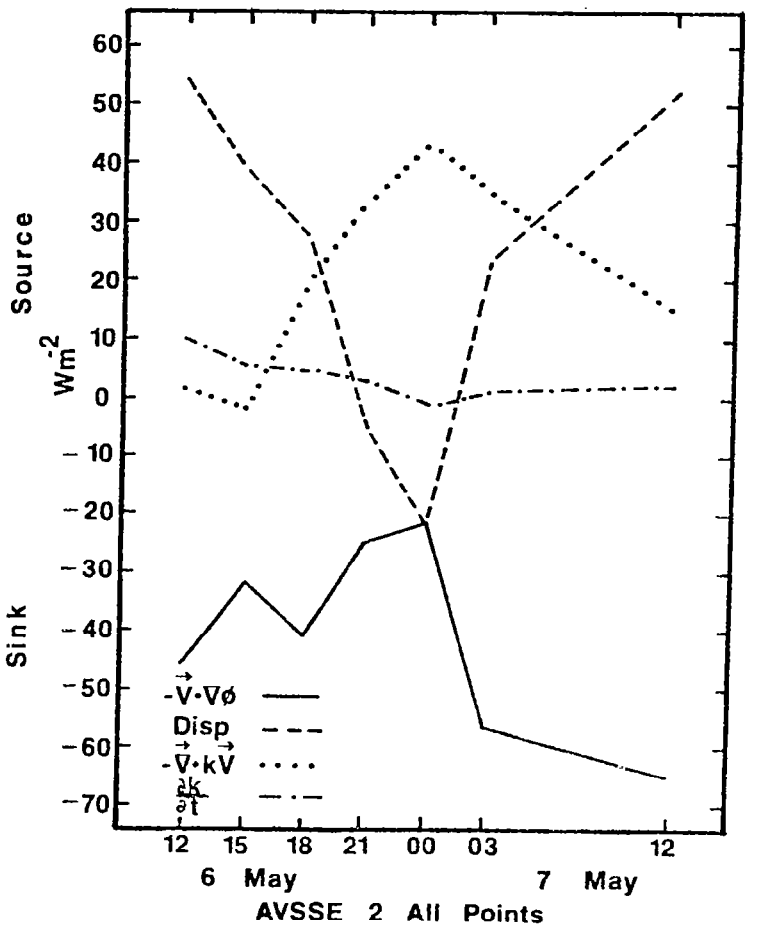

Fig. 11. Time series of kinetic energy budget terms integrated from the surface to 100 mb for the entire AVSSE II area.

in the late afternoon near 0000 GMT. Flux convergence, an external source to the limited volume, also reaches a maximum value near 0000 GMT. During AVSSE II, times of maximum flux convergence do not correspond to the times of maximum destruction of energy by cross-contour flow. While the relationship cited earlier between flux convergence and kinetic energy destruction given by Ward and Smith (1976) seems useful for describing the major features of the AVSSE II energy budget, it does not explain the short term fluctuations in generation seen in Fig. 11.

Values of the energy budget terms at the end of the experiment are not greatly different from those at the beginning, which is consistent with the fact that surface and

upper-level flow patterns also changed little during this 24 h period (Figs. 5, 7). Therefore, the variations seen in Fig. 11 apparently are not due solely to major changes in the synoptic situation. Kung (1967) suggests that organized large-scale variations in winds coupled with diurnal wind variations of a more local scale may produce diurnal variations in the generation term. During AVSSE II, the intense convection occurring within the area may contribute to the observed variations through interactions with coexisting larger and smaller scales of motion. More of the AVSSE II area experienced convection during the afternoon than at other times (Fig. 6). One should note that the profiles of Fig. 11 show relatively smooth time variations. This absence of rapid fluctuations lends credibility to the results.

Time series of energy budget values integrated from the surface to 100 mb for the eight observation times over the entire AVE VII area are shown in Fig. 12. One should recall that in addition to the widespread convection occurring along the southern portions of the regions, an upper-level low moved into the region from the west during the period (Figs. 8-10).

The local time derivative term of Fig. 12 indicates that kinetic energy content varies more during the AVE VII period than during AVSSE II (Fig. 11), but magnitudes of this term are still smaller than those of the other budget terms that are depicted. Generation of kinetic energy by cross-contour flow, which is the major source of energy to the limited region, is largest during the afternoon hours and is smallest at 1200 GMT of both days. Positive dissipation, meaning a transfer of energy from smaller to larger scales of motion, is a maximum in the early morning of both days while a trend toward negative dissipation, a transfer to comparitively smaller scales of motion, occurs between 1200 GMT and 0300 GMT. These findings are similar to those of Kung (1967) although

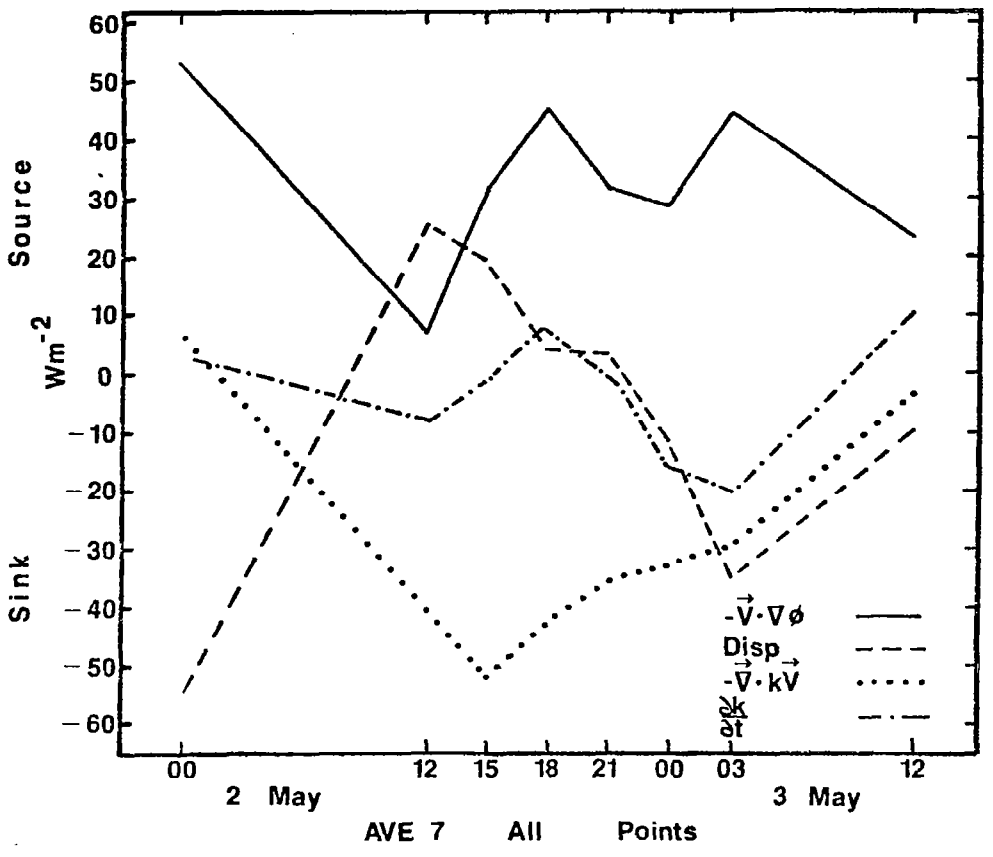

Fig. 12. Time series of kinetic energy budget terms integrated from the surface to 100 mb for the entire AVE VII area.

Kung had only 12 h data. Horizontal flux divergence is a major sink of energy for the area and is greatest near 1500 GMT.

The short term fluctuations seen in the kinetic energy budget terms depicted in Fig. 12 are at least partially related to changes in the synoptic-scale weather patterns, but a careful inspection of the synoptic-scale weather maps does not reveal obvious reasons for most of the variations. Complex interactions between the synoptic-scale features and subgrid scale features including convection also are causes for the variations, but much more additional research will have to be conducted before the nature of these interactions is understood. The smoothly varying nature of the profiles again suggests that data errors or deficiencies in computational

procedures are not major factors in explaining the variability.

b. Energy budgets of individual areas of convection

The synoptic-scale kinetic energy budgets of the environments of two areas of intense convection are described in this section. To isolate the energy processes occurring near the convection from those over the remainder of the experiment area, kinetic energy budgets were computed over small volumes that just enclosed the convection. The horizontal area of these volumes averaged 3.0×10^{11} m^2. The volumes moved as the areas of convection moved so that synoptic-scale energy processes could be related to the life cycle of the convection. The procedure is similar to that used by Fuelberg and Scoggins (1978). The energy budget for each limited volume was computed as the average of grid point values on or within the selected boundaries of the volume. Again, it should be emphasized that the budgets for the limited volumes describe the energetics of the synoptic-scale flow enclosing the intense convection and do not apply to individual mesoscale elements.

Our goal was to describe the energetics of well defined storm areas that formed within the AVE experiment areas during the period of the 3 h rawinsonde observations and remained within the experiment regions for significant portions of their lifetimes. In spite of the widespread convective activity that took place during the three AVE experiment periods that were studied, few areas of storms met the above mentioned criteria.

1) Texas convection area

The energetics of an area of intense storms that occurred in central Texas during the AVSSE II period will be described first. Recall that this area began as scattered rainshowers

near 1400 GMT 6 May 1975, reached peak intensity near 2100 GMT when radar tops reached 18.6 km, and dissipated by 0100 GMT 7 May (Fig. 6). The storm area moved toward the east at about 5 m s^{-1} during its existence. Table 6 gives the budget for this storm area at 2100 GMT when it was near peak intensity. Very large generation of kinetic energy by cross-contour flow occurs with maximum values found near the level of the jet stream. The vertical total of 85.3 W m^{-2} is somewhat larger than the values of 52.2 W m^{-2} and 47.6 W m^{-2} reported by Fuelberg and Scoggins (1978) for the synoptic-scale environments of two squall lines near peak intensity. Kung and Tsui (1975) reported values ranging from 21.3 to 109.9 W m^{-2} during five cases of active convection within the NSSL area. The values reported by Kung and Tsui are averages based on several observation times and do not simply represent the time of peak storm intensity.

Table 6. Average kinetic energy budget for the limited area enclosing the convection in central Texas during AVSSE II at 2100 GMT 6 May 1975.

Pressure Layer (mb)	K (10^5J m^{-2})	$\frac{\partial K}{\partial t}$ (W m^{-2})	$\vec{\nabla}\cdot k\vec{V}$ (W m^{-2})	$\frac{\partial \omega k}{\partial p}$ (W m^{-2})	$-\vec{V}\cdot\vec{\nabla}\phi$ (W m^{-2})	D (W m^{-2})
200-100	8.6	2.8	10.4	-12.7	17.1	-16.6
300-200	9.3	-0.9	3.9	-4.1	21.5	-22.6
400-300	6.3	0.6	-8.4	6.4	13.8	-15.2
500-400	3.5	3.4	4.0	2.3	15.2	-5.5
600-500	2.1	3.0	5.5	2.7	11.5	-0.3
700-600	0.9	2.2	0.5	3.4	5.2	0.9
800-700	0.3	-0.1	-0.9	1.8	1.4	-0.6
900-800	0.1	-0.5	-0.2	0.2	-0.3	-0.2
sfc-800	0.1	-0.2	-0.1	0.0	-0.1	-0.2
Vertical total	31.2	10.3	14.7	0.0	85.3	-60.3

Although large generation of kinetic energy occurs near the severe storms, kinetic energy content shows only a small increase because dissipation of energy and horizontal flux divergence are important sinks. Transfer of energy to subgrid scales of motion occurs throughout most of the vertical column with maximum values found near the level of the jet stream. Weak horizontal flux convergence of energy occurs in the lower troposphere, but this is counteracted by strong horizontal flux divergence in higher levels to yield net flux divergence for the total column. The thin layer between 400-300 mb exhibits the curious phenomena of strong flux convergence although it is bounded on the top and bottom by layers of weaker flux divergence. Since upward motion occurs over the area on the synoptic scale, the vertical flux term indicates that kinetic energy in the lower troposphere where $\partial\omega K/\partial p > 0$ is transported upward to higher levels where $\partial\omega k/\partial p < 0$.

The energy generation and transport processes associated with the Texas area of storms during AVSSE II (Table 6) are generally similar to those observed by Fuelberg and Scoggins (1978). Although the nature of the processes is similar, the energy balance differs somewhat between the two studies. For the Texas area now being described, dissipation is the greatest sink of the generated energy, but in the squall line cases described by Fuelberg and Scoggins, horizontal flux divergence was the major sink. Tsui and Kung (1977) and Kung and Tsui (1975), on the other hand, found that slightly more kinetic energy was dissipated in the mesoscale storm environments than was generated by cross-contour flow. Horizontal flux convergence in the lower half of the atmosphere provided a source of energy to the NSSL Storm region.

By comparing the vertical totals of Table 6 with those of Table 3, it is clear that the energy processes near the Texas area of storms at peak intensity differ greatly from

those of the AVSSE II region as a whole. The near storm environment is characterized by generation of kinetic energy by cross-contour flow while the area as a whole experiences energy destruction. Negative dissipation is found near the Texas storms while positive dissipation occurs for the area as a whole. Finally, the storm area experiences net horizontal flux divergence of kinetic energy within the total vertical column while the area as a whole has horizontal flux convergence.

The storm area located in central Texas underwent a well developed life cycle of development, maturity, and dissipation. Pressure-time cross sections of the various kinetic energy budget terms indicate cyclic changes in the kinetic energy budget that seem related to the life cycle of the storm area. A pressure-time cross section of synoptic-scale vertical motion averaged over the Texas storm area is shown in Fig. 13. Weak upward vertical motion occurs prior to peak storm intensity, but the strongest upward motion (greater than 4 $\mu b\ s^{-1}$) occurs near 2100 GMT when the storms are strongest. After the storms dissipate, downward vertical motion is observed. These results are similar to those observed by Fuelberg and Scoggins (1978). Aubert (1957), Danard (1964), and Ninomiya (1971a and b) have suggested that diabatic heating associated with convection probably is responsible for inducing systematic changes in vertical motions such as those observed in this case study.

The life cycle of the convection is suggested in fluctuations of the generation term, $-\vec{V}\cdot\nabla\phi$ (Fig. 14). Destruction of kinetic energy by cross-contour flow in the middle and upper troposphere at 1200 GMT and 1500 GMT changes to generation of kinetic energy by 2100 GMT, when the storms are most intense, and then reverts back to destruction. In agreement with the present results, Fuelberg and Scoggins (1978) observed

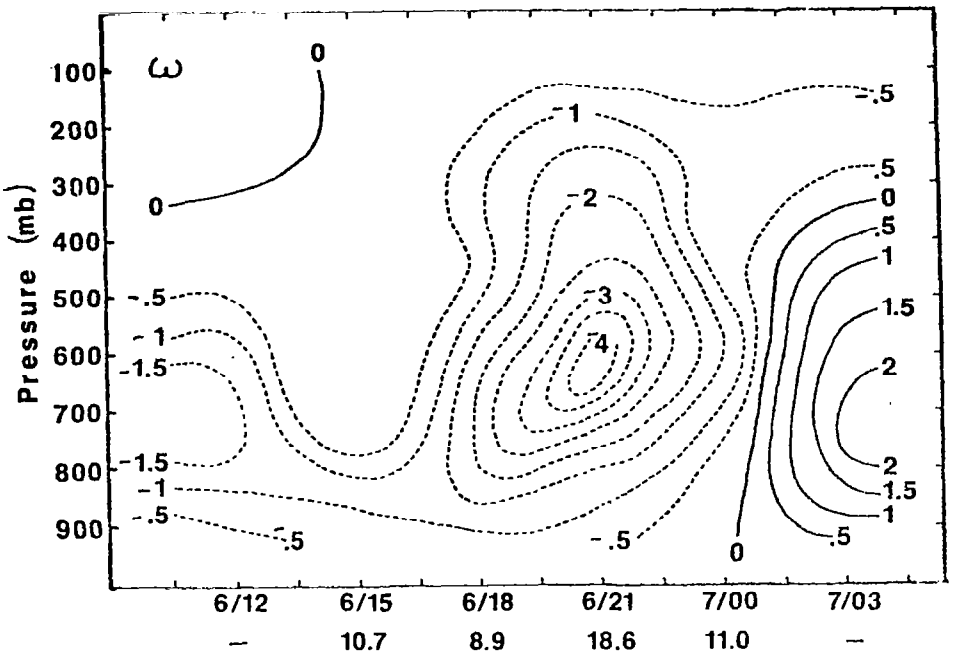

Fig. 13. Pressure-time cross section of vertical motion (ω) in ub s^{-1} for the Texas convection area during AVSSE II. Maximum radar tops (km) are given on the lower horizontal axis.

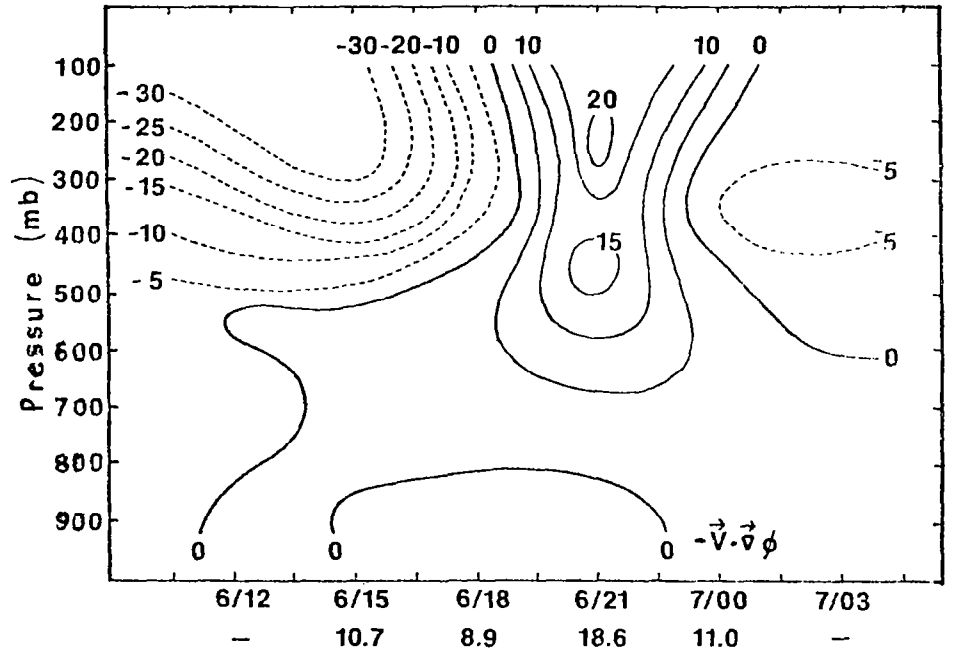

Fig. 14. Pressure-time cross section of generation of kinetic energy ($-\vec{V}\cdot\vec{\nabla}\phi$) for the Texas convection area during AVSSE II in W m^{-2}/100 mb. Maximum radar tops (km) are given on the lower horizontal axis.

enhanced generation of kinetic energy near peak storm intensity; however Tsui and Kung (1977) observed peak generation before and after peak intensity with destruction of kinetic energy occurring near the time of the most violent storm activity. The fact that Kung and Tsui used mesoscale NSSL rawinsonde data may explain the differences in results; they suggest that generation of kinetic energy may surround intense storm areas while destruction occurs within the storm area. This aspect will be investigated when the subsynoptic scale SESAME data become available. As described by Fuelberg and Scoggins (1978), storm induced changes in the geopotential height field coupled with variations in the wind field may explain the changes in the generation term that are observed. Changes in the synoptic-scale weather patterns that are not related to the convection also are contributing factors.

Prior to peak storm intensity, transfer of kinetic energy from subgrid to grid scale motions (positive dissipation) dominates the Texas area of storms (Fig. 15). Maximum values are found near the level of the jet stream. Near peak storm intensity, 2100 GMT, the process reverses so that negative dissipation dominates the upper levels. Negative values decrease after 0000 GMT 7 May. Closer to the surface, an area of positive dissipation occurs between 700-500 mb between 2100 GMT 6 May and 0300 GMT 7 May. Enhanced subgrid scale motions associated with the storms may lead to increased negative dissipation, but the exact mechanism for this is not understood. Results of the squall line cases studied by Fuelberg and Scoggins generally are similar to those of the Texas area; however Tsui and Kung (1977) report enhanced positive dissipation in association with maximum storm intensity.

The pressure-time cross section of the horizontal flux divergence term for the Texas area indicates that rapid changes

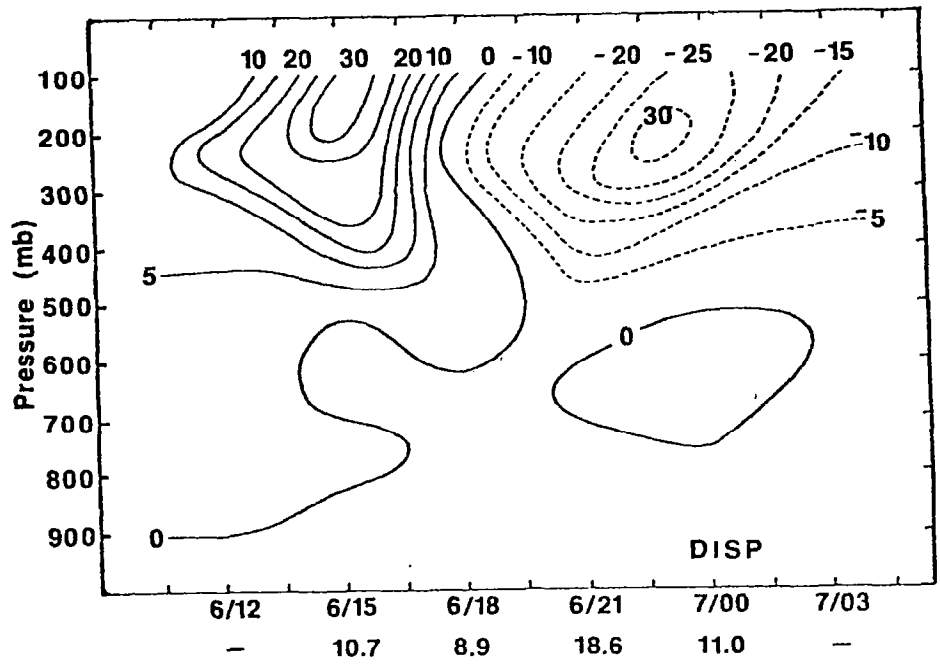

Fig. 15. Pressure-time cross section of dissipation of kinetic energy for the Texas convection area during AVSSE II in W m^{-2}/100 mb. Maximum radar tops (km) are given on the lower horizontal axis.

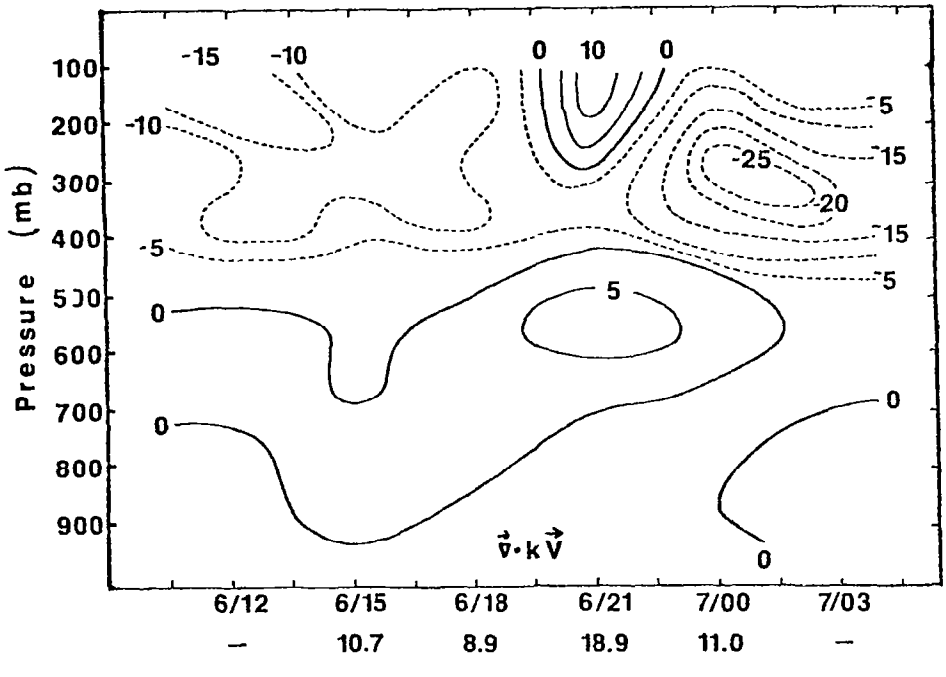

Fig. 16. Pressure-time cross section of the horizontal flux divergence of kinetic energy ($\vec{\nabla}\cdot k\vec{V}$) for the Texas convection area during AVSSE II in W m^{-2}/100 mb. Maximum radar tops (km) are given on the lower horizontal axis.

occur for this term (Fig. 16). The layer of weak low-level flux convergence is deeper at peak storm intensity than at other times and is due to increased low-level velocity convergence. Horizontal flux convergence of kinetic energy occurs above 500 mb before and after peak intensity, but flux divergence dominates the higher levels near 2100 GMT. Variations in velocity divergence are a factor in explaining fluctuations in the term $\vec{\nabla}\cdot k\vec{V}$. Synoptic-scale velocity divergence in the middle and upper troposphere is greatly enhanced near peak storm intensity and leads to positive values of $\vec{\nabla}\cdot k\vec{V}$ (flux divergence). Advection of kinetic energy also affects the sign of $\vec{\nabla}\cdot k\vec{V}$. Both before and after 2100 GMT, strongest winds at the jet stream level are located southwest of the storm area resulting in positive values of $-\vec{V}\cdot\vec{\nabla}k$ that contribute to negative values of $\vec{\nabla}\cdot k\vec{V}$. At 2100 GMT, however, a wind maximum was located over north central Texas, near the location of the storms. Over the western portions of the storm area, values of $-\vec{V}\cdot\vec{\nabla}k$ become negative and contribute to positive values of horizontal flux divergence that are observed at 2100 GMT.

Variations in vertical flux divergence also are related to the life cycle of the storms (Fig. 17). At 2100 GMT, the time of peak storm intensity, vertical flux divergence ($\partial\omega k/\partial p>0$) occurs below 300 mb while vertical flux convergence is indicated at higher levels. Since synoptic-scale vertical motion over the area is upward (Fig. 13), kinetic energy is being transported from the lower levels into levels nearer the jet stream. Weaker values of the vertical flux term occur before and after maximum storm intensity. The observed variations in the vertical flux term are due mostly to the variability of the vertical motion, and to a much lesser extent to changes in kinetic energy content.

The net effects of the various generation and transport processes on kinetic energy content is rather small (Fig. 18) because the sources and sinks tend to cancel each other. One

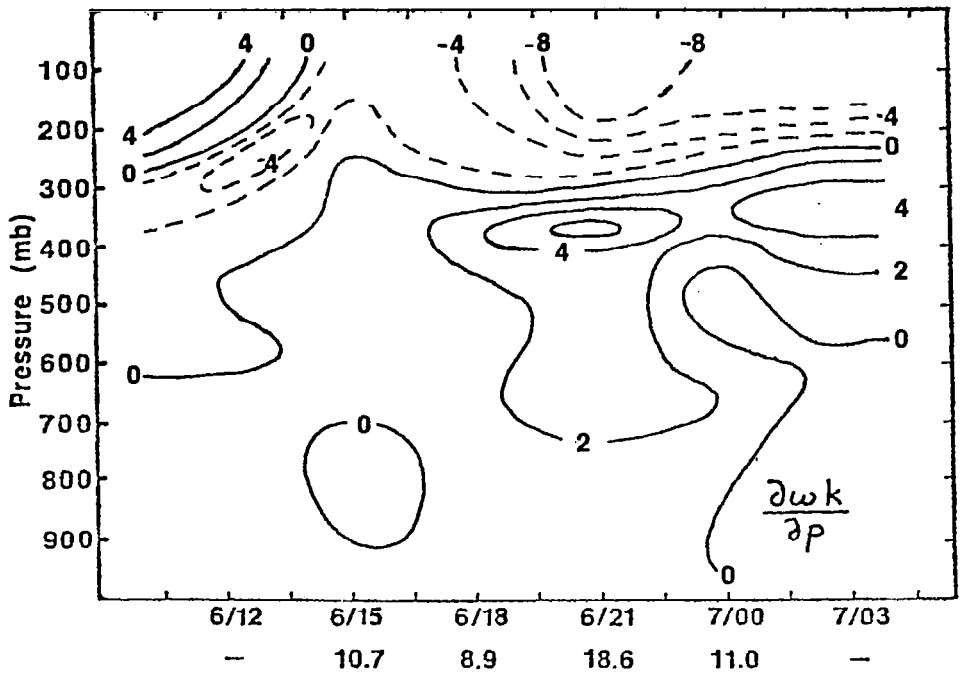

Fig. 17. Pressure-time cross section of the vertical flux divergence of kinetic energy ($\partial \omega k/\partial p$) for the Texas convection area during AVSSE II in W $m^{-2}/100$ mb. Maximum radar tops (km) are given on the lower horizontal axis.

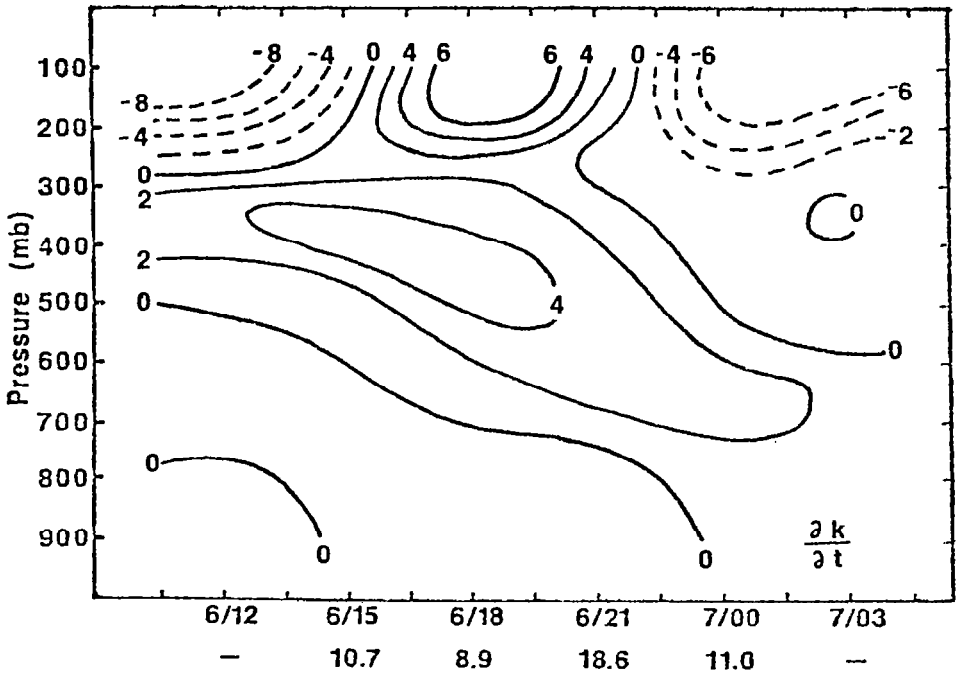

Fig. 18. Pressure-time cross section of the local change of kinetic energy ($\partial K/\partial t$) for the Texas convection area during AVSSE II in W $m^{-2}/100$ mb. Maximum radar tops (km) are given on the lower horizontal axis.

should recall that this term is not a total derivative but is computed as the average local change in kinetic energy for given areas.

2) Gulf Coast convection area

During AVE VII an area of intense storms formed along the coasts of Louisiana and Mississippi that was well suited for the limited volume type of energy study. The area began as light rain near New Orleans at about 1700 GMT 2 May 1978, attained radar tops of 15.8 km (52,000 ft) by 2035 GMT, and continued to expand in areal coverage during the day (Fig. 9). An advancing storm area that had formed in Texas began to merge with the Gulf Coast area near 0900 GMT 3 May. By 1200 GMT 3 May, the end of AVE VII, the large area of storms covered most of Mississippi and eastern Louisiana with radar tops extending to 18.3 km (60,000 ft). Since AVE rawinsonde data were not available after 1200 GMT 3 May, it was not possible to describe energetics of this storm area as it decayed.

Table 7 gives the kinetic energy budget for the limited area that encloses the storms at 1200 GMT 3 May. This rawinsonde observation time most nearly coincides to the time when the storm area was largest and most intense. The close similarity between this budget and that of the Texas area (Table 6) should be noted. Generation of kinetic energy due to cross-contour flow is quite large in the vertical totals for both cases, and dissipation to subgrid scales of motion is a major sink of energy. The vertical total of the local change term is relatively small in both cases. Values of the energy transport terms within individual sublayers are larger for the Gulf area of storms than the Texas area, but the directions of the transports generally are similar. Horizontal flux convergence exists in the lower

Table 7. Average kinetic energy budget for the limited area enclosing the convection along the Gulf Coast during AVE VII at 1200 GMT 3 May 1978.

Pressure Layer (mb)	K (10^5J m^{-2})	$\frac{\partial K}{\partial t}$ (W m^{-2})	$\vec{V}\cdot k\vec{V}$ (W m^{-2})	$\frac{\partial \omega k}{\partial p}$ (W m^{-2})	$-\vec{V}\cdot\vec{\nabla}\phi$ (W m^{-2})	D (W m^{-2})
200-100	7.2	-4.6	44.0	-27.1	39.9	-27.6
300-200	5.5	-5.2	16.2	-5.4	34.8	-29.2
400-300	3.7	-0.6	0.6	-4.2	13.3	-17.5
500-400	3.5	2.7	-6.4	-3.1	-0.6	-6.2
600-500	3.4	4.8	-16.1	10.3	-5.8	4.8
700-600	2.3	4.0	-12.9	18.6	-8.5	18.2
800-700	1.2	2.6	-5.1	7.3	-6.3	11.1
900-800	0.8	1.2	-2.4	2.0	-3.1	3.9
sfc-800	0.5	0.5	-1.6	1.6	0.9	-0.4
Vertical total	28.1	5.4	16.3	0.0	64.6	-42.9

levels while flux divergence exists in the upper levels of both storm areas. Vertical flux divergence exists in the lower levels of both areas while vertical flux convergence occurs at higher levels, indicating upward transport of kinetic energy. A layer of destruction of kinetic energy by cross-contour flow and positive dissipation occur in the middle troposphere over the Gulf area (Table 7) but not over the Texas area of storms (Table 6). An even deeper layer of energy destruction and positive dissipation in the middle troposphere was observed by Tsui and Kung (1977) during times of peak storm intensity. As seen in the Texas storm area of AVSSE II, the energy processes near the Gulf Coast storms are much more intense than those of the AVE VII area as a whole (Table 5).

Pressure-time cross sections of the various kinetic energy budget terms in the near vicinities of the Gulf Coast area of storms show that energy generation and transport become stronger as the convection intensifies and expands in areal coverage. Recall that only light rain was occurring at 1800 GMT 2 May while at 1200 GMT 3 May, radar tops reached 18.3 km (60,000 ft). The pressure-time cross section of synoptic-scale vertical motion indicates that upward vertical motion occurs at all times over the Gulf Coast area (Fig. 19). Values are much larger at the last observation time when the storms are most intense. The peak value of -11.2μb s^{-1} near 500 mb represents very strong synoptic-scale vertical motion.

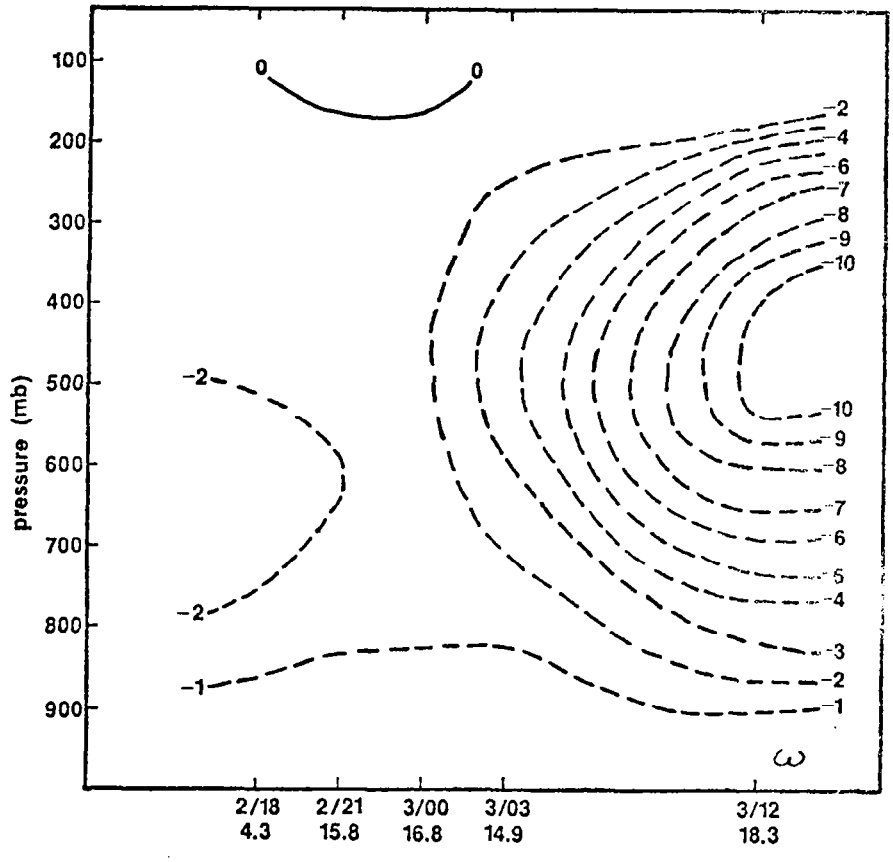

Fig. 19. Pressure-time cross section of vertical motion (ω) in μb s^{-1} for the Gulf Coast area of convection during AVE VII. Maximum radar tops (km) are given on the lower horizontal axis.

Figure 20 shows that values of the generation term $(-\vec{V}\cdot\vec{\nabla}\phi)$ change greatly near the Gulf Coast area of storms. In the middle troposphere a layer of kinetic energy destruction forms near 0000 GMT 3 May and steadily increases in depth and magnitude through the end of the period. Above 500 mb, values of $-\vec{V}\cdot\vec{\nabla}\phi$ are rather small until 0300 GMT when greatly enhanced generation of kinetic energy by cross-contour flow develops. Significant upper-level generation of kinetic energy near times of maximum storm intensity is characteristic of the Texas (Fig. 14) and Gulf Coast storm areas and the two squall lines observed during AVE IV (Fuelberg and Scoggins (1978). On the other hand, Kung

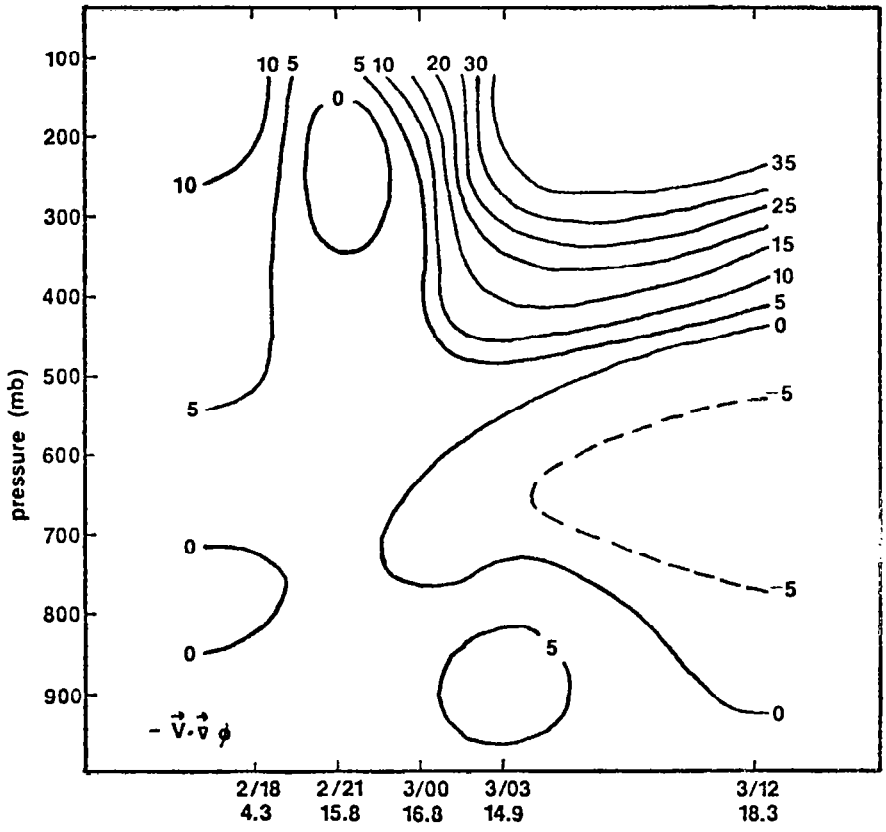

Fig. 20. Pressure-time cross section of generation of kinetic energy $(-\vec{V}\cdot\vec{\nabla}\phi)$ for the Gulf Coast area of convection during AVE VII in W m^{-2}/100 mb. Maximum radar tops (km) are given on the lower horizontal axis.

and Tsui (1977) have reported significant destruction of kinetic energy in the middle and upper troposphere during the intense storm stage and a strong generation before and after peak intensity. Positive generation near peak storm intensity has not been a dominant feature in either of the two current cases or those studied by Fuelberg and Scoggins (1978); however, a later section of this report will show that positive generation is associated with some storms during the AVE periods.

The cross section of the dissipation term (Fig. 21) reveals that energy transfers between grid and subgrid scales

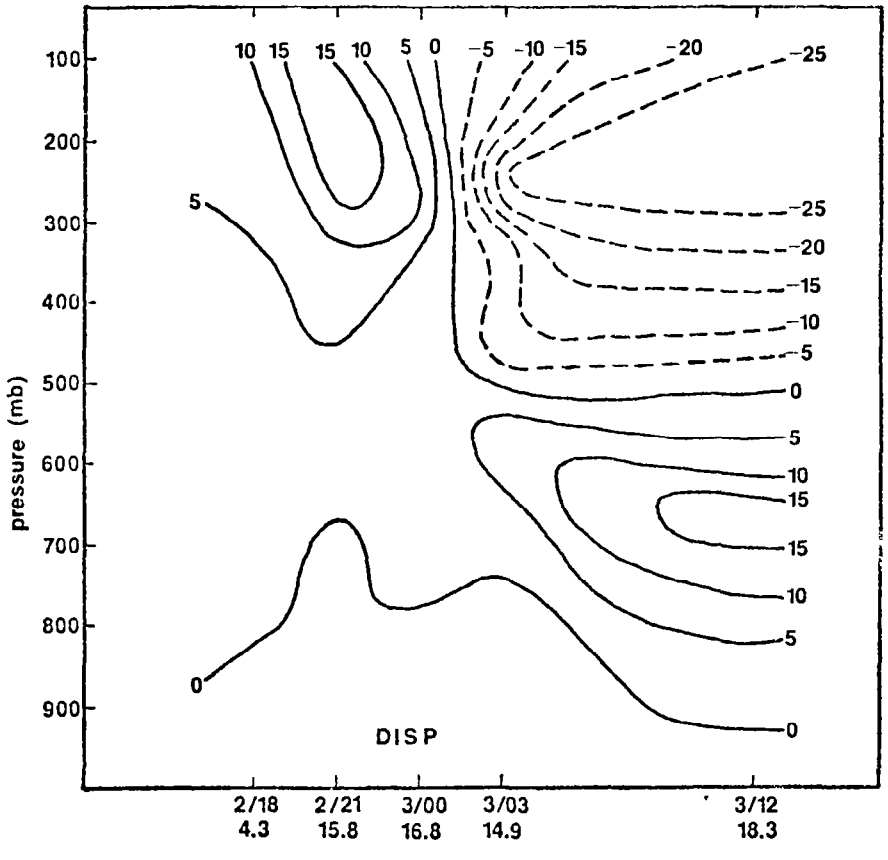

Fig. 21. Pressure-time cross section of dissipation of kinetic energy for the Gulf Coast area of convection during AVE VII in W m^{-2}/100 mb. Maximum radar tops (km) are given on the lower horizontal axis.

of motion undergo major changes during the period investigated. Largest values of dissipation occur near times of maximum convective activity. By comparing Figs. 20-21, a general correspondence is seen between layers of generation of kinetic energy and negative dissipation and between layers of destruction of kinetic energy and positive dissipation. This feature was noted earlier when budgets of the entire experiment areas were described. At peak storm intensity, 1200 GMT 3 May, maximum transfer to subgrid scales occurs near the level of the jet stream while an upwelling of synoptic-scale kinetic energy from subgrid scales occurs in the lower and middle troposphere. The subgrid-scale source of kinetic energy in the middle layers may be associated with the convection and serves to compensate for the destruction of kinetic energy due to cross-contour flow (Tsui and Kung, 1977).

As the storm area increases in size and intensity, low-level horizontal flux convergence and upper-level flux divergence increase in magnitude (Fig. 22). The layer of flux convergence is deeper and more intense than that observed with the Texas storms (Fig. 16). The region of upper-level flux divergence is much more intense as well. At 1200 GMT 3 May, velocity divergence at 200 mb reached 1.0×10^{-4} s^{-1} over the storm area and is the major factor in explaining the large values of upper level flux divergence over the area. The strong velocity divergence just noted formed near 0000 GMT 3 May in association with the advancing trough aloft and the convection over Texas and moved eastward into Louisiana and Mississippi. While the large areas of storms are expected to induce low-level velocity convergence and upper-level velocity divergence on the synoptic-scale, pre-existing synoptic-scale forcing over the area appears to be a major factor as well. It is difficult to separate the two effects or determine which appears first. The values of term $\vec{\nabla}\cdot k\vec{V}$ seen in Table 7 and Fig. 22 for the Gulf area of storms are larger than those seen for the Texas area of storms (Fig. 16). The Gulf area of storms,

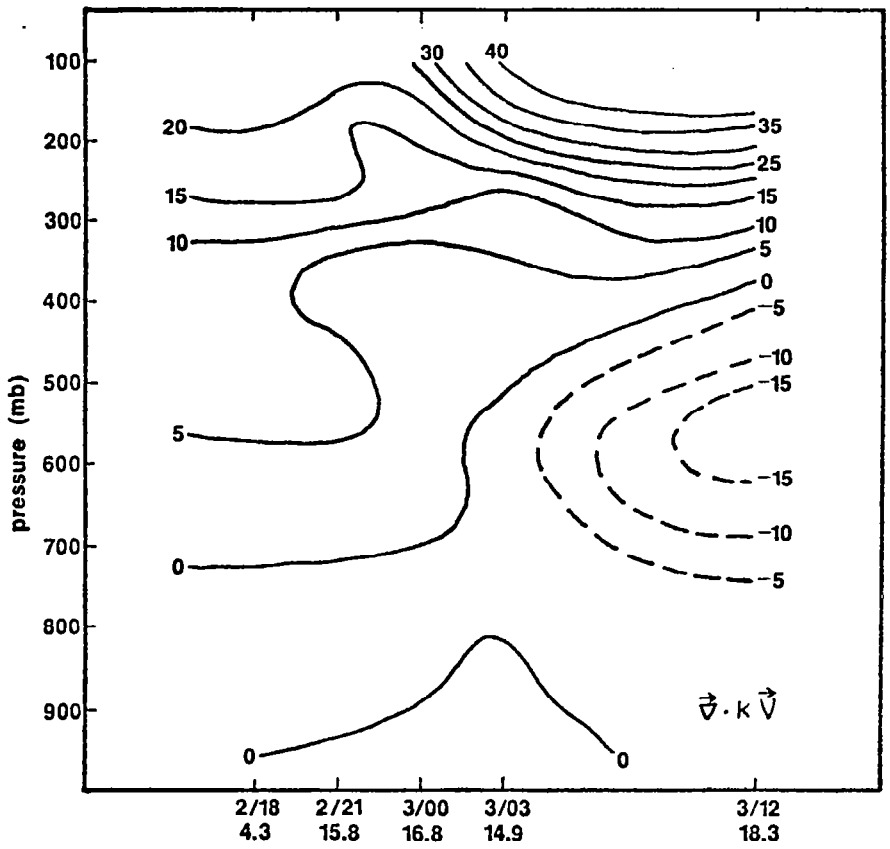

Fig. 22. Pressure-time cross section of the horizontal flux divergence of kinetic energy ($\vec{\nabla}\cdot k\vec{V}$) for the Gulf Coast area of convection during AVE VII in W m^{-2}/100 mb. Maximum radar tops (km) are given on the lower horizontal axis.

however, is more intense, longer lasting, and associated with stronger upper-level forcing than was the Texas area.

The cross section of the vertical flux divergence term for the Gulf area (Fig. 23) shows that kinetic energy from the lower atmosphere is transported aloft by the strong upward vertical motion. This transport is greatest at the last time period. Values of the term are larger for the Gulf area of storms than for the storms occurring in Texas (Fig. 17) and are indicative of the stronger vertical motions observed in the Gulf area.

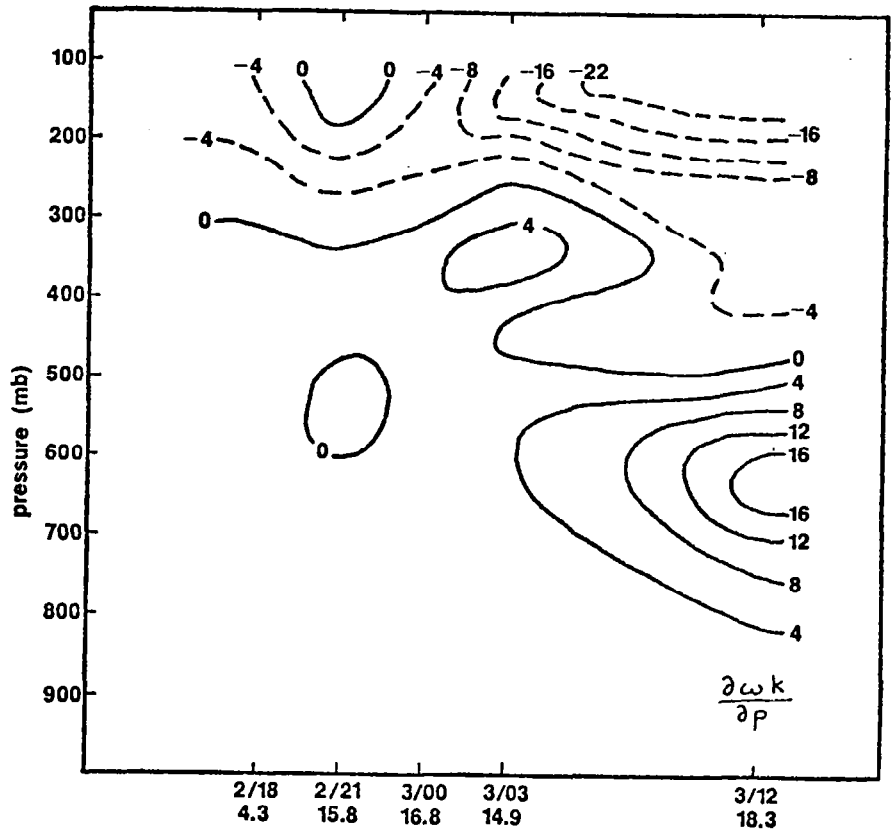

Fig. 23. Pressure-time cross section of the vertical flux divergence of kinetic energy ($\partial\omega k/\partial p$) for the Gulf Coast area of convection during AVE VII in W m^{-2}/100 mb. Maximum radar tops (km) are given on the lower horizontal axis.

Values of the local derivative term (Fig. 24), again, are smaller than other terms of the kinetic energy budget. The largest changes in kinetic energy content occur above 400 mb.

In comparing the kinetic energy budgets of the Texas and Gulf Coast areas of storms, many similarities have been noted between the two cases and between results of previous investigations. To expect identical results between different cases would be unreasonable in view of the highly variable conditions and interactions that occur in the atmosphere. While it is tempting to attribute changes in the kinetic energy parameters solely to the convective activity, this is

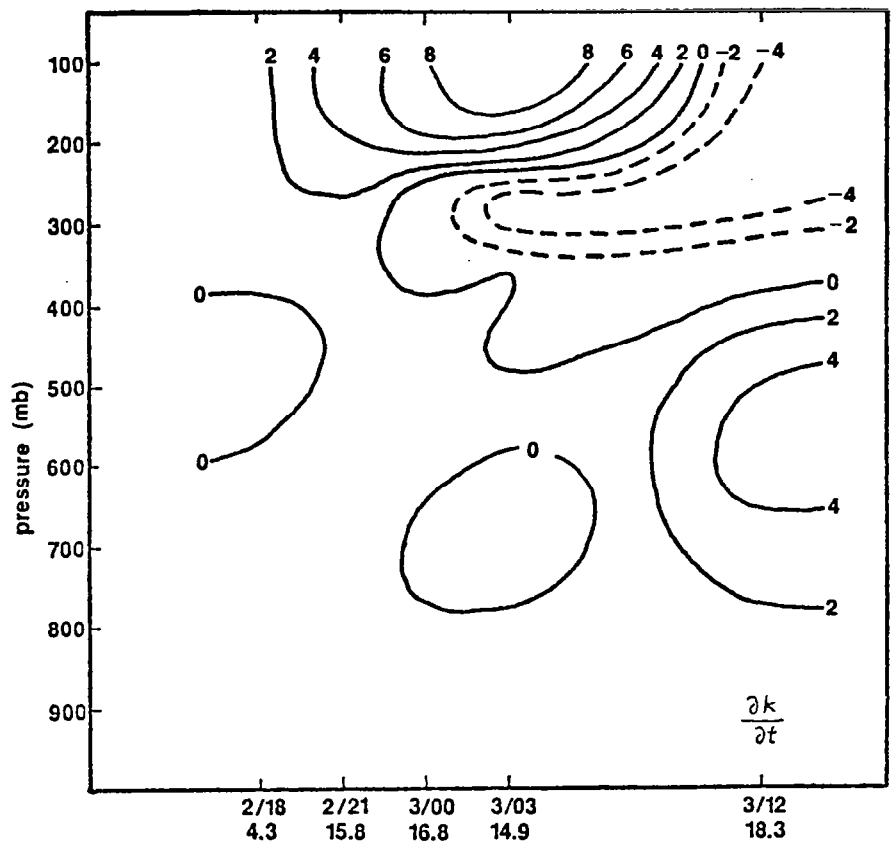

Fig. 24. Pressure-time cross section of the local change of kinetic energy ($\partial K/\partial t$) for the Gulf Coast convection area during AVE VII in W m^{-2}/100 mb. Maximum radar tops (km) are given on the lower horizontal axis.

unwarranted because it is impossible to separate the effects of the storms from the larger-scale effects of the environment. The severe storms studied in this section are modifying their synoptic-scale environments, but it is difficult to determine the degree to which this is done. Since synoptic-scale forcing seems smaller for the Texas storms than for the Gulf Coast storms, it seems reasonable to attribute more of the changes in the kinetic energy budget over Texas to the convection than those in the Gulf Coast case.

c. Energy budgets versus MDR values

In the previous section, energy budgets were computed for limited volumes that enclosed two specific areas of convection. The intensity of the enclosed convection was described on the basis of radar data so that changes in kinetic energy variables could be related to storm intensity. Much of the convection occurring during the AVSSE I and II and AVE VII periods could not be studied using the limited volume approach, however, because many storm areas did not occur at times or locations that permitted them to be monitored for an extended period using the 3 h rawinsonde data. The purpose of this section is to relate energetics to intensity of convection by averaging energy parameters over grid points that have equal MDR values. The procedure differs from that of the previous section since grid points comprising the average of a particular intensity are not necessarily adjacent and since grid points for all times of each experiment are grouped together.

One should remember that a high MDR value (Table 1) does not necessarily mean that an area of storms will exert a major influence on the surrounding synoptic-scale environment. Some severe storms form narrow squall lines or are isolated and may not be large enough in area to have much effect on the surrounding environment that is diagnosed from synoptic-scale data. Other storms that rate a high MDR value are short lived and may not have a noticeable effect on their larger scale surroundings either. Large areas of storms that are comparitively long lasting should have the greatest impact on the synoptic-scale environments.

Table 8 gives energy budgets for grid points having no convection (MDR 0). Values are given for the three AVE type experiments currently being studied and for AVE III (NASA, 1978) and AVE IV (Fuelberg, 1977). The AVE III period (6-7 February 1975) was characterized by a long wave trough

Table 8. Comparisons of energy budget studies for grid points of MDR 0. Values were integrated from the surface to 100 mb.

Author	Data	No. of Grid Points	K (10^5J m^{-2})	$\frac{\partial K}{\partial t}$ (W m^{-2})	$\vec{\nabla}\cdot k\vec{V}$ (W m^{-2})	$\frac{\partial \omega k}{\partial p}$ (W m^{-2})	$-\vec{V}\cdot\vec{\nabla}\phi$ (W m^{-2})	D (W m^{-2})	Internal Source (W m^{-2})
NASA (1978)	AVE 3	1414	42.5	4.2	34.2	-0.4	62.8	-24.7	38.1
Fuelberg (1977)	AVE 4	1114	18.3	-2.1	-1.0	-0.1	-10.6	7.3	-3.3
Current study	AVSSE I	138	24.2	4.7	0.7	0.0	-1.6	7.0	5.4
Current study	AVSSE II	383	26.6	1.6	-27.1	0.0	-47.6	22.1	-25.5
Current study	AVE 7	331	20.4	-3.0	36.1	0.0	29.6	3.5	33.1

centered over the experiment area and by a strong jet stream with speeds as great as 80 m s^{-1}. Convection was relatively light and limited to the southern portions of the region. During the AVE IV period (24-25 April 1975), two short-wave troughs with wavelengths of about 1500 km moved through the region and were responsible for the formation of two large areas of severe storms within the experiment area.

Synoptic conditions of the AVE III and AVE VII periods are similar in that a major trough was located within the experiment region. During AVSSE I and II, however, the major trough axis was located to the west of the experiment region such that upper-level anticyclonic supergradient flow occurred over the areas of study. The upper-level troughs occurring during AVE IV had much shorter wavelengths and amplitudes than those of the other experiments.

The kinetic energy budgets given in Table 8 were integrated from the surface to 100 mb and reflect some of the similarities and differences of the synoptic conditions that they describe. Generation of kinetic energy by cross-contour flow occurs for the grid points of no convection during AVE's III and VII when upper-level waves were located within the experiment areas, but destruction of kinetic energy occurs during AVE IV and AVSSE I and II when conditions were less cyclonic. Kung and Baker (1975), who studied the energetics of many days, found that destruction of kinetic energy and positive dissipation occurred during anticyclonic conditions while the opposite energy transformations were observed for cyclonic conditions. Table 8 shows that positive dissipation, the upwelling of kinetic energy from subgrid scale motions, occurs for the nonconvective grid points of each experiment except AVE III which was the most cyclonic case. Greatest positive dissipation takes place during the AVSSE II period. One should remember that values presented

in Table 8 are averages over all time periods of each particular experiment.

Values of the average "synoptic-scale total derivative" were computed using the formula

$$\frac{DK}{Dt} = -\vec{V}\cdot\vec{\nabla}\phi + D, \qquad (2)$$

indicating that changes in kinetic energy of a "synoptic-scale parcel" are due to cross-contour generation and to dissipation of energy. Smith (1973) calls this term the net internal source or sink of energy. During AVE's III and VII, the strongly cyclonic cases, the grid points of no convective activity were strong sources of kinetic energy. During AVSSE I, the energy contribution due to positive dissipation was greater than that due to cross-contour destruction so that the nonconvective points served as a rather weak source of kinetic energy. The grid points having MDR 0 were a sink of energy during the AVE IV and AVSSE II experiments due to the dominant influence of cross-contour destruction of kinetic energy.

Horizontal import of energy nearly balances the net internal sink for the nonconvective grid points of the AVSSE II period. On the other hand, during AVE's III and VII a large amount of energy is transported outside the region of study. Values of the vertical flux term are near zero due to the boundary conditions specified at the surface and 100 mb. Values of the local derivative term are relatively small in comparison to the other terms of the budget.

Kinetic energy budgets integrated from the surface to 100 mb for grid points having convection (MDR 3-6) are given in Table 9. The budgets for AVE's III, IV, and VII, which are associated with upper-level troughs in the computational region, show generation of kinetic energy by cross-contour flow, negative dissipation of energy (to subgrid scales), and horizontal flux divergence of energy. In addition, the convective grid

Table 9. Comparisons of energy budget studies for grid points of MDR 3-6. Values were integrated from the surface to 100 mb.

Author	Data	No. of Grid Points	K (10^5J m^{-2})	$\frac{\partial K}{\partial t}$ (W m^{-2})	$\vec{V}\cdot k\vec{V}$ (W m^{-2})	$\frac{\partial \omega k}{\partial p}$ (W m^{-2})	$-\vec{V}\cdot\vec{\nabla}\phi$ (W m^{-2})	D (W m^{-2})	Internal Source (W m^{-2})
NASA (1978)	AVE 3	48	51.1	19.4	150.1	-2.9	206.1	-39.5	166.6
Fuelberg (1977)	AVE 4	193	28.9	-9.5	14.8	-0.2	19.3	-14.2	5.1
Current study	AVSSE I	34	31.7	15.6	-12.4	0.0	-42.3	45.5	3.2
Current study	AVSSE II	63	20.6	12.7	9.2	0.0	-14.5	36.4	21.9
Current study	AVE 7	39	25.2	-6.3	20.9	0.0	43.4	-28.8	14.6
Tsui and Kung (1977)	*NSSL convection	--	21.0	4.6	-11.0	-0.2	89.5	-96.0	-6.5
Tsui and Kung (1977)	**NSSL nonconvection	--	9.5	0.2	4.6	0.0	-34.9	39.7	4.8

* Areal average of 4 convection cases
** Areal average of 3 cases of inactive convection

points of these three experiments serve as internal sources of kinetic energy since generation is greater than dissipation. Except for the internal source term, these results are similar to those found by Tsui and Kung (1977) in a study of four cases of active convection using mesoscale data from the NSSL network. Strong cyclonic curvature was evident in their four cases. Their reported values are area averages that are not dependent on storm intensity. The limited area averages of the Texas and Gulf Coast convection areas near peak intensity (Tables 6-7) also are similar to the MDR type averages for these three AVE periods (Table 9). Values of the local time derivative and the vertical flux terms are comparitively small.

The budget of the grid points having convection (Table 9) is somewhat different from the budget of grid points having no convection (Table 8). Since far fewer grid points experience convection than nonconvection, some of the budget differences may be due to a tendency for convection to occur in pre-existing areas of generation, negative dissipative, and horizontal energy export. In addition, the storms themselves may modify their synoptic-scale environments so that the pre-existing generation, dissipation, and horizontal export are enhanced in magnitude. The environmental modification may even result in a reversal of energy processes; for example, destruction of kinetic energy by cross-contour flow may change to energy generation. Fuelberg and Scoggins (1978) cited work by Danard (1964) that suggests that thunderstorms occurring in conjunction with a tilting upper-level trough may produce changes in term $-\vec{V}\cdot\vec{\nabla}\phi$ due to latent heat release and modification of the synoptic-scale wind field. Fuelberg and Scoggins also indicated that storms can induce synoptic-scale fields of velocity divergence/convergence and vertical motion that yield transport of energy together with various kinds of subgrid scale motions.

The energy budgets for the grid points having convection during the AVSSE I and II periods are different from those described for AVE's III, IV and VII (Table 9). Recall that

synoptic conditions during the two AVSSE periods were more anticyclonic than observed during the three previously described AVE periods. The convection grid points of the AVSSE experiments are characterized by destruction of kinetic energy, instead of generation, and transfer of energy from subgrid to grid scale motions (positive dissipation), instead of negative dissipation. Horizontal flux convergence of kinetic energy occurs during AVSSE I while horizontal divergence is observed during AVSSE II. Tsui and Kung (1977) studied three cases of "inactive convection" when storms were "either barely noted or failed to develop" within the NSSL area. These cases were characterized by either anticyclonic curvature in the upper-air flow, as were the two AVSSE periods, or advection of anticyclonic vorticity. Their values of terms $-\vec{V}\cdot\vec{\nabla}\phi$ and D (Table 9) compare favorably with those of the two AVSSE cases.

One should recall that the Texas convection area described in Table 6 occurred during AVSSE II and exhibited generation of kinetic energy and negative dissipation--conditions that are opposite those found in the MDR 3-6 average of Table 9 for the overall AVSSE II period. Other convection areas that are not described in this report show a similar departure from the MDR 3-6 average. By comparing the budget of the MDR 0 points for the two AVSSE periods (Table 8) with that of the MDR 3-6 points (Table 9), we see that some terms increase in magnitude while others decrease in magnitude. For example, term $-\vec{V}\cdot\vec{\nabla}\phi$ has the value -1.6 W m^{-2} for the MDR 0 average of AVSSE I and -42.3 W m^{-2} for the MDR 3-6 average which suggests an enhancement of the anticyclonic type energy conditions described by Kung and Baker (1975). On the other hand, term $-\vec{V}\cdot\vec{\nabla}\phi$ has the value -47.6 W m^{-2} for the MDR 0 category of AVSSE II and -14.5 W m^{-2} for the MDR 3-6 category suggesting a trend to more cyclonic type energy conditions. Perhaps there is no consistent manner in which storms affect the energy budget of the surrounding synoptic-scale environment. The locations of the storms with respect to synoptic-scale features together

with their sizes, lifetimes, and yet to be discovered factors probably influence the scale interactions that determine how the synoptic-scale energy budget will be modified. This aspect will be investigated further as additional cases of convection are studied in future research.

The kinetic energy budget for grid points having intense convection (MDR 5-6) is given in Table 10 for several AVE experiments. The nature of the energy processes is generally similar to that observed for the broader MDR 3-6 category (Table 9). A comparison of the two Tables reveals that convection intensity is not always directly related to the magnitudes of the various energy budget terms. Since comparitively few grid points experienced convection with an MDR 5-6 rating, sample size may contribute to this finding.

To further investigate the energetics of grid points having convection, vertical profiles of the various budget terms will be described for the MDR 3-6 intensity category of several AVE experiments. Vertical profiles of term $-\vec{V}\cdot\vec{\nabla}\phi$ are given in Fig. 25. Generation of kinetic energy by frictionally induced cross-contour flow toward lower pressure occurs near the surface in each experiment. Minimum generation (AVE's IV and VII) or even destruction of kinetic energy (AVSSE I AND II) is found in the middle troposphere. In the upper troposphere and lower stratosphere, two different profiles are noted. The convective grid points of the three cyclonic cases (AVE's III, IV, and VII) are characterized by generation of kinetic energy while the convective grid points of the more anticyclonic AVSSE cases are characterized by cross-contour destruction of energy. The AVE III period with its strong jet stream activity contains the most intense upper-level generation.

Vertical profiles of the dissipation term (Fig. 26) reveal similar differences between experiments. Negative dissipation, due to friction, is observed for the convective grid points near the surface of each experiment. Positive dissipation is observed above 500 mb for the two AVSSE (more anticyclonic)

Table 10. Comparisons of energy budget studies for grid points of MDR 5-6. Values were integrated from the surface to 100 mb.

Author	Data	No. of Grid Points	K (10^5J m^{-2})	$\frac{\partial K}{\partial t}$ (W m^{-2})	$\vec{\nabla}\cdot k\vec{V}$ (W m^{-2})	$\frac{\partial \omega k}{\partial p}$ (W m^{-2})	$-\vec{V}\cdot\vec{\nabla}\phi$ (W m^{-2})	D (W m^{-2})	Internal Source (W m^{-2})
NASA (1978)	AVE 3	16	51.8	23.0	146.2	-3.1	193.5	-27.5	166.0
Fuelberg (1977)	AVE 4	65	25.7	-19.6	34.2	-0.2	32.7	-18.3	14.4
Current study	AVSSE I	17	32.7	15.5	-17.2	0.0	-63.7	62.0	-1.7
Current study	AVSSE II	36	21.4	10.5	3.5	0.0	-22.3	36.3	14.0
Current study	AVE 7	15	29.0	-1.5	48.9	0.0	29.4	18.0	47.4
Tsui and Kung (1977)	*NSSL convection	--	21.0	4.6	-11.0	-0.2	89.5	-96.0	-6.5
Tsui and Kung (1977)	**NSSL nonconvection	--	9.5	0.2	4.6	0.0	-34.9	39.7	4.8

* Areal average of 4 convection cases
** Areal average of 3 cases of inactive convection

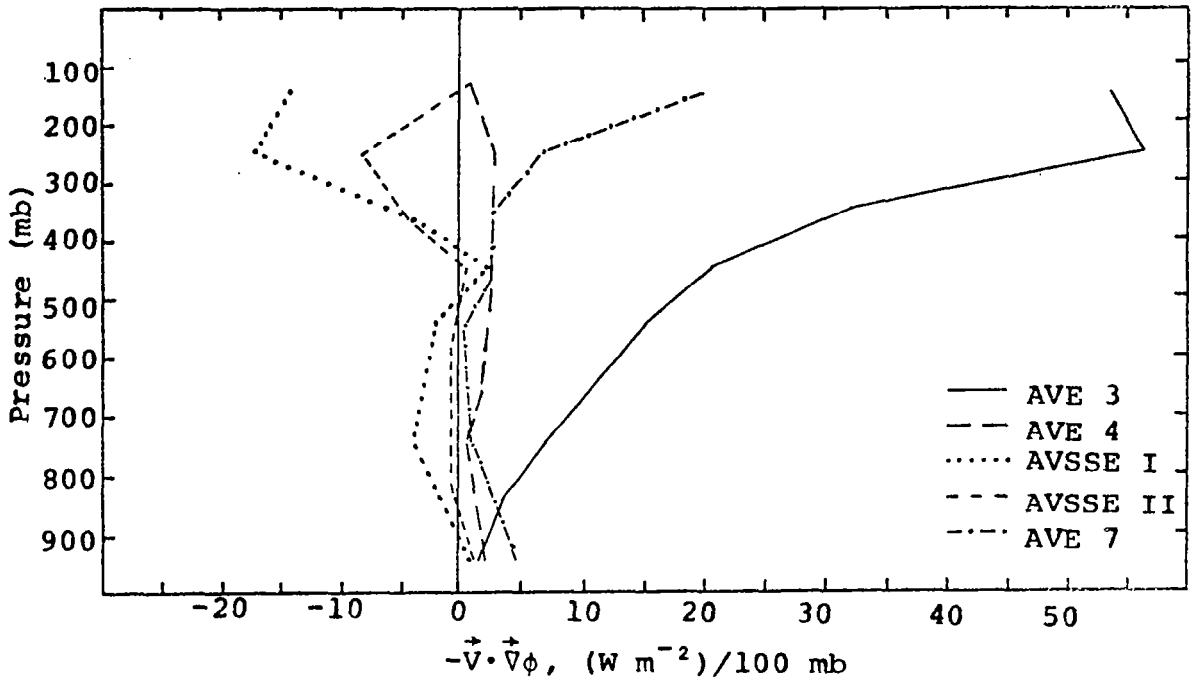

Fig. 25. Vertical profiles of term $-\vec{V}\cdot\vec{\nabla}\phi$ for the MDR 3-6 category of several AVE type experiments.

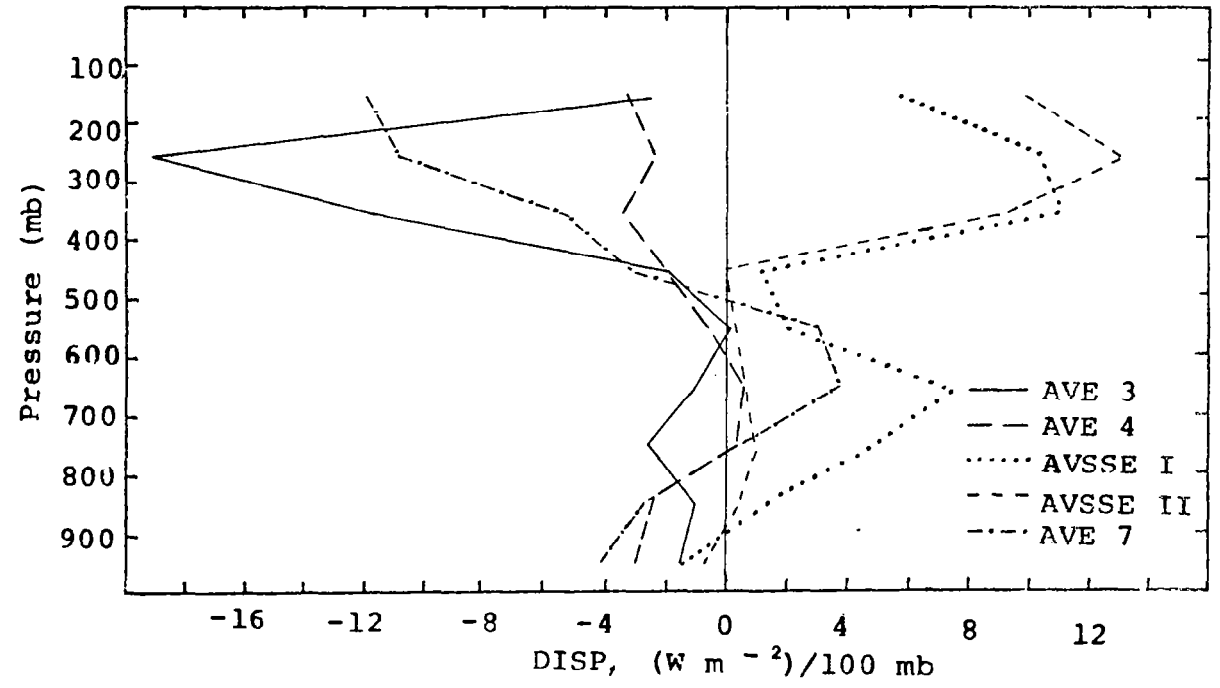

Fig. 26. Vertical profiles of the dissipation term for the MDR 3-6 category of several AVE type experiments.

cases while negative dissipation occurs for the three AVE (more cyclonic) experiments. The importance of subgrid scale motions to the synoptic-scale kinetic energy budget again is demonstrated; unfortunately, we can only speculate about the nature of these small-scale motions.

Vertical profiles of the internal source term $(-\vec{V}\cdot\vec{\nabla}\phi + D)$ do not reveal clear trends among the various AVE experiments (Fig. 27). The vertical totals of Table 9 indicate that the convection grid points of the AVE III period were a greater source of kinetic energy than were convective grid points of the other periods. All grid points having convection, however, provided an internal source of energy.

Largest horizontal transport of kinetic energy for the convection grid points occurs near the level of the jet stream (Fig. 28). Upper-level horizontal flux divergence of energy occurs in all cases except AVSSE I which has convergence. Upper-level velocity divergence due either to pre-existing synoptic-scale motions or produced by the convection is a major factor in explaining the values of flux divergence. The location of the storms with respect to jet maxima influences values of the flux term through advection of kinetic energy. During AVSSE I, advection of larger values of kinetic energy into the storm areas dominates effects due to velocity divergence to give upper-level flux convergence (Fig. 28). Low-level velocity convergence on the synoptic scale associated with the convection contributes to negative values of $\vec{V}$ near the surface of most experiments.

The profiles of term $\partial\omega k/\partial p$ are similar for all experiments since synoptic-scale upward vertical motion occurs in the vicinities of most storm areas (Fig. 29). Vertical flux divergence occurs below about 400 mb while vertical flux convergence occurs at higher levels. On the synoptic scale at least, kinetic energy is transported aloft, but on the cloud scale, much more complicated events take place. Because thunderstorms contain downdrafts as well as updrafts, storms

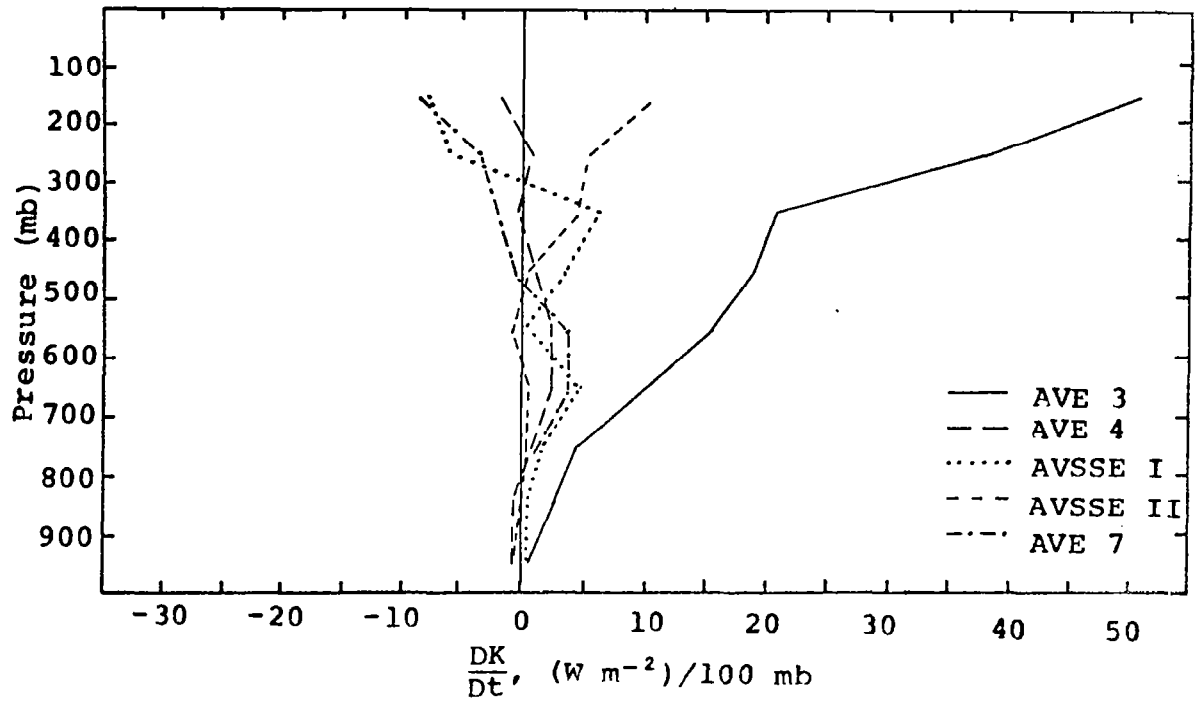

Fig. 27. Vertical profiles of term $\frac{DK}{Dt}$ for the MDR 3-6 category of several AVE type experiments.

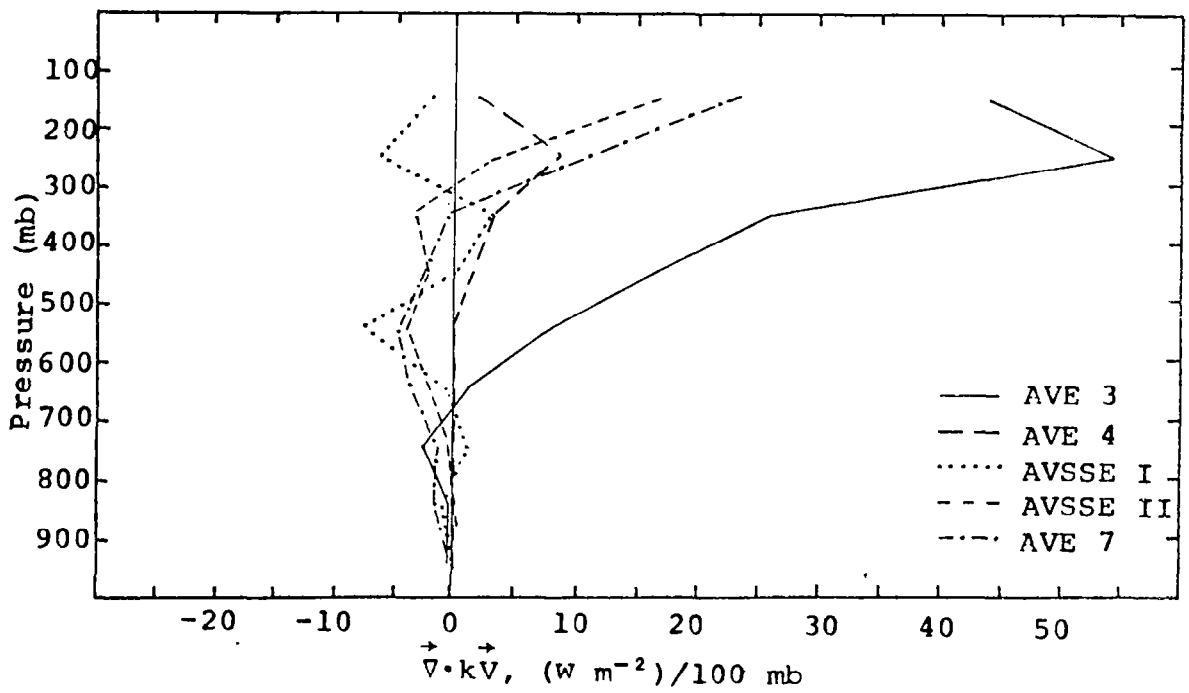

Fig. 28. Vertical profiles of term $\vec{\nabla}\cdot k\vec{V}$ for the MDR 3-6 category of several AVE type experiments.

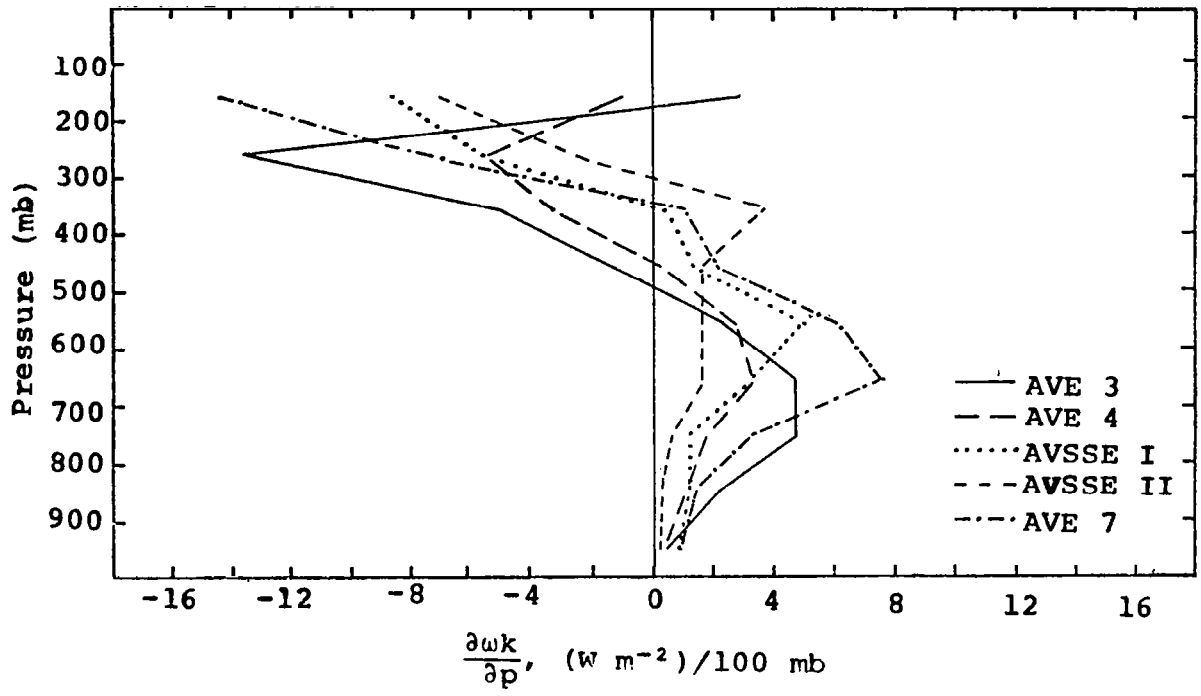

Fig. 29. Vertical profiles of term $\partial\omega k/\partial p$ for the MDR 3-6 category of several AVE type experiments.

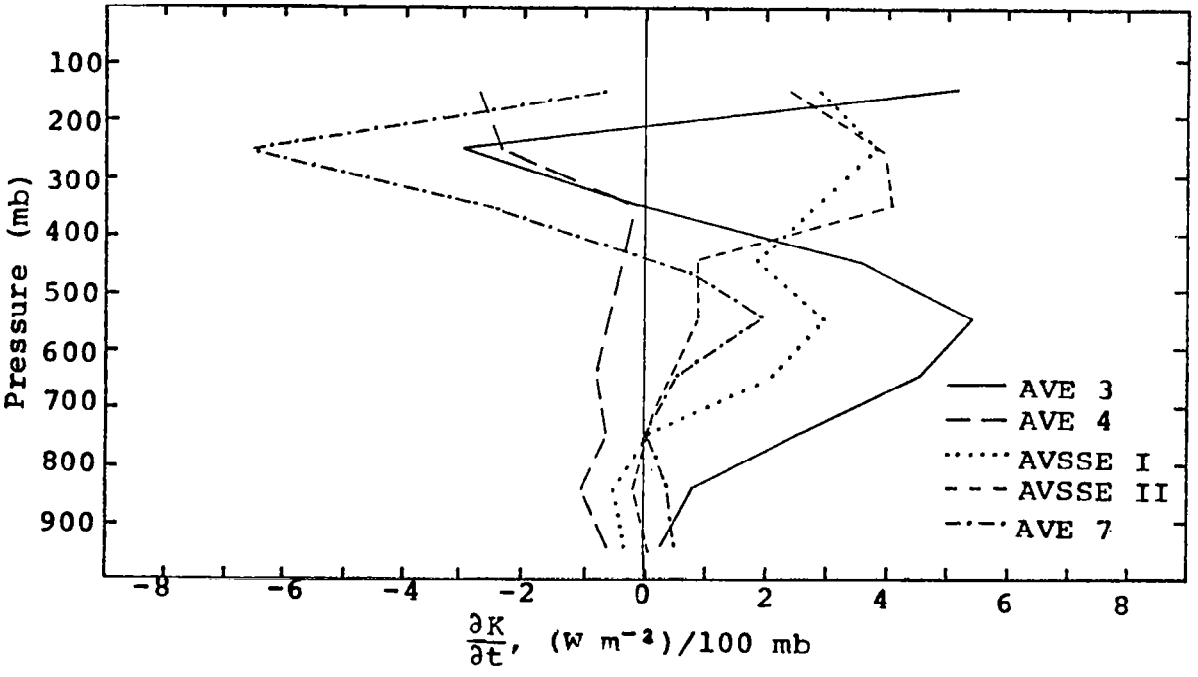

Fig. 30. Vertical profiles of term $\partial K/\partial t$ for the MDR 3-6 category of several AVE type experiments.

can serve as giant mixers of kinetic energy content because of the conservation of momentum. High speed upper-level air that is carried downward should appear as a subgrid-scale source (positive dissipation) in the lower levels (Ward and Smith, 1976). On the other hand, the effects of updrafts and downdrafts should produce a subgrid-scale sink of energy in the higher levels. There is some evidence of this mixing process in the profiles of the dissipation term (Fig. 26), but a host of other subgrid scale processes probably are occurring as well.

Local changes in kinetic energy content are rather small for each experiment (Fig. 30) because the various source and sink terms tend to cancel each other. Both positive and negative values of $\partial K/\partial t$ are seen below about 750 mb. In the middle troposphere, local increases are the general rule. Near jet stream level, local decreases occur for the cyclonic cases (AVE's III, IV and VII) while local increases are observed for the more anticyclonic cases (AVSSE I and II).

d. Spatial maps of kinetic energy budget terms

Spatial maps of the various kinetic energy budget terms provide a means of directly relating energetics to observed areas of convection without averaging over particular areas. It is not possible to present fields of all terms in the energy budget at all times of each AVE experiment studied because of the large number of maps involved. The times selected for discussion in this section contain intense convection; the 400-100 mb layer is selected since energy processes generally are a maximum near the level of the jet stream. Convection with MDR values greater than or equal to 3 is indicated by scalloping.

1) AVSSE I at 0000 GMT 28 April 1975

Intense thunderstorms at this time are located along an advancing cold front located through the Midwest and into west Texas (Figs. 2-4). The storm area had formed during the

morning, and at the current time had maximum radar tops of 16.8 km (55,000 ft) along the border of Oklahoma and Texas. Figure 31a shows that the storms occur east of the maximum wind axis in advance of the upper-level trough (Figs. 2, 4). The storms located over Oklahoma and northern Texas occur partly in an area of generation of kinetic energy by cross-contour flow (Fig. 31b). Maximum values of generation reach 170 W m^{-2} within the 400-100 mb layer. Much of the remainder of the AVSSE I area, including portions of the squall line, experiences destruction of kinetic energy. Recall that the convection grid points of the entire AVSSE I period were characterized by kinetic energy destruction (Table 9).

The storm area is characterized mostly by horizontal flux convergence of kinetic energy ($\vec{V}\cdot k\vec{V}<0$) (Fig. 31c). Near the storms, the positive contribution to term $\vec{V}\cdot k\vec{V}$ by term $k\vec{V}\cdot\vec{V}$, due to upper-level velocity divergence, is completely dominated by the contribution due to advection of higher values of kinetic energy into the storm area. While the present studies and those by Fuelberg and Scoggins (1978) have indicated that times of peak storm intensity often coincide with upper-level horizontal flux divergence of energy, this is not observed in the current case study. Tsui and Kung (1977), who studied several cases, found that the sign of this term fluctuated between their cases. While severe thunderstorms often occur just downwind of jet maxima, this is certainly not always true. In addition, the contribution of velocity divergence may either reinforce or cancel the advective contribution to give either a positive or negative value to the horizontal flux term.

The area of vertical flux convergence in the upper levels ($\partial\omega k/\partial p<0$) coincides closely with the storm area (Fig. 31d). Since synoptic-scale upward vertical motion occurs over the storm area, kinetic energy is being transported aloft. An area of downward motion and associated vertical flux divergence is located to the west of the storm area near the Texas

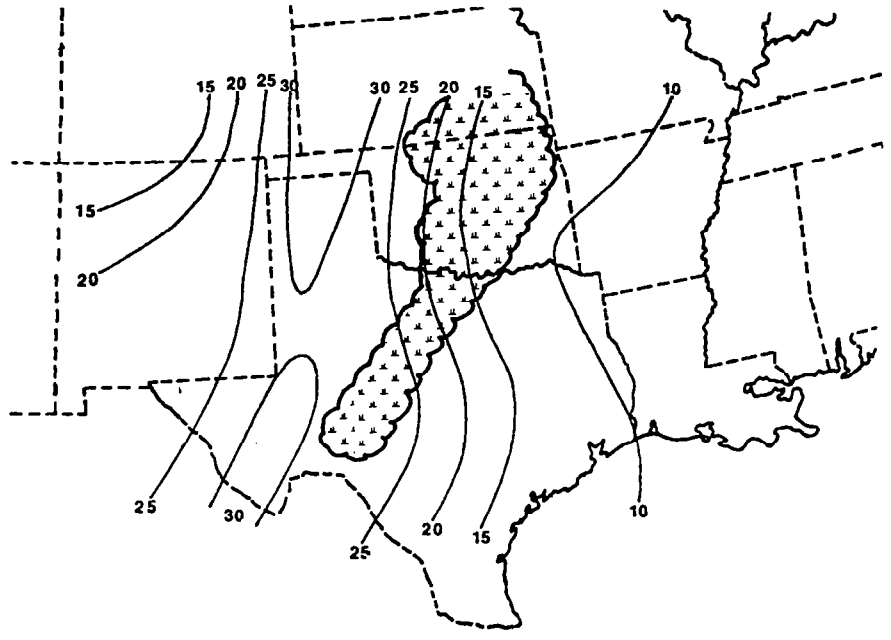

(a) Kinetic energy content, K, 10^5 J m^{-2}, 400-100 mb

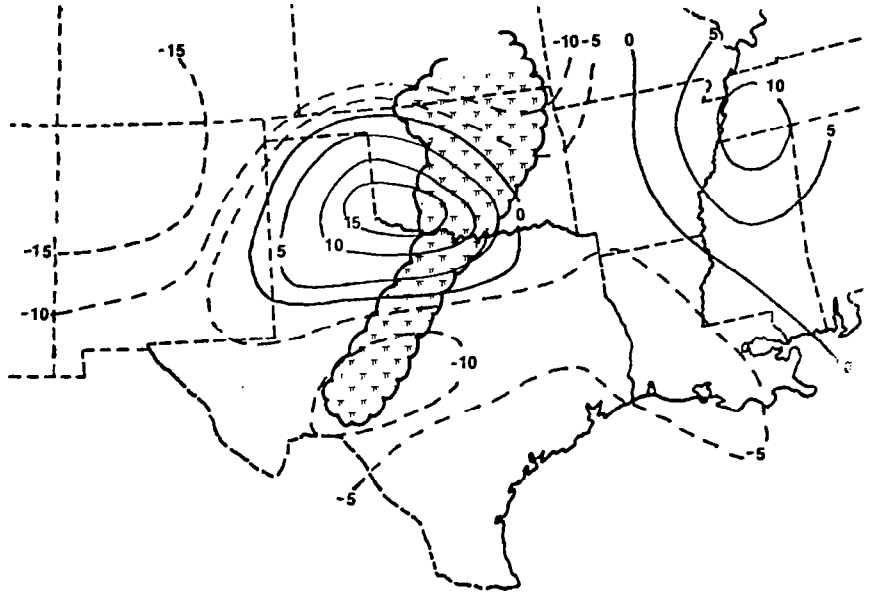

(b) Generation term, $-\vec{V}\cdot\vec{\nabla}\phi$, 10^1 W m^{-2}, 400-100 mb

Fig. 31. Spatial fields of kinetic energy budget terms for the 400-100 mb layer of AVSSE I at 0000 GMT 28 April 1975. Superimposed are areas of MDR values $\geq$ 3.

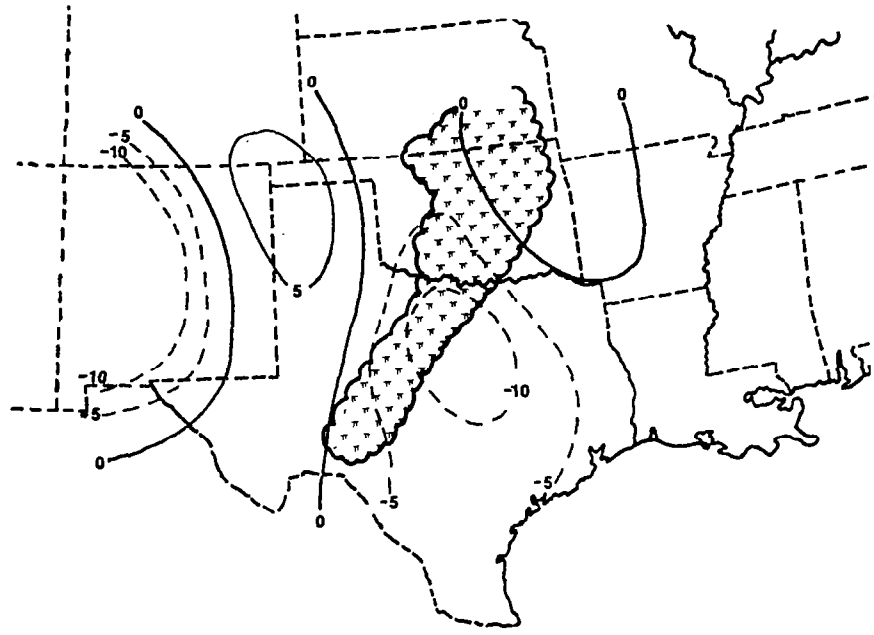

(c) Horizontal flux divergence term, $\vec{\nabla}\cdot k\vec{\nabla}$, 10^1 W m^{-2}, 400-100 mb

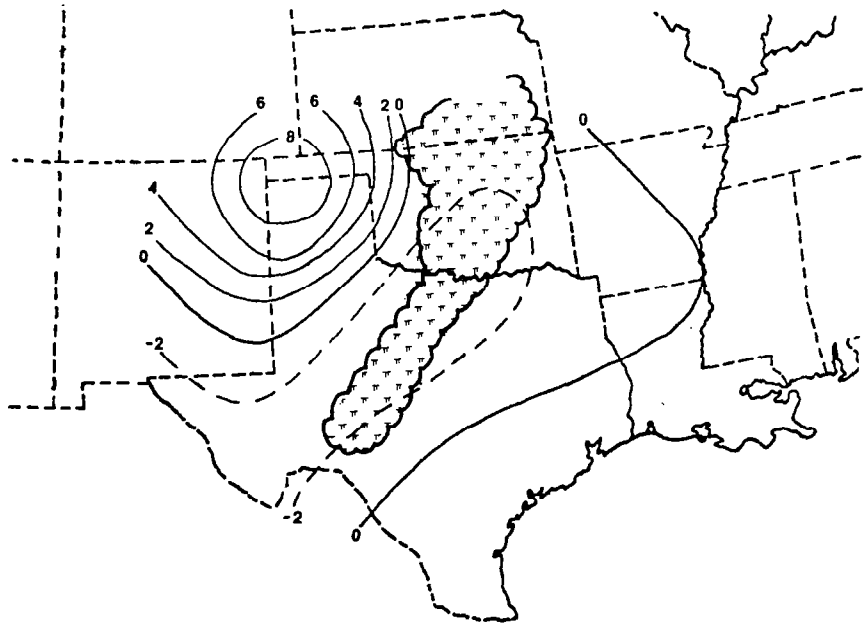

(d) Vertical flux divergence term, $\partial\omega k/\partial p$, W m^{-2}, 400-100 mb

Fig. 31. (Continued)

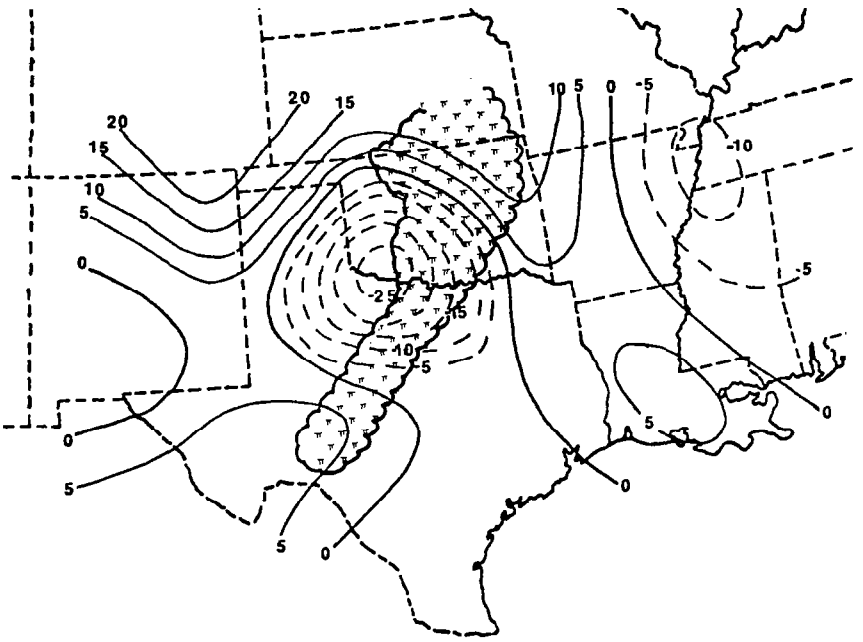

(e) Dissipation term, 10^1 W m^{-2}, 400-100 mb

Fig. 31. (Continued)

and Oklahoma panhandles.

Dissipation of kinetic energy to subgrid scales of motion occurs over much of the storm area (Fig. 31e). Since peak dissipation of 250 W m^{-2} occurs in the area while peak generation is 170 W m^2, the storm area is using up more kinetic energy than is generated locally, the remainder is imported from the surroundings.

2) AVSSE II at 2100 GMT 6 May 1975

The Texas area of convection that was described in Section 5b is near peak intensity at this time. The Texas storm area is located near an upper-level wind maximum while storms in Oklahoma occur to the north of the wind maximum (Fig. 32a). The storm area in Arkansas is comparitively weak and is dissipating and will not be described further. The Texas storms at peak intensity occur in an area of generation of kinetic energy by cross-contour flow (Fig. 32b). Maximum values over Texas are 80 W m^{-2}, somewhat smaller than observed during the AVSSE I case of the previous section. Most of the remainder of the AVSSE II area at this time and level exhibits destruction of kinetic energy by cross-contour flow which is due to supergradient winds on the eastern side of the trough located to the western side of the experiment area. The storm area over Oklahoma occurs in this region of kinetic energy destruction. Recall from Fig. 14 that destruction of kinetic energy occurred over the Texas storm area prior t peak intensity but then changed to generation of kinetic energy at 2100 GMT, the time of Fig. 32.

The Texas storm area is located partly within an area of horizontal flux convergence ($\vec{\nabla}\cdot k\vec{V}<0$) and partly within an area of flux divergence (Fig. 32c) due to the location of the wind maximum over north central Texas (Fig. 32a). The area averaging procedure gives divergence for the limited area average (Table 6). Much of the remainder of the AVSSE II area is downwind of this wind maximum and experiences flux convergence of kinetic energy at 2100 GMT, including the storm

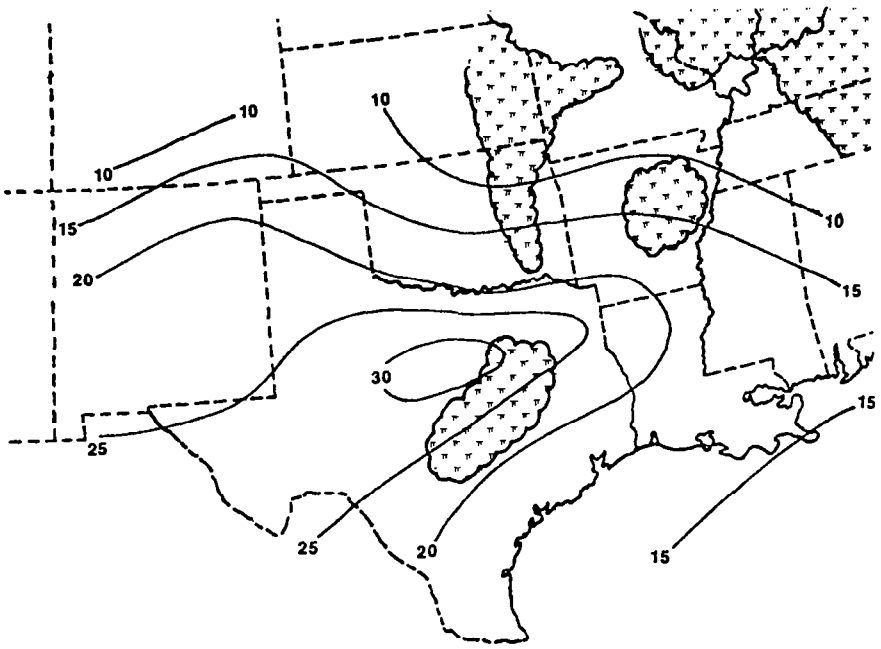

(a) Kinetic energy content, K, 10^5 J m^{-2}, 400-100 mb

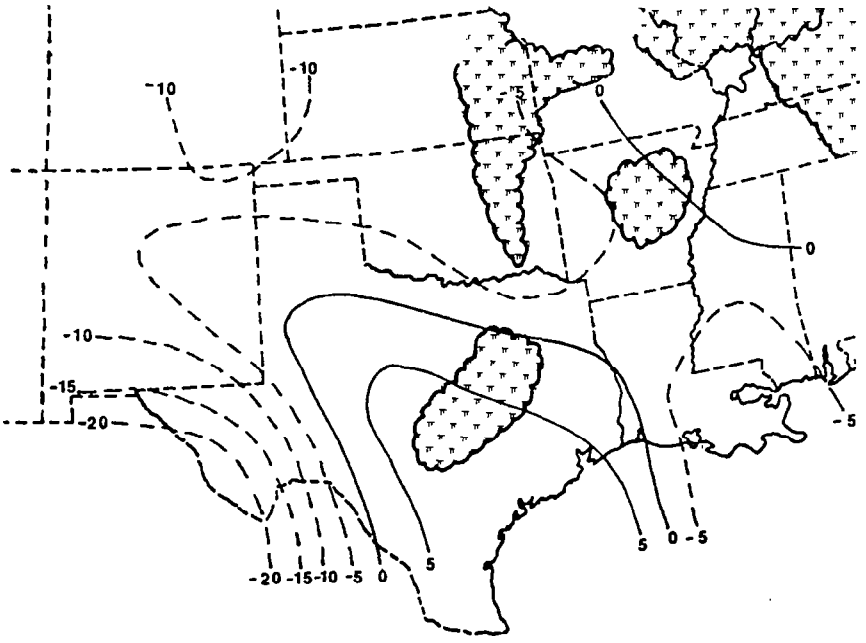

(b) Generation term, $-\vec{V}\cdot\vec{\nabla}\phi$, 10^1 W m^{-2}, 400-100 mb

Fig. 32. Spatial fields of kinetic energy budget terms for the 400-100 mb layer of AVSSE II at 2100 GMT 6 May 1975. Superimposed are areas of MDR $\geq$ 3.

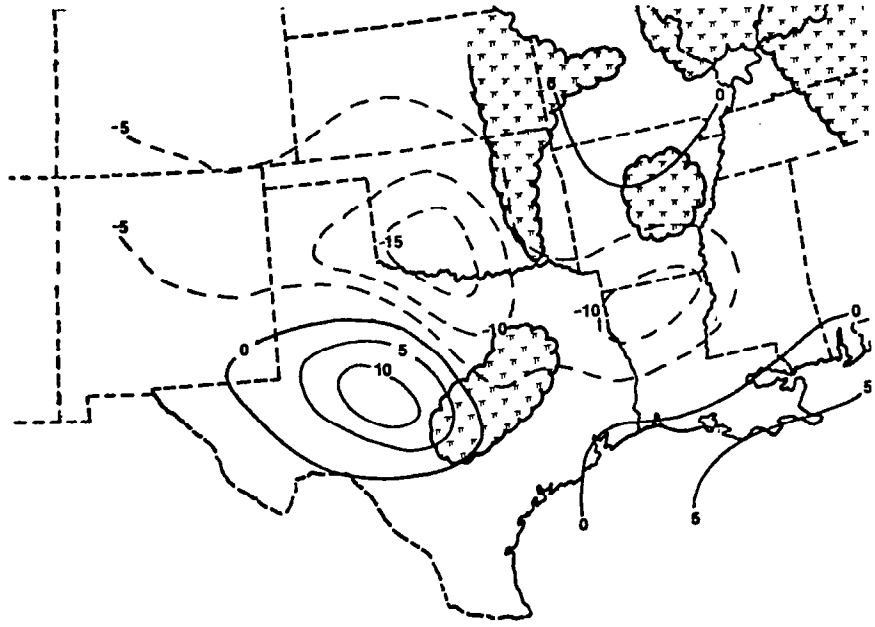

(c) Horizontal flux divergence term, $\vec{V} \cdot k\vec{V}$, 10^1 W m^{-2}, 400-100 mb

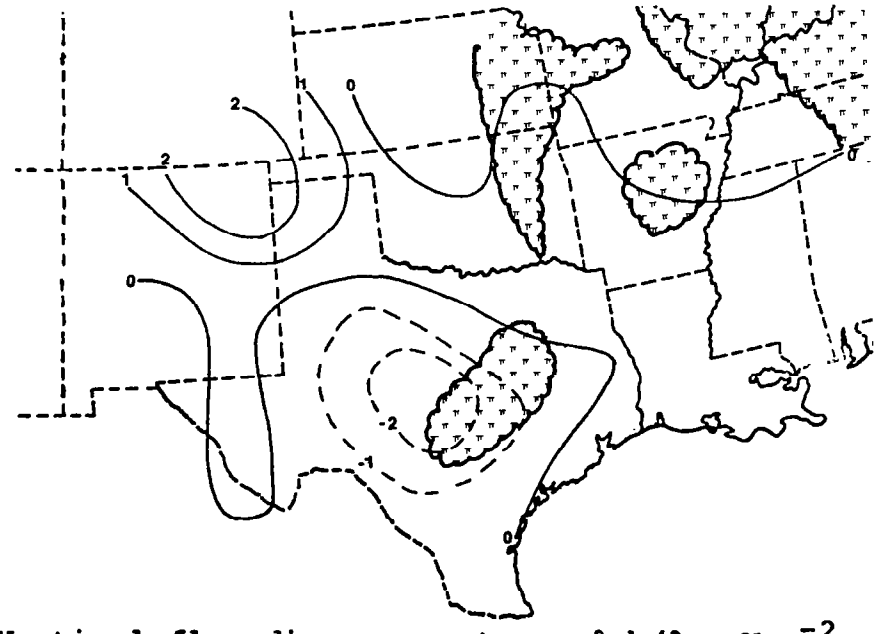

(d) Vertical flux divergence term, $\partial \omega k / \partial p$, W m^{-2} 400-100 mb

Fig. 32. (Continued)

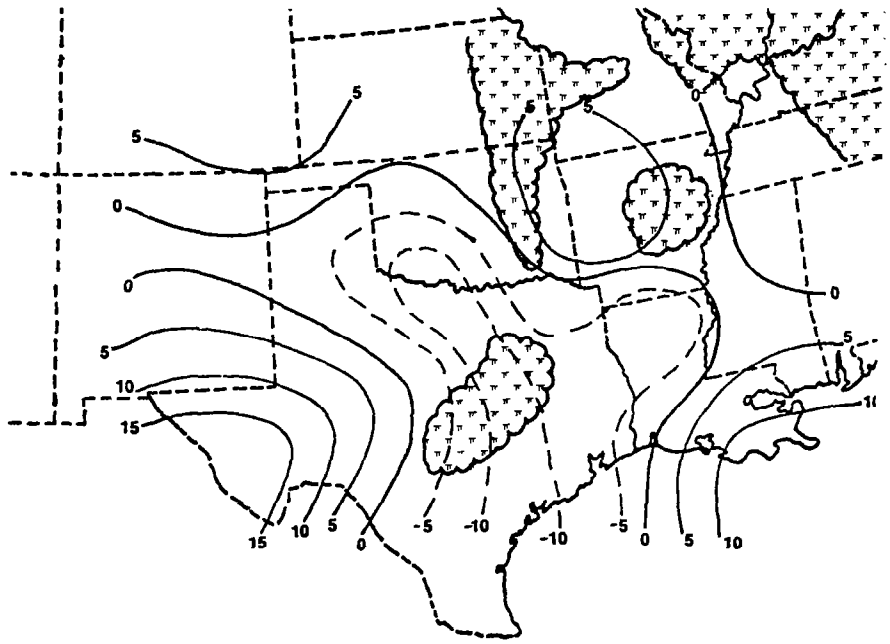

(e) Dissipation term, 10^1 W m^{-2}, 400-100 mb

Fig. 32. (Continued)

area over Oklahoma.

As a general rule, fields of term $\partial\omega k/\partial p$ show good agreement with storm location and the life cycle of the storms because the vertical motion fields from which the flux term is computed show this same good agreement (see Figs. 13, 19). Figure 32d indicates that the Texas storm area occurs near a well defined region of upper-level flux convergence of kinetic energy that is due to upward vertical motion. The storms over Oklahoma do not occur in a well defined region of upward vertical motion, and therefore do not exhibit strong vertical flux convergence. Since the Oklahoma storms did not even enhance the synoptic-scale vertical motion field, their failure to produce changes in the energy budget is more understandable. Those portions of the AVSSE II region that do not contain convection generally experience weak values of vertical flux divergence. An exception is northeast New Mexico where strong subsidence and associated large values of flux divergence occur.

Transfer of kinetic energy to subgrid scales of motion (negative dissipation) occurs over much of Texas and northern Louisiana (Fig. 32e). The Texas area of storms is located near the center of this negative region. Significant areas of positive dissipation that include the Oklahoma storm region also are evident at this time. By comparing Figs. 32b and e, the close correspondence between areas of destruction of kinetic energy by cross-contour flow and areas of positive dissipation is evident.

In summary, the Texas area of storms is associated with a region of well defined upward vertical motion, generation of kinetic energy, and negative dissipation. These findings agree with those of the Gulf Coast area of storms described in this report and findings by Fuelberg and Scoggins (1978). On the other hand, the storms over Oklahoma are not associated with a well defined area of synoptic-scale vertical motion, and values of generation and dissipation differ greatly from those

of the Texas area. Apparently, the Oklahoma storms had little impact on their synoptic-scale environments or were overwhelmed by it even though the storms themselves were quite intense and obviously had a large effect on their more local environments.

3) AVE VII at 1200 GMT 3 May 1978

Intense thunderstorms were located over eastern Louisiana and all of Mississippi in advance of an upper-level low located over Texas (Figs. 9-10). Figure 33a shows that the storms over Louisiana occur in advance of a wind maximum over south Texas. Light winds and small values of kinetic energy content occur over the northwest portion of the experiment area.

Two areas of kinetic energy generation by cross-contour flow occur at 1200 GMT; the strongest is centered over Mississippi near the Gulf Coast storm region while the second occurs in central Texas where storms are not observed (Fig. 33b). Areas of comparitively weak destruction of kinetic energy are located through Kansas, Oklahoma, and along the Gulf Coast.

Much of the AVE VII area exhibits horizontal flux convergence of kinetic energy due to advection of higher values of energy into the area from south Texas (Fig. 33c). The relative minimum of kinetic energy content over Missouri (Fig. 33a) manifests itself as an area of horizontal flux divergence over the northeast portion of the experiment area. Strong horizontal flux divergence of energy occurs along the coasts of Louisiana and Mississippi near the locations of the stro gest thunderstorms. Although higher values of energy are being advected into the storm area contributing to $\vec{\nabla}\cdot k\vec{V}<0$, the effect of strong upper-level divergence dominates to give $\vec{\nabla}\cdot k\vec{V}>0$ (flux divergence).

Strong upward synoptic-scale vertical motion near the storms that reaches 21 $\mu b\ s^{-1}$ at 500 mb transports kinetic energy into the 400-100 mb layer and appears as a well defined area of vertical flux convergence in Fig. 33d. A much weaker

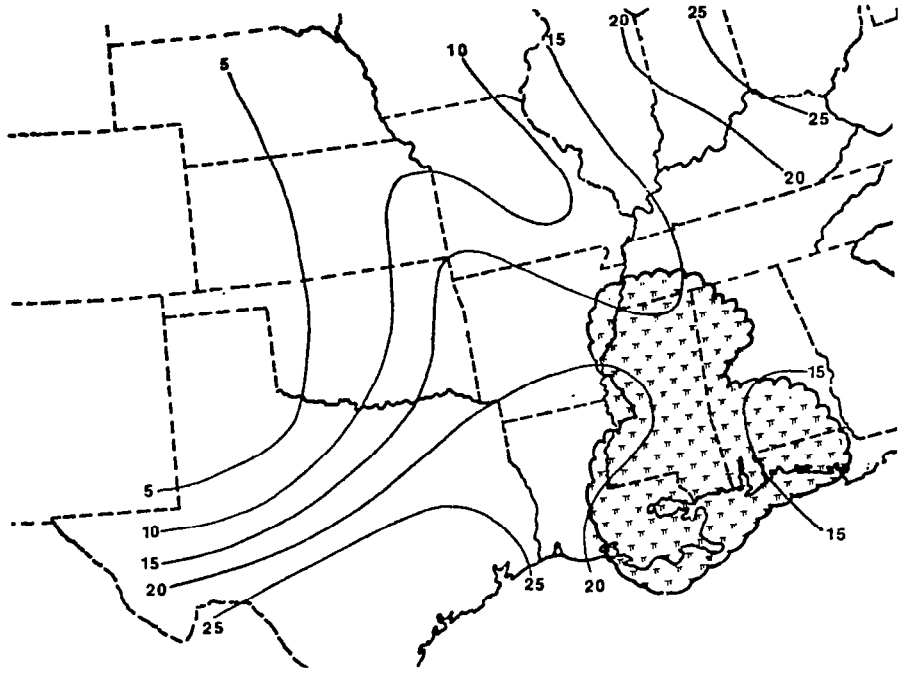

(a) Kinetic energy content, K, 10^5 J m^{-2}, 400-100 mb

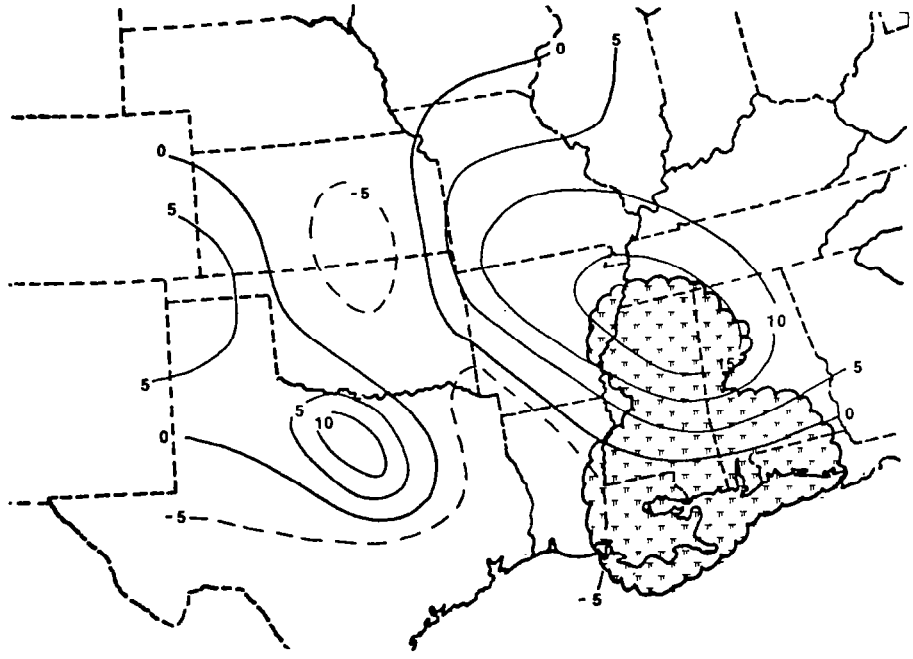

(b) Generation term, $-\vec{V}\cdot\vec{\nabla}\phi$, 10^1 W m^{-2}, 400-100 mb

Fig. 33. Spatial fields of kinetic energy budget terms for the 400-100 mb layer of AVE VII at 1200 GMT 3 May 1978. Superimposed are areas of MDR values $\geq$ 3.

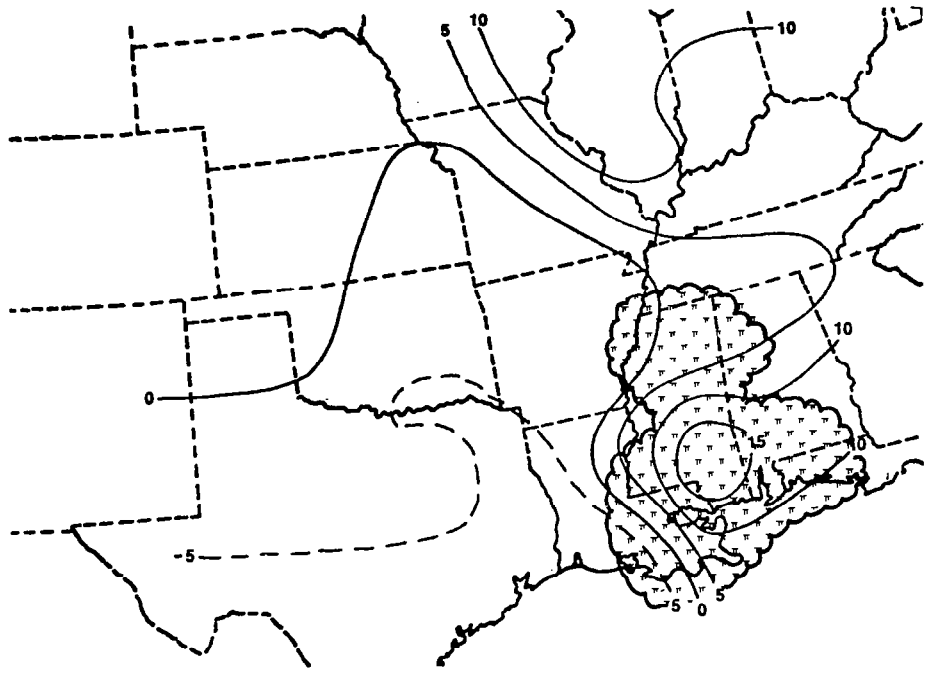

(c) Horizontal flux divergence term, $\vec{\nabla}\cdot k\vec{V}$, 10^1 W m^{-2}, 400-100 mb

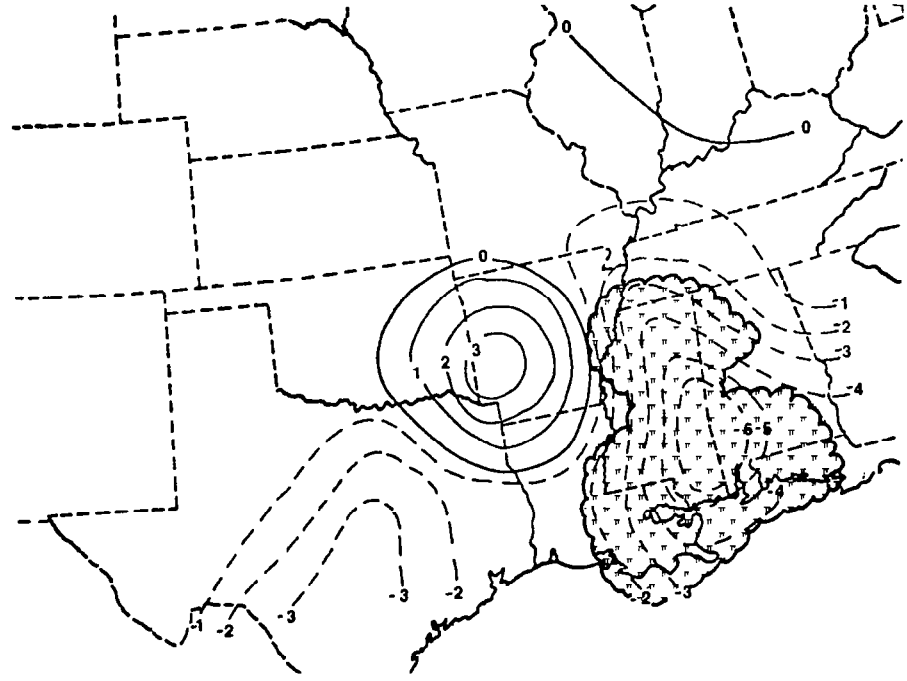

(d) Vertical flux divergence term, $\partial\omega k/\partial p$, W m^{-2}, 400-100 mb

Fig. 33. (Continued)

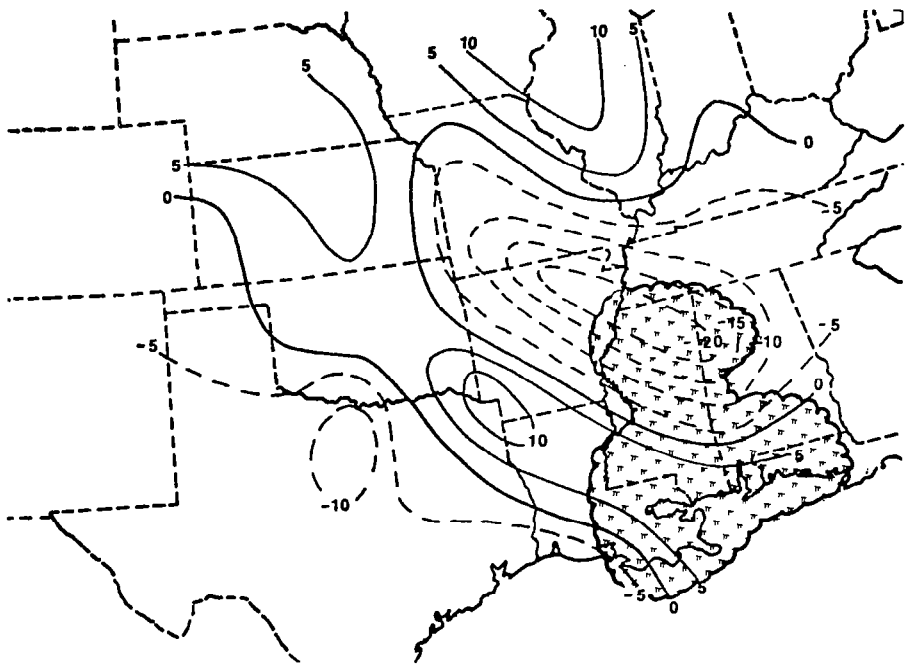

(e) Dissipation term, 10^1 W m^{-2}, 400-100 mb

Fig. 33. (Continued)

area of vertical flux convergence is located over southcentral Texas in association with rainshower activity. Strong downward motion over Arkansas is evidenced by vertical flux divergence of energy over that area.

Areas of positive and negative dissipation occur over the AVE VII area (Fig. 33e). An area of negative dissipation centered over Arkansas and Mississippi is the dominant map feature. The strongest storms along the Gulf Coast are located partly in the negative area and partly in a region of positive dissipation centered over Louisiana. In this particular case, the field of the dissipation term does not show close resemblance to the field of cross-contour generation (Fig. 33b).

6. SUMMARY AND CONCLUSIONS

Synoptic-scale budgets of kinetic energy have been computed during periods of intense convection. The availability of 3 and 6 h synoptic-scale rawinsonde data from three AVE experiments enabled temporal resolution of features that ordinarily would be undetected.

Several conclusions are drawn from the research:

1) The kinetic energy budget for each AVE area as a whole exhibits significant temporal variability with periods as short as 6 h. Some of the variability is due to synoptic-scale features that can be observed on carefully hand analyzed synoptic maps. Other aspects of the observed fluctuations are not readily explainable on the basis of synoptic-scale features and are presumably due to subsynoptic-scale phenomena such as thunderstorms and their interactions with the larger scales.

2) The kinetic energy budgets of limited volumes that barely enclose large areas of intense convection exhibit variations that are even greater than those observed for the area as a whole. Some of this variability is due to the modification of the synoptic-scale environment by the storms due to latent heat release and alteration of the wind field. Another portion of the variability would have occurred without the presence of the intense storms. Further research must be conducted to isolate the relative contributions of the storms.

3) The various energy generation and transport processes in the vicinities of some large areas of intense storms are greatest near the times when the storms are most intense. Storm areas that are weak, small, or short lived do not appear to modify their environments to a degree that is detected with synoptic-scale data.

4) All storm areas at peak intensity do not exhibit the same kinetic energy generation and transport processes. This seems reasonable because storms and their environments do not always interact in the same way. The time of peak storm

intensity is often, but not always, characterized by large values of generation of kinetic energy by cross-contour flow, dissipation of energy to subgrid scales, low-level horizontal flux convergence of energy, upper-level horizontal flux divergence of energy, and upward transport of energy into the upper troposphere and lower stratosphere. These energy processes are not always characteristic of peak storm intensity, however; destruction of kinetic energy and positive dissipation sometimes occur in the vicinities of the severe storms. The nature of the synoptic-scale upper-level flow, i.e., whether cyclonic or anticyclonic, seems to have a major influence on the energetics of the imbedded storm areas.

5) Spatial fields of kinetic energy budget terms show that the locations of severe storms often coincide with the locations of the most intense energy generation and transport for the area.

6) The more we study the energetics of severe storm situations, the more we realize that storm-environment interactions are very complex. Yet, a better understanding of these interactions is needed if we are to make advances in severe storms forecasting and in modelling the atmosphere. Additional research, of the type presented in this report, is planned for the upcoming year.

REFERENCES

Aubert, E.J., 1957: On the release of latent heat as a factor in large-scale atmospheric motions. J. Meteor., 14, 527-542.

Barnes, S.L., 1964: A technique for maximizing detail in numerical weather map analysis. J. Appl. Meteor., 3, 396-409.

Chen, T., and L.F. Bosart, 1977: Quasi-Lagrangian kinetic energy budgets of composite cyclone-anticyclone couplets. J. Atmos. Sci., 34, 455-464.

_____, 1977: Synoptic and kinetic energy analyses of Hurricane Camille (1969) during transit across the southeastern United States. Mon. Wea. Rev., 106, 67-77.

Danard, M.B., 1964: On the influence of released latent heat on cyclone development. J. Appl. Meteor., 3, 27-37.

_____, 1966: On the contribution of released latent heat to changes in available potential energy. J. Appl. Meteor., 5, 81-84.

Davis, J.G., H.E. Fuelberg, and R.E. Turner, 1978: NASA's AVE VII experiment: 25-mb sounding data. NASA TM-78197, George C. Marshall Space Flight Center, Alabama, 222 pp.

Fucik, N.F., and R.E. Turner, 1975a: Data for NASA's AVSSE I experiment: 25-mb sounding data and synoptic charts. NASA TM X-64959, George C. Marshall Space Flight Center, Alabama, 174 pp.

_____, and _____, 1975b: Data for NASA's AVSSE II experiment: 25-mb sounding data and synoptic charts. NASA TM X-64957. George C. Marshall Space Flight Center, Alabama, 185 pp.

Fuelberg, H.E., 1974: Reduction and error analysis of the AVE II pilot experiment data. NASA CR-120496, George C. Marshall Space Flight Center, Alabama, 131 pp.

_____, 1977: Atmospheric energetics in regions of intense convective activity. NASA CR-2826, National Aeronautics and Space Administration, Washington, D.C., 148 pp.

Fuelberg, H.E., and J.R. Scoggins, 1977: Relationship between the kinetic energy budget and intensity of convection. Preprints Tenth Conf. on Severe Local Storms, Omaha, Amer. Meteor. Soc., 265-270.

_____, and _____, 1978: Kinetic energy budgets during the life cycle of intense convective activity. Mon. Wea. Rev., 106, 637-653.

Kornegay, F.C., and D.G. Vincent, 1976 : Kinetic energy budget analysis during interaction of tropical storm Candy (1968) with an extratropical frontal system. Mon. Wea. Rev., 104, 849-859.

Kung, E.C., 1966: Kinetic energy generation and dissipation in the large-scale atmospheric circulation. Mon. Wea. Rev., 94, 67-82.

_____, 1967: Diurnal and long-term variations of the kinetic energy generation and dissipation for a five-year period. Mon. Wea. Rev., 95, 593-606.

_____, and W.E. Baker, 1975: Energy transformation in middle-latitude disturbances. Quart. J. Roy. Meteor. Soc., 101, 793-815.

_____, and P.J. Smith, 1974: Problems of large-scale kinetic energy balance--A diagnostic analysis in GARP. Bull. Amer. Meteor. Soc., 55, 768-777.

_____, and T.L. Tsui, 1975: Subsynoptic-scale kinetic energy energy balance in the storm area. J. Atmos. Sci., 32, 729-740.

McInnis, D.H., and E.C. Kung, 1972: A study of subsynoptic scale energy transformations. Mon. Wea. Rev., 100, 126-132.

National Aeronautics and Space Administration, 1978: Studies of vorticity imbalance and stability, moisture budgets, atmospheric energetics, and gradients of meteorological parameters during AVE III. NASA CR-3084, National Aeronautics and Space Administration, Washington, D.C., 128 pp.

National Weather Service, 1978: Digital radar code users guide. Silver Spring, Maryland, 25 pp.

Ninomiya, K., 1971a : Dynamical analysis of outflow from tornado-producing thunderstorms as revealed by ATS III pictures. J. Appl. Meteor., 10, 1103-1121.

_____, 1971b: Mesoscale modification of synoptic situations from thunderstorm development as revealed by ATS III and aerological data. J. Appl. Meteor., 10, 1103-1121.

O'Brien, J.J., 1970: Alternate solution to the classical vertical velocity problem. J. Appl. Meteor., 9, 197-203.

Smith, P.J., 1969: On the contribution of a limited region to the global energy budget. Tellus, 21, 202-207.

_____, 1970: A note on energy conversions in open atmospheric systems. J. Atmos. Sci., 27, 518-521.

_____, 1973: The kinetic energy budget over North America during a period of major cyclone development. Tellus, 25, 411-423.

_____, and S.P. Adhikary, 1974: The dissipation of kinetic energy in large-scale atmospheric circulations. Rev. Geophys. Space Phys., 12, 281-284.

Tsui, T.L., and E.C. Kung, 1977: Subsynoptic-scale energy transformations in various severe storm situations. J. Atmos. Sci., 34, 98-110.

_____, and L.N. Chang, 1975: Kinematic energy budgets of moving systems: Case studies for an extra-tropical cyclone and hurricane Celia, 1970. Tellus, 27, 215-233.

Ward, J.H., and P.J. Smith, 1976: A kinetic energy budget over North America during a period of short synoptic wave development. Mon. Wea. Rev., 104, 836-848.

ACKNOWLEDGEMENTS

Special thanks are due to David Ebel and Bill Abeling for their help during the course of the research and in the preparation of the final report with its many figures. Cathy Nicksich did a superb job of typing the final report.

1. REPORT NO.	2. GOVERNMENT ACCESSION NO.	3. RECIPIENT'S CATALOG NO.
NASA CR-3166		

4. TITLE AND SUBTITLE	5. REPORT DATE
Kinetic Energy Budgets in Areas of Convection	AUGUST 1979
	6. PERFORMING ORGANIZATION CODE

7. AUTHOR(S)	8. PERFORMING ORGANIZATION REPORT #
Henry E. Fuelberg	

9. PERFORMING ORGANIZATION NAME AND ADDRESS	10. WORK UNIT NO.
Department of Earth and Atmospheric Sciences Saint Louis University St. Louis, Missouri 63103	SLU-M-286
	11. CONTRACT OR GRANT NO. NAS8-32838
	13. TYPE OF REPORT & PERIOD COVERED Contractor (Final - 3/20/78 - 4/19/79)

12. SPONSORING AGENCY NAME AND ADDRESS	14. SPONSORING AGENCY CODE
National Aeronautics and Space Administration Washington, D. C. 20546	

15. SUPPLEMENTARY NOTES

Prepared under the technical monitorship of the Atmospheric Sciences Division, Space Sciences Laboratory, NASA Marshall Space Flight Center

16. ABSTRACT

Synoptic-scale budgets of kinetic energy are computed using 3 and 6 h data from three of NASA's Atmospheric Variability Experiments (AVE's). Numerous areas of intense convection occurred during the three experiments.

Large kinetic energy variability, with periods as short as 6 h, is observed in budgets computed over each entire experiment area and over limited volumes that barely enclose the convection and move with it. Kinetic energy generation and transport processes in the smaller volumes are often a maximum when the enclosed storms are near peak intensity, but the nature of the various energy processes differs between storm cases and seems closely related to the synoptic conditions. A commonly observed energy budget for peak storm intensity indicates that generation of kinetic energy by cross-contour flow is the major energy source while dissipation to subgrid scales is the major sink. Synoptic-scale vertical motion transports kinetic energy from lower to upper levels of the atmosphere while low-level horizontal flux convergence and upper-level horizontal flux divergence also occur. Spatial fields of the energy budget terms show that the storm environment is a major center of energy activity for the entire area.

17. KEY WORDS	18. DISTRIBUTION STATEMENT
Kinetic energy Convection Synoptic scale Atmospheric Variability Experiment	Category 47

19. SECURITY CLASSIF. (of this report)	20. SECURITY CLASSIF. (of this page)	21. NO. OF PAGES	22. PRICE
Unclassified	Unclassified	103	$6.50

* For sale by the National Technical Information Service, Springfield, Virginia 22161

NASA-Langley, 1979